Author:
Naduthottathil, Mincy R

Title:
Biomimetic Gelatin Nanofibrous Scaffolds for the Mechanical Modulation of Cardiac Pericyte Fate

Biomimetic Gelatin Nanofibrous Scaffolds for the Mechanical Modulation of Cardiac Pericyte Fate

Mincy Raj Naduthottathil

A dissertation submitted to the University of Bristol in accordance with the requirements for award of the degree of Doctor of Philosophy in the Faculty of Health Sciences

Bristol Dental School

June 2019

Word Count : 46,041

ABSTRACT

Congenital heart disease (CHD) is the most common and deadly congenital anomaly, accounting for up to 7.5% of all infant deaths. Survival in children born with CHD has improved dramatically over the past several decades, this positive trend being counterbalanced by the fact that more patients develop heart failure. Seminal data indicate an alteration of the extracellular matrix occurs with time in these hearts due to diffuse and abundant interstitial fibrosis. This results in an escalation in stiffness of the local microenvironment. However, the influence of matrix stiffness in regulating the function of resident human stromal cells has not been reported. The objective of this study was to determine the impact of stiffness on the antigenic and functional profile of cardiac pericytes (CPs) isolated from patients with CHD. To this aim, firstly, gelatin nanofibrous scaffolds with varying degree of stiffness using an *in-situ* electrospinning technique were produced. The Young's Modulus were assessed and then performed a comprehensive physicochemical characterisation of the scaffolds employing scanning electron microscopy, atomic force microscopy, and Fourier-transform infrared spectroscopy. This study next evaluated the changes induced by different scaffold stiffness on CPs morphology, antigenic profile, viability, proliferation, angiocrine activity, and induced differentiation. Results indicate that soft matrixes (Young's modulus ≤ 0.3 MPa) with larger fiber diameter (~400 nm), increase CPs adhesion, proliferation, secretion of Angiopoietin 2, Vascular Endothelial Growth Factor A (VEGF A) and F-actin stress fiber formation upon induced differentiation into vascular smooth muscle cells. There was no effect of stiffness on CPs antigenic profile or viability. To the best of my knowledge, these data indicate for the first time that human CPs can be functionally influenced by subtle changes in matrix stiffness. The study elucidates the importance of mechanical/morphological cues in modulating stromal cell behaviour and the feasibility of exploiting matrix stiffness to increase key features instrumental to the CPs regenerative potential.

ACKNOWLEDGEMENTS

Aum… A silent hymn before I begin. His wish that I should be here at the University of Bristol. To be inspired, motivated, encouraged and accompanied. Thanking each one of you all who have helped me in immeasurable ways. Not only to complete this prestigious degree but also to bundle up memories, to cherish.

I would firstly like to thank **Professor Bo Su**, for his supervision and helpful guidance over the last four years. I really appreciate his concerns on me as his student, when I was struggling in the initial stages of my Ph. D to cope up with the work-life balance. I express my deep sense of gratitude and sincere thanks to him for his valuable assistance and creative suggestions throughout my work.

I am thankful to **Professor Paolo Maddedu**, the one whom I am indebted to, for he stood with me with his own caring way, especially in writing the manuscript. He had been a pillar of strength with his tremendous insight and constant guidance and support in conducting the cell studies.

I am grateful to **Dr Sean Davis** for giving his valuable instructions and support in performing the mechanical characterisation of my material and access to the Chemical Imaging Facility.

With great gratitude, I thank **Dr Terry McMaster**, who gave me this excellent opportunity to pursue a Ph. D, which was my dream. Also, I would like to express my sincere appreciation to **Dr Annela Seddon** and all the faculty members of Bristol Centre for Functional Nanomaterials and Bristol Dental School who gave generously of their time and expertise.

Perhaps more than that of anyone, the always willing and generous help of **Dr Elisa Avolio**, was significant to the successful fulfilment of this work. Her constant advice, supervision, and crucial contribution helped me immensely for the timely completion of this thesis.

My heartfelt gratitude to **Dr Jean-Charles Eloi**, **Dr Robert Harniman**, **Dr Michele Carraba**, **Dr Nick Schumacker**, **Dr Sadie Slater**, and **Marco Fagnano** for helping me with the equipment, their tricky software and all the messy just-before-the-last-minute-file transfers, so that I could meet the deadlines with confidence.

The episode of acknowledgement cannot end without mentioning the role of my husband **Dr Aathish Bhanu**, without his support, I would not have done this tedious task. I would like to thank him for his extreme patience and understanding, and also for being the reason for the successful completion of this work. I am incredibly appreciative for the constant co-operation from my daughter **Amiyah Aathish,** especially in the last stages of writing this thesis. I also thank my **Parents,** who laid the basic foundation in achieving this award. I am very grateful to my **Brother** and my **In-laws,** for their constant support and encouragement in following my passion. I wouldn't have made it this far, without your love and support. It is my thesis, but in some ways, it is your achievement. I would also like to thank my friend **Dr Sana Algharaibeh**, for being a constant source of 'healthy' distraction from work and in creating a beautiful work environment.

Finally, I would like to gratefully acknowledge the financial support offered by the Engineering and Physical Sciences Research Council for conducting this project and funding my scholarship. I would also like to express my sincere gratitude to British Heart Foundation

(BHF) and the grant from National Institute for Health Research (NIHR) Biomedical Research Centre at University Hospitals Bristol NHS Foundation Trust and the University of Bristol. I wish to express my sincere thanks to the research nurses and administrators from the NIHR Biomedical Research Centre at University Hospitals Bristol NHS Foundation Trust and the University of Bristol for collection of patient samples used in this study.

Above all, I thank God Almighty for all the blessings and giving me the much-needed strength and enthusiasm to carry out this work successfully.

I declare that the work in this dissertation was carried out in accordance with the requirements of the University's Regulations and Code of Practice for Research Degree Programmes and that it has not been submitted for any other academic award. Except where indicated by specific reference in the text, the work is the candidate's own work. Work done in collaboration with, or with the assistance of, others, is indicated as such. Any views expressed in the dissertation are those of the author.

SIGNED: DATE:

Mincy Raj Naduthottathil

LIST OF TABLES

LIST OF ILLUSTRATIONS

1. INTRODUCTION

In this chapter, the factors concerned with successful cardiovascular regeneration and tissue engineering with a particular focus on congenital heart defects (CHDs) and the current situation of research into correcting CHDs and the future strategies for treating CHDs will be introduced. The stem cell therapy and cardiac pericytes (CPs) as potential stem cells for cardiovascular regeneration and tissue engineering will also be discussed. The biomimetic ECM and the factors affecting the stem cell fate, notably the matrix stiffness/elasticity of the material and the evaluation of nanofiber matrix stiffness will be reviewed in detail. The electrospinning technique, gelatin and the cross-linking method of gelatin will also be appraised in detail and areas that require further research will be highlighted.

The native extracellular matrix (ECM) can be regarded as a dynamic and hierarchically organised nanomaterial that not only provides mechanical support for embedded cells, but also interacts with the cells and regulates cellular functions such as adhesion, migration, proliferation, and differentiation (1). A typical ECM is composed of structural protein nanofibers such as collagen, with dimensions ranging from tens to hundreds of nanometers in the three-dimensional form (1-3). It is expected that such 3D biomimetic ECM will play a similar role in supporting cell growth *in vitro* as native ECM does *in vivo*. Creation of such a niche is thus imperative to basic stem cell biological studies and tissue engineering applications (4, 5).

Stem cell-based therapies are gaining widespread attention in the field of tissue engineering and regenerative medicine because of their self-renewal capacity and pluripotency (5). In i*n vivo* conditions, stem cells are surrounded by a specialised microenvironment called “stem cell

niches" consisting of soluble and surface-bound signalling factors, cell-cell contacts, stem cell niche support cells, ECM, and local mechanical microenvironment (5, 6). The stem cell fate is affected by all these microenvironmental factors and how these biophysical signals are filtered and taken up by the stem cells to regulate tissue regeneration based on physiological demand is still incompletely understood (4, 5). Moreover, it is hard to mimic the same microenvironmental conditions *in vitro* because of its complex nature. So, the critical aspect of enabling stem-cell based therapies is the ability to manipulate the interactions with the local microenvironment (5, 7).

Currently, most studies of cell culture system are focused on chemical cues, i.e. cell-binding proteins and peptides, or topographical cues, i.e. nanofibrous form (8-10). There has been increasing evidence that mechanical stiffness is also a sufficient cue to modulate cellular behaviours of stem cells, particularly their fate (self-renewal and differentiation). It is known that native ECM consisting of collagen or fibrin nanofibers often have a much higher local stiffness (elastic modulus of ~MPa at the individual-fibre level) than the bulk ECM (elastic modulus of ~kPa). Therefore, the mechanical stiffness of ECM is not just dependent on its material property of individual fibre but also on its 3D structure (11-13). Even though stem cells have been widely used for many clinical applications, our knowledge on how they are engaged in the differentiation process via cell-scaffold interaction is somewhat limited. Hence, a thorough understanding of how the mechanical properties of scaffolds influence these stem cells is of fundamental importance to functional tissue engineering and regenerative medicine applications (8).

Electrospinning is the most common method used for the fabrication of nanofibers utilizing both natural and synthetic polymers. The polymer selected in this work is gelatin as gelatin is

a natural polymer, and hydrolysed form of collagen which is the most common protein in the animal kingdom. However, the electrospinnability of gelatin is poor compared to synthetic polymers with defined molecular weight and distribution, such as Polycaprolactone (PCL), Polylactic acid (PLA) and Polylactic-co-glycolic acid (PLGA) as electrospinnability is strongly dependent on polymer chain confirmations and entanglements. Gelatin is polyelectrolytic in nature and possesses a 3-D macromolecular cross-linked network because of the strong hydrogen bonds formed at room temperature, which in turn reduces the mobility of polymer chains (14). Hence, for the successful electrospinning of gelatin, high-polarity solvents such as 2,2,2, -trifluoroethanol (TFE) and hexafluoroisopropanol (HFIP) are commonly used and are cytotoxic and expensive. This work exploits an alternative biocompatible and cheap water solvent system to obtain gelatin nanofibers using an *in situ* electrospinning method. Despite other conventional cross-linking methods, which cross-links by diffusion, *in situ* electrospinning technique with a double-barrel syringe benefits homogeneous mixing of the polymer solution with the cross-linker, and hence the formation of internally cross-linked uniform gelatin nanofibrous scaffolds. Additionally, this technique will also allow the fine-tuning of the requisite amount of cross-linking agent and reduces the unwanted deposition of cross-linker on the surface of the material.

Therefore, in this work, electrospun gelatin nanofibrous scaffolds with different crosslinking densities were fabricated to understand the effect of matrix stiffness on cardiac stem cell fate. Currently, a great deal of research is going on in examining various types of fibers and how they interact with stem cells to drive differentiation into specific cell lineages (8, 15, 16). An ideal ECM substrate should be biocompatible, highly porous, biodegradable and mechanically durable depending upon the application (17, 18). Nanofibrous scaffolds can be fabricated with tunable porosity and mechanical strength, and its three-dimensional (3D) architecture can

enhance cell adhesion, alter focal-adhesion signalling cascades, and thereby the stem cell fate (19, 20). Similarly, the high surface to volume ratio of nanofibrous scaffolds can aid better cell adhesion, proliferation and differentiation (21). Hence, the best way to mimic the ECM is to create a nanofibrous matrix to achieve specific stem cell lineages.

The stem cells under investigation in this study are cardiac pericytes (CPs). They are CD34 positive cells, negative for the endothelial markers CD31 and CD146. They reside in the heart as an interface between the coronary vasculature and cardiomyocyte compartment and play an essential role in maintaining cardiac homeostasis and repair. The previous studies from our group have revealed the possibility of immunosorting and expanding CPs from small biopsies of the human heart (22). There are also reports showing that pericytes can be effectively used for the repair of infarcted heart, myocardial ischemia, cardiovascular repair, skeletal muscle tissue engineering, etc.(23-28). Hence CPs have potential applications in the cardiovascular regeneration, and it is crucial to understand how these cells behave to different mechanical cues to be used in a stem cell engineered graft for cardiovascular reconstruction.

This study addresses the problem of Congenital Heart Defects (CHDs), which affects 9 in every 1000 babies born in the United Kingdom (UK) (20). For the reconstruction of complex cardiac defects, surgeons are using prosthetic materials such as xenografts, autografts, allografts and synthetic Gore-tex (29). For example, it has been reported that decellularized porcine small intestinal submucosa extracellular matrix (SIS-ECM) can be used as a vascular graft for tissue regeneration in animal models and noncardiac human applications. However, these implants are often a failure in repairing an infant's heart due to their lack of cardiomyocytes and remodelling capacity when it comes clinically (30). It is also associated with a higher risk of infections and thrombotic complications (29). Hence, stem cell engineered grafts or cell

therapy are gaining a wide range of attention in correcting the heart defects nowadays because they can grow as the child's body grows and remodels physiologically (31).

Changes in stiffness occur in the hearts and arterial vessels of patients with congenital heart disease (CHD), currently acknowledged as the most common congenital anomaly responsible for 7.5% of all infant deaths and for an increased heart failure morbidity and mortality (32). A previous study examining the effects of matrix stiffness on the behaviour of ovine and murine adult cardiac side population cells documented that rigid substrates caused a reduction in cardiomyogenic differentiation, accelerated cell ageing and stimulated the upregulation of extracellular matrix and adhesion proteins gene expression (33). Nonetheless, to the best of our knowledge, no study has assessed the effect of stiffness on the behaviour of stromal cells from the heart of patients with congenital cardiac defects. Investigating this matter could not only improve the current understanding of cell behaviour during maladaptive heart remodelling but also help to refine the biocompatibility of matrices for tissue engineering correction of cardiac defects.

Therefore, in the present study, *in situ* electrospun gelatin nanofibrous scaffolds (CLGS) with different crosslinking concentrations, prepared in a cheap and biocompatible water system were used as an *in vitro* platform to investigate the effect of matrix stiffness on CP antigenic profile, morphology, viability, proliferation, angiocrine activity and capacity to differentiate into vascular smooth muscle cells (VSMCs).

1.1. Cardiovascular Regeneration and Tissue Engineering

It is considered that heart disease remains the number one cause of mortality in both developed and developing countries. This can be due to many pathophysiological conditions of the heart such as the myocardial infarction, atherosclerosis, diabetic and ischemic diseases and loss of cardiomyocytes (CMs) due to ageing. All these circumstances can lead to fatal conditions from cardiac arrhythmias to heart failure (34).

Tissue engineering has been considered as a prospective bioengineering technology for treating cardiovascular diseases with the objective of creating biomimetic 3D synthetic or natural substitutes made of polymers usually known as scaffolds. Mostly these scaffolds were used along with autologous stem cells and differentiated cells, to permit individual patients' therapy with physiological remodelling and tissue regeneration (29, 35, 36). The scaffolds act as a matrix and support cell adhesion, proliferation, differentiation and finally new tissue formation in the *in vivo*.

The cardiovascular disease under consideration of this study was congenital heart defects (CHDs), which is the most common and deadly congenital anomaly, accounting for up to 7.5% of all infant deaths. Children born with CHD are surviving, and this rate has improved dramatically over the past several decades, but this positive trend being counterbalanced by the fact that more patients develop heart failure.

1.1.1. Congenital Heart Defects (CHDs)

CHDs are becoming a leading cause of death among infants in developed countries. It has been reported that every year, around 4600 babies are born with CHD in the United Kingdom alone (21). Despite the advances in foetal care, surgical and medical technologies with CHDs, the mortality and morbidity rates associated with CHDs are still a cause of concern. According to the researchers, 80% of the patients born with CHDs are expected to reach their adulthood and later develop heart dysfunction and other neurological and respiratory problems. Hence, there is a necessity to extend the clinical needs of CHDs not only to the young patients but also to adulthood (37).

Palliative surgery for CHDs has allowed patients to survive in most cases, with lethal heart abnormalities. However, these patients have to undergo repeated surgeries associated with an increased risk of surgical complications and considerable psycho-social stress for young patients and their families. Moreover, these surgical procedures often place a burden on the heart over time and cause heart failure due to the low inherent capacity of mammalian heart to form new cardiomyocytes.

Depending on the severity of the defects, the CHDs are classified into different types. It varies from common congenital heart abnormalities such as valves or septal defects, alterations of pulmonary veins and arteries, to severe malfunctions such as the absence of one or more chambers or valves. This condition results in abnormal blood circulation, which eventually results in heart failure and death (29, 38, 39). Among these, septal defects are the most common CHDs in infants which are associated with holes between the two ventricles or atrium. This causes abnormal blood circulation due to the mixing of oxygenated and deoxygenated blood

between the two chambers of the heart. The complex CHDs include Tetralogy of Fallot (ToF) and Hypoplastic Left Heart Syndrome (HLHS) (or univentricular heart syndrome) (29, 35, 38). Tetralogy of Fallot (ToF) is a condition which occurs due to the combination of different heart abnormalities. They are narrowing of the pulmonary artery, the hole between two ventricles, the position of the aorta above the aperture of ventricular chambers and right ventricle hypertrophy (39, 40). HLHS is due to the hypoplastic conditions of both aorta and left ventricle. In this condition, blood from the systemic circulation and the lungs mixes before it is being pumped by the right ventricle. This causes increased pressure and workload on the right ventricle and finally, the failure of the right ventricle (41). The classifications of CHDs are shown in figure.1.1.

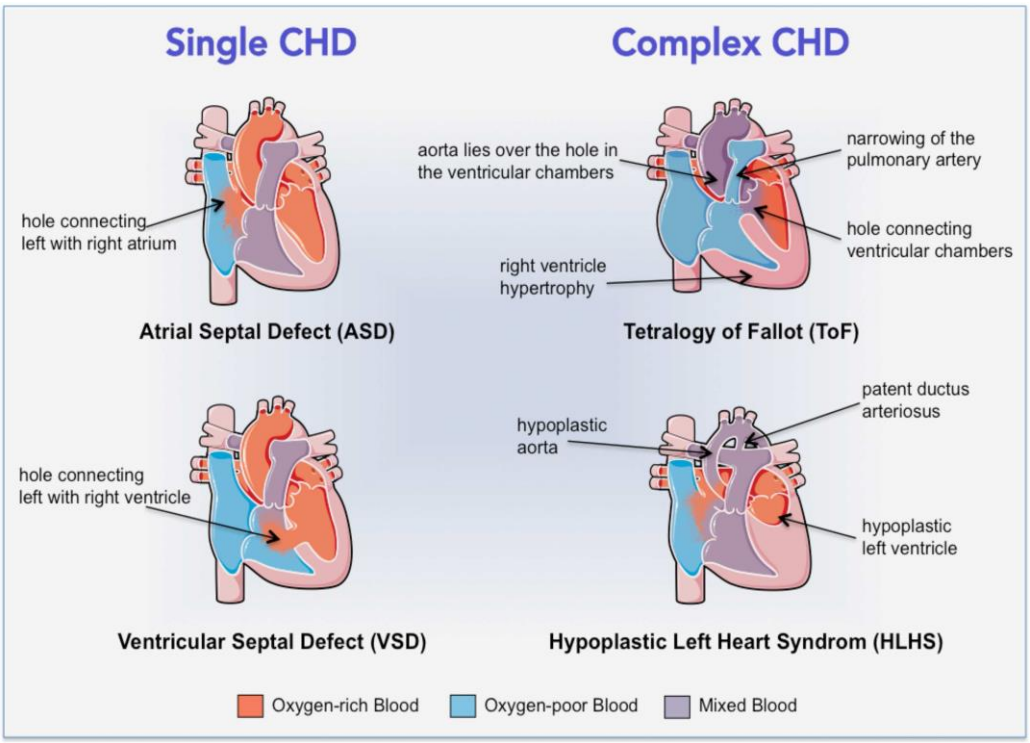

Figure.**1.1**. Classifications of CHDs based on their complexity (29).

1.1.2. Current treatment for CHDs and their limitations

The ideal treatment option for CHD patients is the corrective surgery, during which the holes in the heart are corrected with stitches or a patch, repairs or substitutes valves, broadens arteries, and alter the position of major blood vessels for active blood circulation (29). However, to correct complex structural defects, patients should undergo repeated open-heart surgeries, which are expensive and distressing to the patients (29, 38, 39). The deterioration of implanted grafts is another reason for these risky operations (42). On the other hand, heart transplantation is the only option for patients who are at the highest risk of death, which is very rare due to the lack of donors (43).

Currently, for the reconstruction of complex cardiac defects, surgeons are using prosthetic materials such as xenografts, autografts, allografts and synthetic Gore-tex (29). For example, it has been reported that decellularized porcine small intestinal submucosa extracellular matrix (SIS-ECM) can be used as a vascular graft for tissue regeneration in animal models and noncardiac human applications. However, these implants are often a failure in repairing an infant's heart due to their lack of cardiomyocytes and remodelling capacity when it comes clinically (40). It is also linked with a higher risk of infections and thrombotic complications (29). The advantages and disadvantages of using the current treatment modality are shown in table.1.1. Hence, stem cell therapy and stem cell engineered grafts is being investigated extensively to overcome the heart regeneration barrier, particularly in neonatal hearts (44).

Table.**1.1.** Schematic representation of different grafts currently used for surgical correction of CHD in children and their advantages and limitations (29).

Substitutes	**Advantages**	**Disadvantages**
Autografts	• Not immunogenic • No thromboembolism risk • Growth potential	• Replacement surgeries required
Allografts	• Good hemodynamic profile • Non antigenic ECM is repopulated after implantation • Preservation of morphology	• Lack of growth potential • Shortage and rare in small size • Decellularization weakens ECM • Immunogenic response if decellularization is not complete
Xenografts	• Limitless supply • Adequate anatomic structure	• Lack of growth potential • Toxic glutaraldehyde cross-linking • Decellularization weakens ECM • Risk of calcification • Immunogenic response

Stem cell therapy offers enormous therapeutic potential and is currently used to treat many diseases and disorders, including neurological conditions, orthopaedics and traumatology and cardiovascular diseases. This treatment modality is based on the injection of stem cells directly to the site of damage, aimed at the restoration of the damaged tissue by the self-renewing

capacity of stem cells and thereby recovering the lost function. This approach has been trialed used in the treatment of cardiovascular diseases, particularly in adult patients with myocardial ischemia (45). Only recently, it has also been proposed for the correction of CHDs (31, 46). A recent pre-clinical study was also conducted in a piglet ToF model and disclosed the safety and feasibility of intramyocardial administration of human MesP1 (mesodermal posterior 1)-embryonic stem cell-derived cardiac progenitors. But, at 3 months follow-up, the animals that had received cell therapy showed some improvements in RV (right ventricle) remodelling, and there was no substantial progress in RV function compared to control animals (47). A clinical study was also performed recently by administrating autologous umbilical cord blood-derived stem cells in a 4-months-old baby during a second palliative surgery. At 3 months of follow-up, the patient exhibited positive results in the improvement of right ventricular ejection fraction (RVEF) from 30 to 50% (48).

Tissue engineering is considered as one of the promising strategies for the regeneration of impaired tissues. Various synthetic biodegradable polymers such as polycaprolactone (PCL) polyglycolic acid (PGA) and poly-L-lactic acid (PLLA) have been commonly used in cardiovascular tissue regeneration. However, the mechanical properties, biodegradation rates and cytotoxicity of degradation products still remain as a factor of concern (49-51). In addition to these polymeric scaffolds, cell sheets engineering is another methodology used for tissue engineering and regenerative medicine applications. This technology makes use of confluent cell sheet constructs by harvesting the cells along with their deposited ECM. For this, the cells are grown on petridishes coated with temperature-responsive poly (N-isopropylacrylamide) (PIPAAm) and these cells form cell-cell junctions and ECM as they become confluent which favours the extraction of intact cell sheets. The cells are cultured at 37°C and the hydrophobic nature of the plates help the cells to adhere and proliferate. When the temperature is lowered,

the polymer is hydrated and become hydrophilic. This reduces the interaction with the ECM and hence the cell sheets are harvested. Three-dimensional cell sheet constructs are also developed by layering the cell sheets and are currently used for myocardial tissue engineering (52-54).

Even though there are not many clinical trials on treating CHDs with tissue engineered grafts, there are few pieces of evidence of positive outcomes involving the application of tissue engineered-grafts for correcting CHDs. Usually, the scaffolds were made with any of the above-mentioned polymers or combination of polymers and the most commonly used cell types were bone marrow-derived mononuclear cells (BMMNCs) or endothelial cells (ECs) because of the ease of harvesting from the bone marrow and peripheral veins (29). In 2001, cells were isolated from the peripheral vein of a 4-years-old girl affected with univentricular heart and pulmonary atresia and were seed on to a biodegradable graft made of PLLA/PCL which is reinforced with PGA. This trial was successful, and after 7 months of implantation, there was no evidence of occlusion and aneurysm. Two years later, the same group performed this trial in another 5-years-of-old child with the same scaffold incorporated with BMMNCs, and that was also successful with no stenosis (55). In 2010, Hibino *et al.* published a paper, and they performed a human trial for evaluating the remodelling potential of a tissue-engineered vascular graft. They isolated mononuclear cells from bone marrow (BMMNCs) from 25 patients (17 out of 25 patients recruited were <7 years of old) and were seeded onto a biodegradable scaffold made of PLLA/PCL/PLGA and implanted as conduits in patients with single ventricle physiology. They found that there was no evidence of rupture, infection or calcification of the grafts, but graft stenosis was reported in a few patients (56). Despite these successful trials, the application of these tissue engineered grafts in treating CHDs still needs

to be investigated thoroughly, since it is entirely a new field of study which will be explored in the future.

Thus, in cell therapy, the cells are isolated from different sources and are transplanted directly to the dysfunctional myocardial areas. This approach has been hampered due to the significant cell death followed by the cell transplantation clinically. There has been increasing evidence that the administrated cells may die soon after the implantation into the heart, and their therapeutic function is just to secrete the paracrine factors in the initial post-transplantation phase. So, this approach is not sufficient to correct complex CHDs as they require additional tissues in the form of grafts, valves and patches to recreate the fundamental biological structures (51), (29, 57). When the polymer scaffolds were used with BMMNCs or endothelial cells, their limitations were the inadequate supply of cell populations for tissue regeneration. Hence, stem cell therapy and tissue engineering are the two areas which hold together for the repair of complex heart defects (31).

1.1.3. Future Strategies for treating CHDs

As mentioned in the above section, it is imperative to have a matrix substrate that mimics the anatomy of heart tissue and suitable cell populations for the efficient creation of cell engineered scaffolds for correcting CHDs. The future strategies for correcting CHDs described by Avolio *et al*. in 2015 is displayed in figure.1.2.

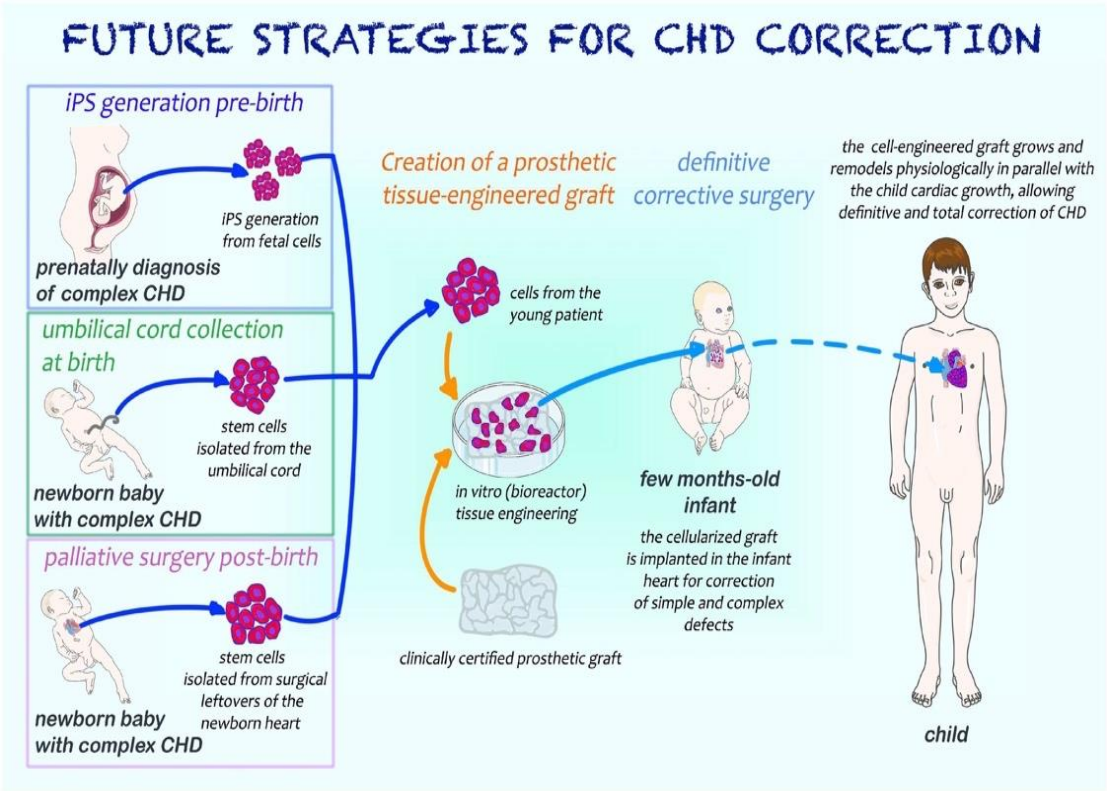

Figure.**1.2.** Cartoon illustrating possible future strategies for treating CHDs (29).

The advancements in the diagnostic screening allow the early detection of CHDs nowadays. Hence, if diagnosed prenatally, either the foetus cells can be harvested and induced pluripotent cells is generated, or during birth, the stem cells can be isolated from the umbilical cord and used for further treatments. On the other hand, if the diagnosis is made after birth, the cells can be isolated from the surgical leftovers of patients who undergo corrective surgeries. The isolated cells are then cultured on the scaffolds, and they are kept in the bioreactor, which provides all the essential nutrients for the cells to grow, proliferate and differentiate. The cells incorporated implants are then implanted to the defected part of the heart and can remodel the child's heart physiologically and grow simultaneously with the child's growth (29, 41).

In this study, cardiac pericytes isolated from the heart biopsies obtained from young patients who undergo palliative surgery in the Bristol Royal Infirmary were used. The details of clinical characteristics and pathology of the tissue donors recruited for this study are mentioned in the Materials and Methods chapter.

1.2. The Extracellular Matrix (ECM)

The ECM can be considered as a dynamic and physiologically active component of all living organisms. It provides structural and mechanical support to the cells embedded within a tissue as well as regulates the cell division, growth and development. In other words, ECM interacts with the cells and regulates cellular functions such as adhesion, migration, proliferation and differentiation.

1.2.1. Components of ECM

The ECM is mainly composed of proteoglycans, water, minerals, and fibrous proteins. Among them, proteoglycans and fibrous proteins are the major components of ECM. Proteoglycans are composed of a protein core surrounded by long chains of starch-like molecules called glycosaminoglycans. They provide resistance to stretching forces while fibrous proteins provide resistance to compressive forces. The fibrous proteins in the ECM consist of collagen, elastin, fibronectin and laminin (1-3). The ECM and its components present in all living organisms are presented in figure.1.3. The plasma membrane and cell surface receptors called integrins are also shown in the figure.

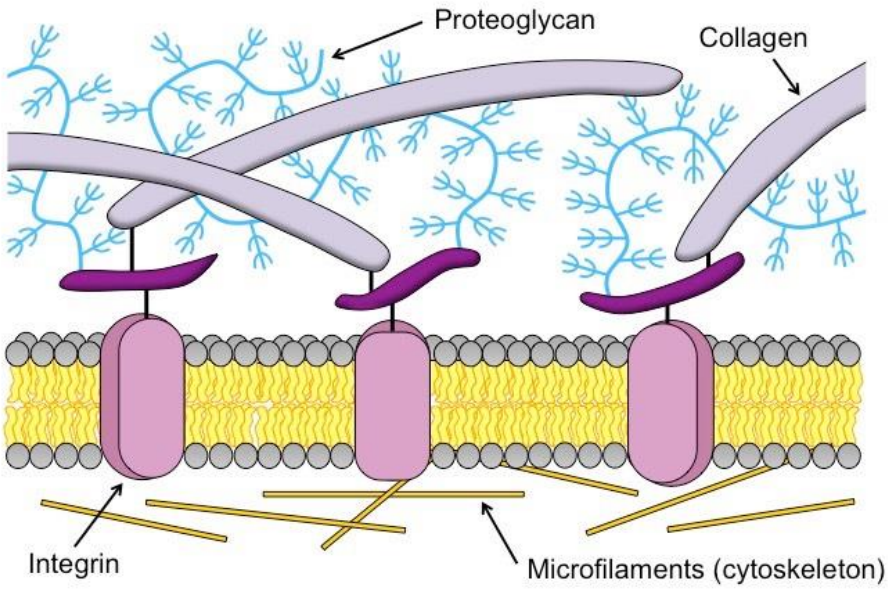

Figure.**1.3.** Representative image of ECM and its components (https://ib.bioninja.com.)

1.2.2. Cardiac ECM

In the heart, the ECM consists of all these components and provide a specialised microenvironment for the cells to survive and maintain a homeostasis. The ECM here acts as a structural and functional unit in maintaining the integrity of the organ by providing mechanical support for the cardiomyocytes, cardiac fibroblasts and endothelial cells and acts in response to the actomyosin contractions. Usually cardiomyocytes are differentiated and non-proliferating cells which allows the heart to pump blood into the pulmonary and systemic circulations by generating electric impulses and thereby coordinating the contractile behaviour. The coronary vasculature act as a tissue compartment by providing oxygen and helps in the waste removal. The coronary vasculature consists of both arterial and venous tissue. Both the cardiomyocytes and coronary vasculature are embedded in an ECM which mainly consists of collagen, proteoglycans and glycoproteins. Among these cells, cardiac fibroblasts form the largest population on the ECM(58). The stiffness of the cardiac ECM varies according to different factors such as ageing, blood pressure and diseased conditions(59). It has been

reported that the increased deposition of collagen results in a condition called fibrosis and fibrotic hearts are stiffer compared to normal myocardium. The stiffness of normal myocardium reported is 18 to 60 kPa and 55 to 295 kPa in fibrotic myocardium(60).

1.3. Stem Cells

Stem cells are the undifferentiated cells found in all multicellular living organisms. They can differentiate into specialized cells as well as they can divide itself to produce more stem cells (Figure.1.4). This ability of self-renewal makes the stem cells more attractive among the researchers to work on stem cell-based therapies. Stem cells can be divided into two main types. They are embryonic stem cells and adult stem cells. Embryonic stem cells can divide into any kinds of cells, while the adult stem cells can differentiate into specialized lineages (5).

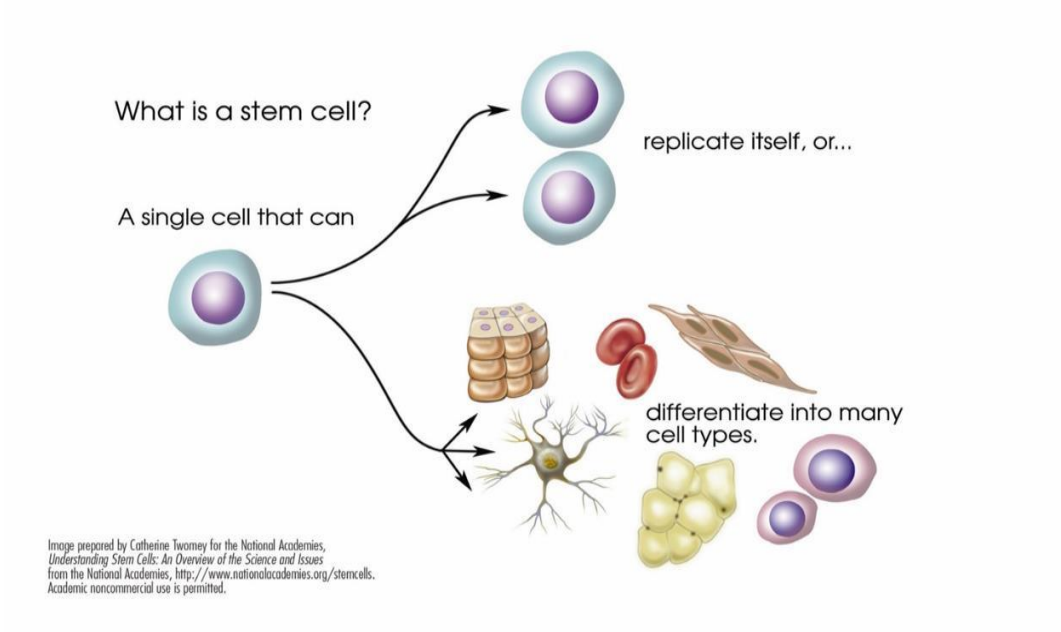

Figure.**1.4.** Diagrammatic representation of a stem cell replication and differentiation (61).

In this study, the stem cells under investigation are Cardiac Pericytes. Cardiac pericytes (CPs) are NG2 and PDGFRb expressing stromal cells that typically locate around capillaries and in close vicinity of coronary arterioles. They are CD34 positive cells, negative for the endothelial markers CD31 and CD146. They reside in the heart as an interface between the coronary vasculature and cardiomyocyte compartment and plays a vital role in maintaining cardiac homeostasis and repair. Our group have previously reported the antigenic profile, expansion/differentiation capacity, paracrine activity, and pro-angiogenic potential of CPs from neonatal and adult human hearts (21). In addition, we succeeded in immunosorting and expanding CPs from small biopsies of neonatal human hearts and demonstrated their engrafting capacity in clinically certified prosthetic grafts (21). There are also preclinical reports showing that pericytes can be effectively used for treating many cardiovascular diseases. For example, saphenous vein-derived pericytes (SVPs) along with cardiac stem cells (CSCs) were isolated and administrated to the infarcted heart of Beige mice affected with SCID (severe combined immunodeficiency) and tested their synergistic effect in repairing the heart defect. The coculture system showed reduction in the size of infract and interstitial fibrosis. They also reported SVPs capability in inducing angiogenesis while CSCs promoted cardiomyocyte proliferation and endogenous stem cells recruitment and hence proved the ability of this coculture system in repairing infarcted heart (22). In another study, SVPs were isolated from patients undergoing coronary artery bypass surgery and tested their therapeutic potential such as antigenic profile, proangiogenic potential and expansion of SVPs in treating patients with ischemic hearts. They observed the integration of CPs into endothelial cells and enhanced angiogenesis. Moreover, when these cells were administrated to the ischemic limbs of mice, they exhibited improved blood flow and neovascularization (23).

Furthermore, pericytes are attaining greater focus in cardiac tissue engineering, and researchers have been doing many works to differentiate cardiac pericytes into cardiac specific lineages. Even though, there are reports showing that pericytes can be effectively used for the repair of infarcted heart, myocardial ischemia, cardiovascular repair, skeletal muscle tissue engineering etc. only minimal studies are associated with combining CPs on scaffolds and assessing their capability to regenerate heart tissues. Our group has also stated CPs potential to be used as a graft in treating CHDs. The isolated CPs were incorporated into a patch called *CorMatrix* which is a decellularized patch, and when they were kept in a bioreactor for up to 3 weeks, they showed engraftment and viability of cells suggesting their potential to be used as a graft in treating CHDs. Still there exist a lack of investigations regarding the capacity of CPs to grow, proliferate and differentiate on biodegradable scaffolds to be used as a promising substitute for the prosthetic grafts and valves. As mentioned in the above section, it is a new field of study, and hence, more researches are adequate in expanding the use of CPs in tissue engineering scaffolds. In this scenario, it is, therefore, crucial to understand how these cells behave in response to mechanical cues in their native environment as well as in artificially modified substrates for the optimal design and preparation of scaffolds.

Usually, a cardiac stem cell differentiates into three types of cells known as cardiomyocytes, smooth muscle cells and endothelial cells. In the studies reported so far, only the differentiation of pericytes into smooth muscle cells have been reported (21-28, 62). For example, our group has also evaluated CPs potential to differentiate into any of these lineages by treating with corresponding differentiation inductive media containing specific growth factors. The results were only positive towards the differentiation of CPs into VSMCs while no differentiation has occurred towards the other two lineages (21). The cardiac stem cell differentiation and its specific lineages are shown the figure 1.5.

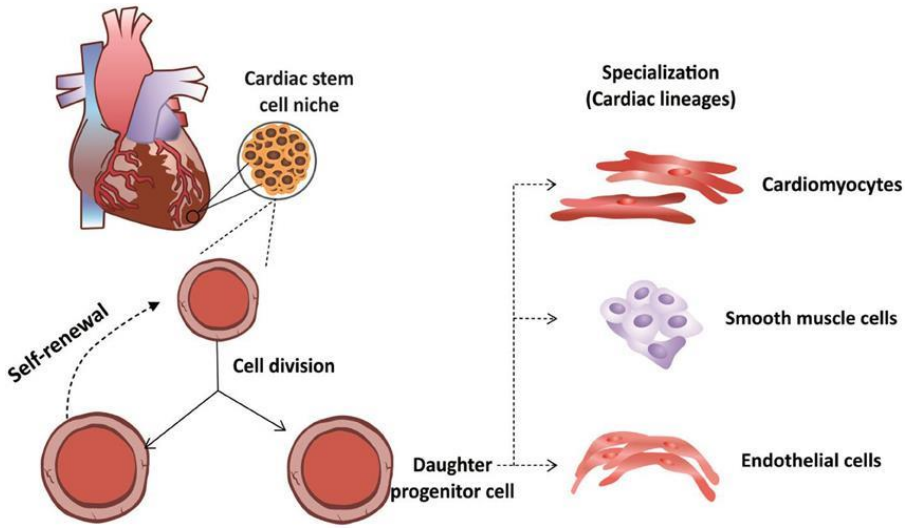

Figure.**1.5**. Differentiation of cardiac stem cells into their specific lineages (63).

1.4. Factors Affecting Stem Cell Fate

In *in vivo* stem cells are surrounded by a group of supporting cells, ECM and many soluble factors such as growth factors, cytokines, enzymes etc. A variety of chemical/biochemical cues, structural, mechanical and electrical cues are responsible for directing stem cells to the desired behaviour for the tissue engineering and regenerative purposes. Stem cells respond to these microenvironmental factors via numerous interactions with the adjacent cells and also with the tissue matrix, thereby the remodelling occurs consequently (64, 65). Regulation of stem cell fate is controlled by a wide range of microenvironmental factors such as matrix rigidity and topography, flow shear stress, strain forces, and other mechanical forces exerted by adjacent support cells. Figure 1.6. depicts the various biophysical factors/signals in the stem cell niche and their molecular interactions in the microenvironment for regulating the stem cell fate (5-8).

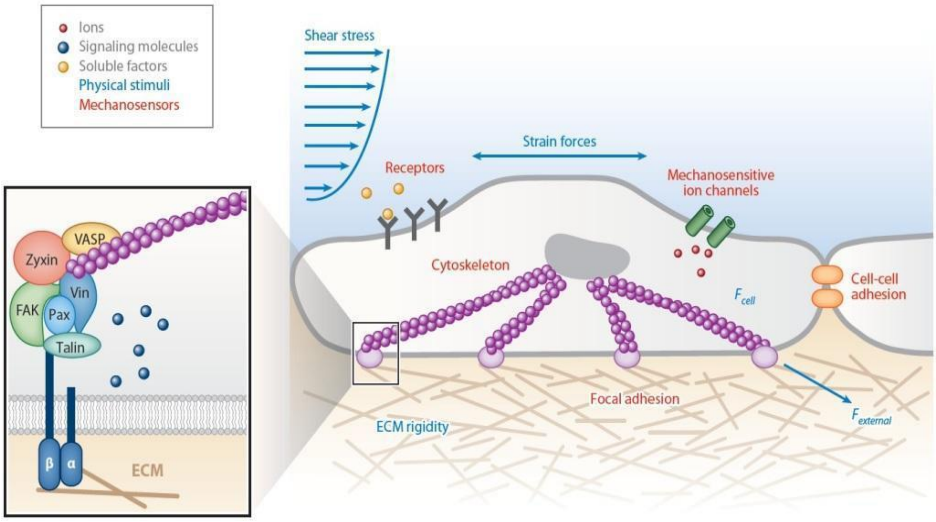

Figure. **1.6.** Schematic representation of various biophysical signals/factors acting in the stem cell niche (5).

Cells are exposed to mainly three types of forces such as extracellular, intercellular and intracellular forces. The extracellular forces are the forces exerted to the cells from the outer regions, and this includes the shear forces and tensile forces. Intercellular forces are the forces created when the cells contact each other. Finally, intracellular forces are cytoskeletal generated contractile forces due to actomyosin contraction, microtubule polymerisation and depolymerisation, osmotic forces etc. All these forces can create a mechanical stimulus in the stem cell niche, and the cells are subjected to adjust themselves to the external forces from the microenvironment by modulating their cytoskeletal contractility. The cytoskeletal contractility is dependent on the elastic modulus (stiffness) of the ECM. Thus, there occurs a tensional homeostasis or force balance between the external forces from the microenvironment to the cells and the force exerted by the cells (traction force) due to their endogenous cytoskeletal contractility. This plays an essential role in the basic cellular functions such as adhesion,

proliferation, differentiation, survival and apoptosis (5, 66, 67). Any variations in maintaining this tensional homeostasis can cause severe disease conditions such as arteriosclerosis, osteoarthritis, osteoporosis and cancer (5, 68-70).

There has been increasing evidence that the stem cells can sense all these stimuli through cell surface receptors called integrins and convert them into intracellular biochemical and functional responses through a series of cell signalling pathways (Ras/MAPK, PI3k/Akt, RhoA/ROCK, Wnt/β-catenin, TGF-β) by a process known as mechanotransduction (5, 70, 71). Integrin provides a mechanical linkage between the ECM and the actin cytoskeleton. Any mechanical forces acting on the cells such as shear stress or strain can activate integrins which are bound to the focal adhesion points. This, in turn, results in the recruitment of signalling proteins to strengthen the focal adhesion sites and to transmit biochemical signals to the cells. These mechanotransduction pathways can activate actin-myosin cytoskeletal contractility with the help of integrin engagement. Figure.1.7. explains how such mechanotransduction results in the modulation of protein expression and cellular functions such as survival, proliferation and differentiation (5, 72).

In a study by Chowdhury *et al.*, reported that mESCs cultured on soft polyacrylamide gels (~500 Pa) could maintain their pluripotency for 15 passages without exogenous leukaemia inhibitory factor (LIF; a soluble factor critical for maintenance of pluripotency of mESCs). This demonstrated the mechanosensitivity of pluripotent ESCs to matrix mechanics and showed that they are sensitive to subtle changes in external mechanical forces (73). In another study, fluid shear stress-induced the differentiation of Flk-1-positive mouse ESCs into vascular endothelial cells *in vitro* than the mouse ESCs incubated in a static culture condition (74). These observations suggest that matrix mechanics is a crucial regulator in controlling the stem cell function and differentiation (75, 76).

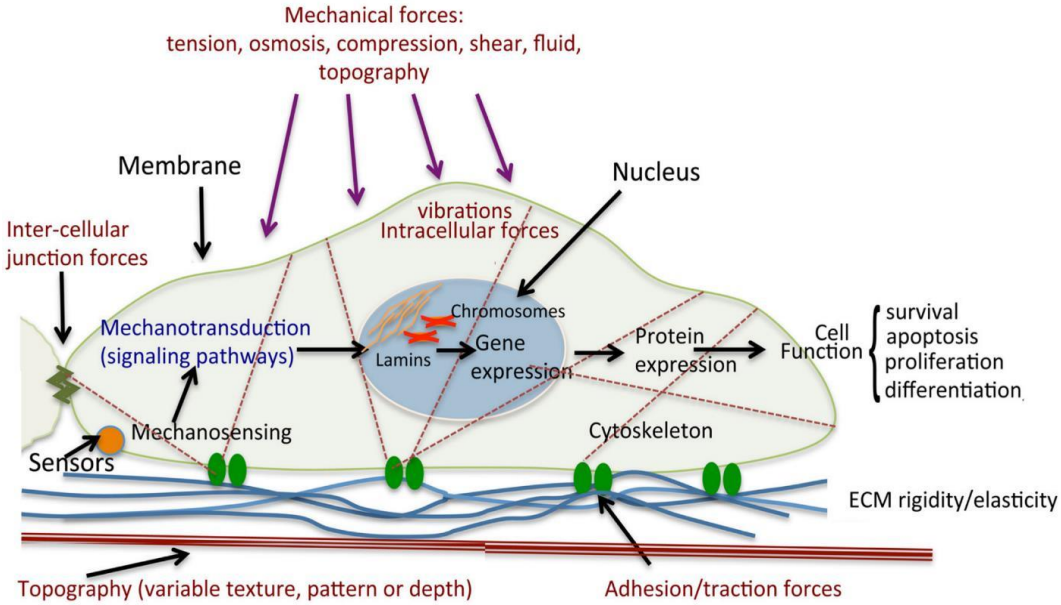

Figure.**1.7.** Schematic representation of cell mechanical stimulation (5).

1.4.1. Matrix Stiffness

Matrix stiffness is another crucial factor in determining stem cell self-renewal and commitment (11, 77-79). Stiffness of the ECM is usually represented as elastic modulus or Young's modulus. As mentioned earlier, the cytoskeletal contractility is directly dependent on the ECM stiffness. This can activate various mechanotransduction pathways with the help of integrins and regulates the stem cell fate (5, 11, 72). There are studies regarding the effect of ECM stiffness in determining stem cell fate. For example, MSCs were grown on polyacrylamide gel having different matrix stiffness, and it was found that the cell properties were not similar in the substrates with less stiffness. The stiffer substrates induced stiffer cells and differentiated into MSCs specific lineages than in the soft substrates. Furthermore, soft substrates with mechanical properties similar to that of brain tissue were found to be neurogenic, intermediate stiffness substrates with mechanical properties similar to muscle tissues were myogenic, and relatively rigid substrates with mechanical properties similar to bone were found to be

osteogenic (77, 80). Matrix stiffness also has effects on cell adhesion, migration, proliferation and differentiation. For example, different gel matrices were prepared with varying cross-linking degrees, and ligand densities and the cells were seeded to understand their adhesion on various substrates. It was found that most of the cells anchored firmly towards the stiffer substrates forming focal adhesion points and actin-myosin stress fibers (65, 77). Also, when MSCs were cultured on a rigid substrate differentiated into osteoblasts instead of adipocytes while on soft hydrogel substrates, they maintained self-renewal *in vitro* (65) (79, 81).

Even though there are plenty of studies based on hydrogel systems for regulating stem cell fate, only a few studies have reported the effect of nanofibers and its mechanical stiffness that determines the stem cell fate. In 2012, Wingate *et al.* fabricated three-dimensional nanofiber matrixes with the variable elastic modulus (2-15kPa) by adjusting the photopolymerization time, and MSCs were seeded to see their differentiation into vascular endothelial cells and smooth muscle cells (82). Nam *et al.* fabricated a core-shell poly (ether sulfone)-poly(ε-caprolactone) (PES-PCL) fibers of modulus 30.6 MPa, which is four times more than that of PCL alone. The embryonic mesenchymal progenitor cells behaviour was studied, and they found that the cells seeded on PES-PCL showed chondrogenesis, whereas the cells on PCL showed osteogenesis. Hence, by changing the nanofiber matrix modulus, the stem cell fate could be altered (8). This can be achieved in many ways such as introducing one more polymer and thereby creating a composite scaffold as done by Nam *et al.* or by changing some factors such as crosslinking density, functionalizing the nanofibers with nanoparticles etc. All these can have a significant influence in affecting the stem cell mechanisms (8, 83, 84).

Matrix stiffness is usually evaluated by measuring Young's modulus (YM). It is considered as the ability of the material to withstand the changes in length under tension or compression. YM is measured by the longitudinal stress divided by the strain.

$$E = (FL)/A \times \Delta L$$

where F is the force applied, L is the initial length, A is the area, ΔL is the change in length, and E is Young's modulus in Pascals (Pa).

The YM of electrospun nanofibers can be measured using a Nano tensile testing machine and Atomic Force Microscopy (AFM). Both single fibers and entire scaffolds are subjected to YM measurements depending on their applications. In tensile testing, MTS Nanomechanical Testing System or Instron machinery are usually used by researchers to measure the YM of nanofibers. In 2006, Chew *et.al*., performed YM analysis of single electrospun nanofibers composed of poly(ε-caprolactone) (PCL) and its copolymer, poly (caprolactone-co-ethyl ethylene phosphate) (PCLEEP) by electrospinning fibers on an aluminium frame, and a single fiber was then mounted on a cardboard mount to test the YM. The vertical sides of the cardboard mount were cut off before performing the tensile testing, and the fiber specimen was pulled at a constrain strain rate of $0.001s^{-1}$. The same method was followed by Naraghi *et al.* in 2007, but the nanofibers were collected on a Transmission Electron Microscopy (TEM) grid to perform the YM measurements (85). The YM was calculated from the obtained stress-strain curves (86). This method has certain limitations particularly the practical difficulty in the selection and mounting a single fiber for measurements, and a large number of measurements should be required to minimise the standard deviation as the fibers formed will be of different diameter. Hence, most of the studies are based on evaluating the YM of the whole nanofibrous scaffolds. Carrabba *et al*., investigated the YM of PCL nanofibrous scaffolds by holding the scaffolds between a custom-made gripping system and a strain rate of 0.01 min^{-1} were applied until failure (87). Studies which involve the application of cell/tissue engineering usually investigates the YM of the scaffolds in wet condition as well, since the scaffolds will be in the hydrated form when it is associated with the cells. Therefore, it is crucial to check the YM of

scaffolds in wet condition as different mechanical properties of the scaffolds will affect the cellular functions. For example, Dias et al., studied the YM of gelatin meshes, crosslinked with varying concentrations of 1,4-butanediol diglycidyl ether (BDDGE) both at the wet state and dry state and found a significant difference in the YM of the scaffolds when measured in both conditions (88). The picture of commercial nano tensile testing machine is shown in figure.1.8.

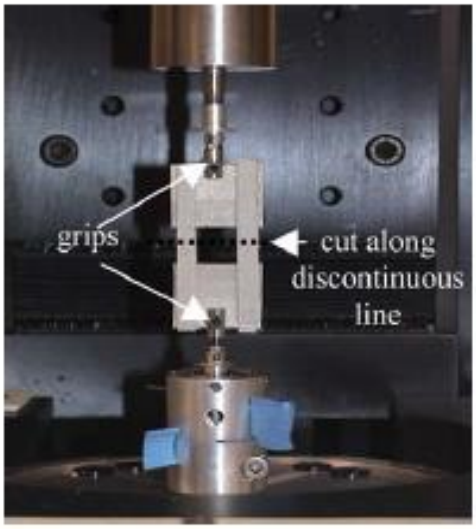

Figure.**1.8**. Nano tensile testing machine (78).

AFM utilizes different experimental methods commonly nanoindentation, tensile testing and three-point bend test to characterize the mechanical properties of nanofibers. Of all these characterisation techniques, nanoindentation is the most convenient method because of its easy sample preparation. To perform nanoindentation, a nanofiber is mounted on a hard and flat substrate, and an AFM tip is used to indent the nanofiber (89). AFM is operated in the force mode, in which the depth of the indent is always monitored relative to the indentation load and sample surface. The cantilever deflection is measured according to the vertical displacement of the cantilever tip as the loading and unloading occur through piezoelectric transducer expansion. Later, the force curves (force versus displacement) can be detected, and mechanical

properties such as YM and hardness can be derived (89). In 2005, Tan *et al.* reported the nanoindentation study of individual PCL nanofiber to measure the YM using AFM (90). The same group has also published the AFM based nanoindentation system for the tensile testing of nanofibers. This involves the use of a nanoindenter to pull a single fiber by clamping the nanofiber between the nanoindenter tip and the base, and the stepper motor of the AFM was used to stretch the fiber. In another approach by the same group, one end of the nanofiber was attached to (AFM) cantilever tip and the other end to, a movable optical microscope stage to perform the YM analysis. The nanofiber was stretched by moving the stage and the force was measured by the deflection of the cantilever. The YM of Polyethylene oxide (PEO) nanofibers (700 nm) measured by this method was found to be ~45 MPa (91). A schematic representation of this approach is shown in figure.1.9.

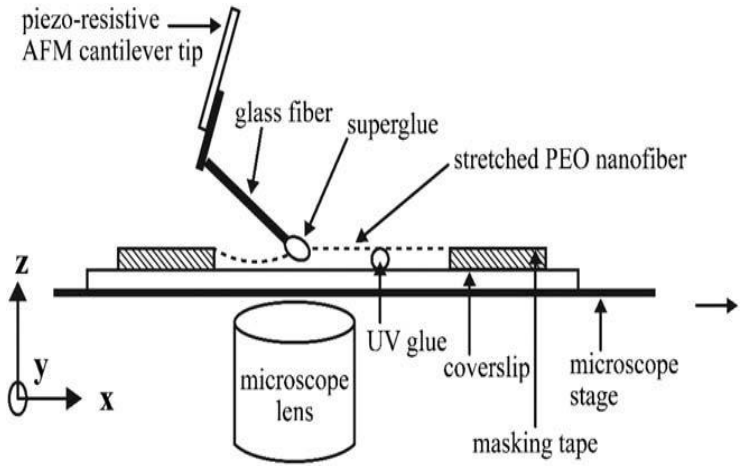

Figure.**1.9.** Schematic diagram of AFM based nanoindentation system for the tensile testing of nanofibers (91).

In three-point bend test, a nanofiber is suspended across an etched groove which is clamped by adhesives at both ends. An AFM tip is then used to apply a point load at the centre point of the suspended nanofiber (92). The YM of PLLA nanofibers with a diameter of less than 350 nm were found to be 1.0±0.2 GPa when measured by using this method (93). The schematic representation of AFM based three-point test is shown in figure.1.10.

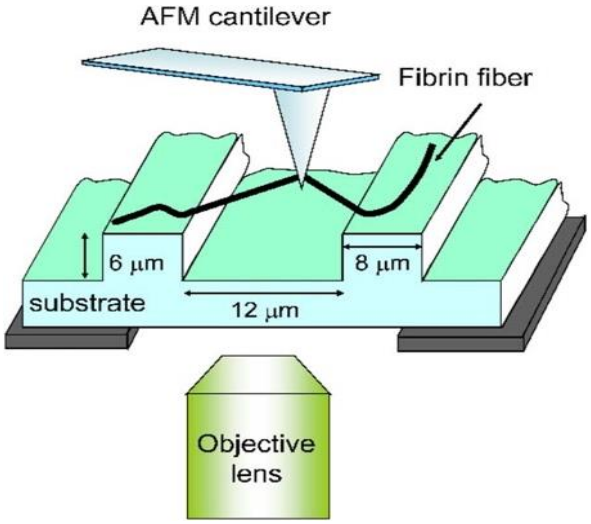

Figure.**1.10**. The schematic representation of AFM based three-point test using fibrin nanofiber (84). The dimensions of the substrates are also shown.

There are many limitations of using AFM for the mechanical characterisation of nanofibers, particularly the selection and mounting of ultrafine nanofiber and the complexity of the technique. Thus, the sample preparation and manipulation of nanofibers for their mechanical characterisation still remains the most significant challenge to date. Although AFM nanoindentation is convenient compared to other techniques, the uncertainties in the nanoindenter tip shape, the surface roughness, the curvature, the relative configuration of tip-fibre, and the adhesion force between the sample and the indenter makes this technique less reliable (85). In the AFM three-point bend test, the angles of inclination formed between the

deformed and original position of the nanofiber could give an axial fiber force value which may lower than the actual value and could lead to the misinterpretation of the data (85).

In this work, matrix stiffness of the fabricated gelatin nanofibrous scaffolds was evaluated by measuring the YM using tensile testing machine both at the dry state and wet state. More details about the experiment are explained in the Materials and Methods section. An attempt to measure the YM of individual fibers using AFM is also carried out, and the details of this are described in the Future Work section.

1.4.2. Matrix topography

For the regulation of stem cells, the matrix topography and its interactions with the cell is also a crucial factor. The recent advancements in the field of nanotechnology paved the way for the new possibilities to regulate the stem cell fate with specially designed nano topographies. It has been reported that the nanopatterned surfaces (ridges, steps, grooves, pillars and pits) can affect the cellular functions such as adhesion, morphology and gene expressions which in turn results in cell survival, apoptosis, proliferation and differentiation (81, 94). Macbeth *et al*., in 2004, showed that the nano-topography caused significant changes in the focal adhesion and resulted in the cytoskeletal changes, which also altered the gene expression (81). Dalby *et al.* were the first one to report that based on the degree of variation in the nanoscale order in the nano pit array, the hMSCs are capable enough to produce bone mineral *in vitro* without any osteogenic supplements. Also, the cells cultured on ordered arrays of nano pits showed less osteoblastic differentiation (95).

There are various methods for creating the nano-topography similar to the ECM. Nanolithography is one among them to control the shape, size, spacing, symmetry etc. of nanomaterials which are generally used for surface patterning. Phase separation , self-assembly

and electrospinning are other methods to synthesise nanofibers from synthetic as well as natural polymers (96). These techniques are reviewed in detail in the next section.

It has been reported that the nanofiber alignment is also an essential factor in affecting the stem cell adhesion, proliferation and differentiation. For example, Schwann cells cultured on aligned fiber scaffolds were shown to have more focal adhesion and proliferation than on the random meshes. The cells cultured on the aligned fibers can grow in the direction of the alignment of fibers, and it is a significant aspect in the neural tissue engineering. Fiber alignment has also been investigated for the regeneration of the anterior cruciate ligament. Also, there are studies showing the change in diameter can create a significant difference in the spreading, adhesion, proliferation and differentiation of the stem cells. Hence the fiber morphology and alignment can directly affect the mechanical properties of the scaffolds, which in turn affects the cellular behaviours (97).

Therefore, it is evident that ECM plays a vital role in regulating the stem cell fate, particularly in terms of its mechanical forces acting on it (stress and strain), stiffness and topography. The use of biomaterials is a useful tool to create a biomimetic ECM in the *in vitro* conditions.

1.5. Biomimetic ECM

To better mimic ECM, polymers have been widely used in the field of tissue engineering and regenerative medicine. Both synthetic and natural polymers are widely used to create ECM in the form of hydrogels, nanofilms, nanofibers etc. (96, 98-100). For example, natural polymers like hyaluronic acid, alginate, chitosan, gelatin, silk etc. have been widely used both individually and as composites using different fabrication process to study the stem cells (101-106). Some of the synthetic polymers using in this field are Poly (L-lactic acid) (PLLA), Poly (lactic-glycolic acid) (PLGA), Polycaprolactone, Polyvinyl alcohol (PVA) etc. (14, 78).

A typical ECM is composed of structural protein nanofibers such as collagen with dimensions ranging from tens to hundreds of nanometres in three-dimensional form. It is expected that such 3D biomimetic ECM will play a similar role in supporting cell growth *in vitro* as native ECM does *in vivo.* An ideal ECM substrate should be biocompatible, non-toxic, highly porous biodegradable and mechanically strong enough depending upon the application.

In the present study, I focused on creating nanofibrous matrixes for investigating the effect of CPs behaviour on substrates with different stiffness/elasticity.Nanofibrous scaffolds can be fabricated with tunable porosity and mechanical strength, and it's three- dimensional (3D) architecture can enhance the cell adhesion, alter the focal-adhesion signalling cascades, and as a result the stem cell fate (18, 19). Also, the high surface to volume ratio of nanofibrous scaffolds can aid better cell adhesion, proliferation and differentiation. Hence, the best way to mimic the ECM is to create a nanofibrous matrix in order to achieve specific stem cell lineages.

Currently, a great deal of research is going on in examining various types of fibers and how they interact with stem cells to push differentiation into specific cell lineages. In a study using a composite nanofibrous material, made of PCL and collagen increased the proliferation of nerve-like cells. Moreover, the incorporation of collagen increased the biocompatibility of PCL and the amino groups of collagen help in cell adhesion and proliferation (15). Another pioneering work in the field of stem cell research using nanofibers is the differentiation of MSCs into chondrocytes using electrospun PCL fibers containing chondrogenic medium TGF-β1. Also, electrospun nanofibers with different chemical compositions were fabricated using poly [(L-lactide)-*co*-(ε-caprolactone)] (PLCL) and gelatin, and its osteogenic differentiation of MSCs was studied. It was found that hMSCs cultured on PLCL/gelatin nanofibers showed better *in vitro* cell growth and osteogenic differentiation than hMSCs grown on PLCL-only

nanofibers (16). In another work done by Kang et al., PCL scaffolds were found to be an appropriate matrix for the mouse ES cells to grow and differentiate into adipocytes (17).

As discussed above, there are many works related to the efficient use of electrospun nanofibers for various tissue engineering applications. In the field of cardiac regeneration, recently a research group revealed the potential of using beta-PVDF as a nanofibrous implantable electrospun scaffold in conjugation with stem cells for the reconstruction of damaged heart muscles. The fabricated nanocomposite material was found to be mechanically stable and showed enhanced cardiomyocyte differentiation with respect to control (107). In another work, FDA approved polymer PCL was functionalized with gold nanoparticles and mesenchymal stem cells and cardiomyocytes were cocultured on to the scaffolds to investigate the scaffolds potential in the regeneration of infarcted myocardium. Notably, the scaffolds mechanical strength of 2.56 MPa was similar to the native myocardium and the gold nanoparticle incorporated PCL scaffolds exhibited positive expression of cardiac-specific markers in differentiated mesenchymal cells suggesting its ability to support and cardiogenic differentiation potential (108).

Alternatively, self-assembly and phase separation has been used for synthesizing nanofibers. Phase separation is the most commonly used technique for the production of highly porous polymeric scaffolds or membranes. This process is usually accomplished by the thermally-induced polymerization, which involves several steps such as the dissolution of the polymer with an appropriate solvent, gelation by applying adequate gelling temperature and finally, the solvent separation (109). This will result in the production of the porous nanofibrous structure whereas self-assembly is an entirely different approach for nanofiber formation; which utilizes the bottom-up approach that relies on weak noncovalent bonds to form nanofibers from peptides (109). Both these approaches have their own advantages and disadvantages. For

example, self-assembled nanofibers are excellent for drug delivery applications, and phase separation is exceptional for obtaining highly porous scaffolds for various tissue engineering applications, particularly for bone regeneration. However, both these systems would be difficult to scale up to a commercial setting and only limited number of polymers can be utilized for these approaches. Also, these techniques consume tremendous time as they involve various steps. Compared to these processes, electrospinning is the most feasible and reproducible nanofiber fabrication technique, which is less expensive, scalable and can be performed with any type of polymers.

There are works based on the fabrication of nanofibers using phase separation and self-assembly. For example, differentiation of mouse ES cell and MEF to osteoblast-like cells were studied using self-assembled peptide nanofibers, which also expressed osteopontin and collagen type I with high alkaline phosphatase activity and calcium phosphate mineralization. Smith et al. used phase separation method to form poly (L-lactic acid) (PLLA) nanofibrous matrices for osteogenic differentiation of both mouse and human ES cells and compared this with the 2D flat films and 3D solid-wall scaffolds. It showed the importance of nanofibrous architecture in promoting osteogenic differentiation (35, 106, 110, 111).

Hence nanofibers hold promising applications in the cardiac tissue regeneration and the nanofiber production technique called electrospinning is commonly used for the fabrication of nonwoven fibers.

1.6. Electrospinning for producing nanofibrous scaffolds

Electrospinning is the most widely used technique for the manufacture of ultra-fine polymer fibers (112). It has been widely used for various applications such as wound dressing, drug delivery applications and in the field of tissue engineering and regenerative medicine (113-

117). This old technique was first observed in 1897 by Rayleigh, and a detailed study on this technique was done by Zeleny (1914) and patented by Formhals in 1934. The work of Taylor (1969) on electrically driven jets has laid the groundwork for electrospinning. It is believed that the term “electrospinning”, is derived from “electrostatic spinning” since it uses electrostatic forces to produce ultrafine fibers ranging from nanometre scale to micrometre. (118, 119). It consists of a high voltage power supply in the range of several tens of kVs to generate the electrospinning. This voltage is essential to inject charge to the polymer solution and is accelerated towards the collector plate having opposite charge. The collector can be either static or rotating mandrel. In most of the spinning setups, the collector is usually a metal screen or plate (119). Also, it has a pipette tip known as spinneret to eject the polymer solution to the collector. Currently, there exist two different methods for electrospinning, vertical and horizontal. With the advancement of technologies, more sophisticated spinning techniques have been introduced and used by various research groups which can form more complex nanofibrous structures in a controllable and efficient way (119, 120) (121-123). The polymers are dissolved in appropriate solvents before spinning, and the polymer solution is then introduced to the spinneret. The high voltage supply can create a charge on the polymer solution, and when it reaches a critical value, the electrostatic force of the solution overcomes the surface tension, and Taylor cone is formed. Eventually, a charged polymer jet is ejected from the tip of the Taylor cone and is collected on the collector which is positioned at a specific distance from the spinneret. This creates an unstable and rapid whipping of the jet in the space between the tip and collector, which leads to evaporation of the solvent (124-126). The diagram of the conventional electrospinning technique is shown in figure.1.11.

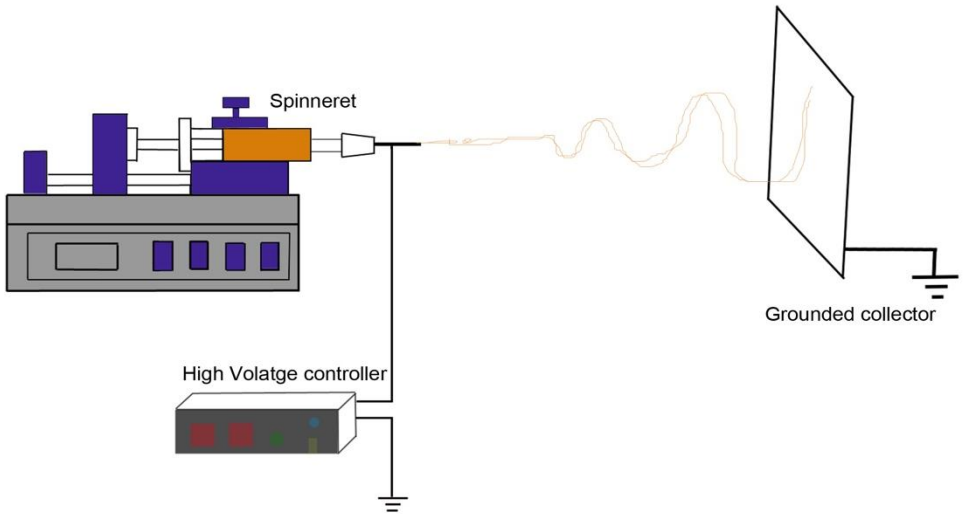

Figure**. 1.11**. Schematic representation of the conventional electrospinning technique.

1.6.1. Principle of electrospinning

There are three stages involved in the process of electrospinning, namely jet initiation, propagation and termination. In the first stage, the ejection of polymer solution occurs by forming a spinning jet from the spinneret. In the second stage, the polymer jet acquires a smooth stretching due to the applied electrical forces. In the final step, jet undergoes splitting and whipping instability, making it travel in a helical path until they are stopped by the collector (120). These three stages are briefly explained below.

1.6.1.1. Jet initiation

The polymer solution taken in a needle forms a droplet at the tip of the spinneret and remains in equilibrium because of the gravitational force and surface tension acting on it, and this prevents the solution from flowing out of the spinneret (127). When a high voltage is applied, the polymer solution attains a charge, and these charges get accumulate at the droplet surface. This causes the surface to be pulled into the shape of '*a section of the sphere'*. At a particular point, the electrical force overcomes the force of surface tension, and the meniscus bulges out;

hence, charges get accumulated on the protruding part of the meniscus (128). Further accumulation of charges on the meniscus causes the meniscus to be pulled out in the shape of a cone – "Taylor cone", which was mathematically reported by Taylor (124).When the applied voltage attains a threshold value, the electric force exceeds the surface tension, and a fine jet of the fluid is pulled out from the spinneret tip.

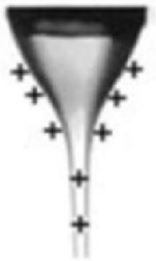

Figure**.1.12**. Schematic representation of Taylor cone formation and the charge accumulation at the surface (129).

1.6.1.2. Jet propagation

During the jet propagation, the diameter of the jet decreases with increase in length while the total mass per unit time remains the same at any point in the Z axis (130). Under this condition, the velocity of this polymer jet surpasses the speed of sound in air (131). The elongation of the polymer jet and evaporation of solvent results in the further reduction in the diameter of the spinning jet. Hence jet elongation is initiated by electric forces and gravitational forces, which is counter-balanced by viscosity, surface tension, and inertia (132).

1.6.1.3. Jet termination

The jet elongation results in the process of jet thinning, and according to Feng, this generates a fluctuation in the surface charge density, which alters the electric field and increases the viscosity. This results in the deceleration of the jet along the straight path. The viscous

resistance continues to grow as the jet undergoes a steady acceleration under the influence of electrical force. At a certain point, the jet experiences instability when the viscous resistance defeats the electrical force and even a slight perturbation caused by air may result in oscillations (131). The electrospun nanofibers remain charged throughout the flight and travel down the stream until they deposit on the collector as randomly oriented nanofibers in the form of nonwoven mats. It has also been reported that the deposited nanofibers have a tendency to repel the incoming fibres due to the force of repulsion (125). Moreover, the nanofibers form as coils or loops if the nanofibers are deposited onto the collector is at higher velocity (133). For the successful deposition and overlapping of fibers, it is essential for the fibres to have a random orientation.

1.6.2. Parameters involved in the electrospinning process

The process of electrospinning is controlled by many parameters which are widely categorized into solution parameters, process parameters, and ambient parameters. Viscosity, conductivity, molecular weight, and surface tension are the solution parameters. Process parameters include applied voltage, tip target distance and flow rate. All these parameters drastically affect the fibre morphology, and thus, proper optimization of these parameters can yield nanofibers of required morphology and diameter (134). The effect of each parameter on fibre diameter and morphology have been briefly explained in table 1.2.

Table **1.2**. Details of processing parameters which influence the electrospinning process (119).

Parameters	Effect of fiber morphology
Polymer Concentration	Increase in fiber diameter with increase in polymer concentration
Viscosity	High viscosity-Increase in fiber diameter and absence of beads Low viscosity-Appearance of beads
Conductivity	Increase in conductivity reduces the fiber diameter
Molecular weight	Absence of beads and droplets with increase in molecular weight
Surface tension	No conclusive evidence that link with fiber morphology, but as surface tension increases the jet instability also increases
Applied voltage	Increase in voltage reduces the fiber diameter
Tip target distance	Increase in tip target distance reduces the fiber diameter Change for bead formation if the distance is too large or too small
Flow rate	Decrease in flow rate decreases the fiber diameter
Humidity	Formation of circular pores if the humidity is high
Temperature	Increase in temperature decreases the fiber diameter

1.7. Gelatin for electrospinning

The polymer used in this study is gelatin, which is a naturally occurring polymer. Gelatin is widely used in the field of tissue engineering as it occurs abundantly and is less expensive. It is the hydrolysed form of collagen; hence, it is the most suitable polymer for mimicking the ECM. Ideally, the ECM should be biocompatible, nontoxic and biodegradable to be used as a right candidate for tissue engineering and regeneration applications. Gelatin favours all these

properties which enable this material as a good choice for mimicking the ECM (135-137). The structure of gelatin is shown in figure.1.13.

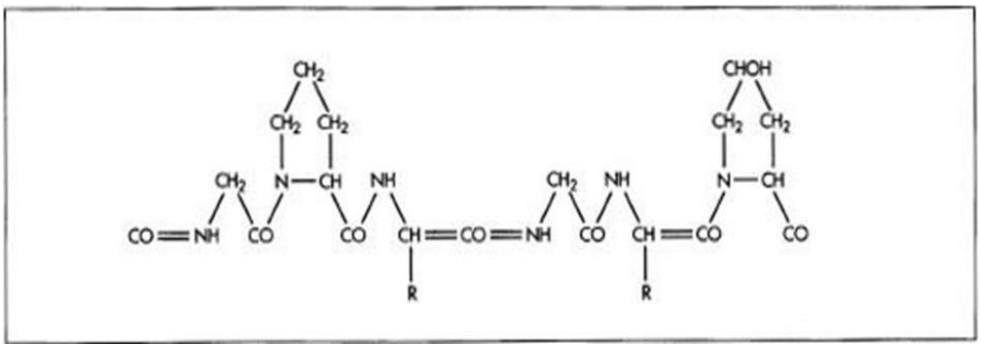

Figure.**1.13.** Structure of gelatin (adapted from http://www.madehow.com/Volume-5/Gelatin.html)

One of the unique properties of the gelatin is its temperature dependent cross-linking ability. The gelation temperature of gelatin is at 40°C in a water solvent. Hence to aid electrospinning in aqueous solution, it is necessary to overcome this characteristic feature of gelatin. In most of the electrospinning experiments, gelatin is electrospun using organic solvents, which is expensive, and toxic. This challenge was approached by setting up the whole electrospinning apparatus in an enclosed incubator with facilities to raise the temperature and humidity, which assisted the successful electrospinning of gelatin nanofibers in a pure water solvent. Further details regarding the novelty of the electrospinning technique used in this work are explained in the Results and Discussions section.

1.7.1. Cross-linking of gelatin

The term cross-linking refers to the “linking of polymer chains” to enhance the physical and mechanical properties of polymers. Since the polymer used in this study is gelatin, which is readily soluble in water, it should be cross-linked physically or chemically to retain its structure to be used in cell culture studies. There are different cross-linking methods such as physical

and chemical processes by which the water resistance and the mechanical properties of the nanofibers can be increased (138). The physical processes include dehydrothermal (DHT) treatment and plasma treatment or UV irradiation, which is less efficient in cross-linking gelatin nanofibers because the cross-linking occurs only on the surface of the gelatin. Hence, chemical cross-linking is the most widely used method for cross-linking gelatin nanofibers. This includes 1-ethyl-3-(3-dimethylaminopropyl) carbodiimide hydrochloride/Sulfo-NHS (N-hydroxysulfosuccinimide (EDC/NHS) and glutaraldehyde (GA) vapour cross-linking, which can cross-link the entire material rather than on the surfaces alone (139, 140).

DHT treatment is the process of applying a high temperature of above 98°C under vacuum. This results in the evaporation of water molecules and leads to the formation of intermolecular crosslinks through condensation reactions. It has been widely used for the stabilization of collagen scaffolds and natural biopolymers for the enhanced mechanical properties and reduced degradation rates. It has also been reported that DHT treated collagen fibers supported cell proliferation and tissue formation. Another advantage of DHT treatment is that it does not involve the use of toxic chemical reagents and provide biocompatibility (141-143).

1.7.1.1. EDC/NHS Cross-linking

EDC/NHS facilitates the activation of carboxylic acid residues of aspartic and glutamic acid on gelatin and reacts with the free amino groups of EDCs to form O-acylisourea intermediate residues. NHS acts as a catalyst to carry out this reaction process by reacting with the activated carboxylic acid groups and forms NHS-activated, a carboxylic acid group which in turn reacts with the amine groups in the lysine residues of gelatin to form amide bonds (Figure.1.14). Compared to GA cross-linking, EDC/NHS is less toxic, and there is evidence to support the cell viability and proliferation on EDC/NHS cross-linked scaffolds (144, 145).

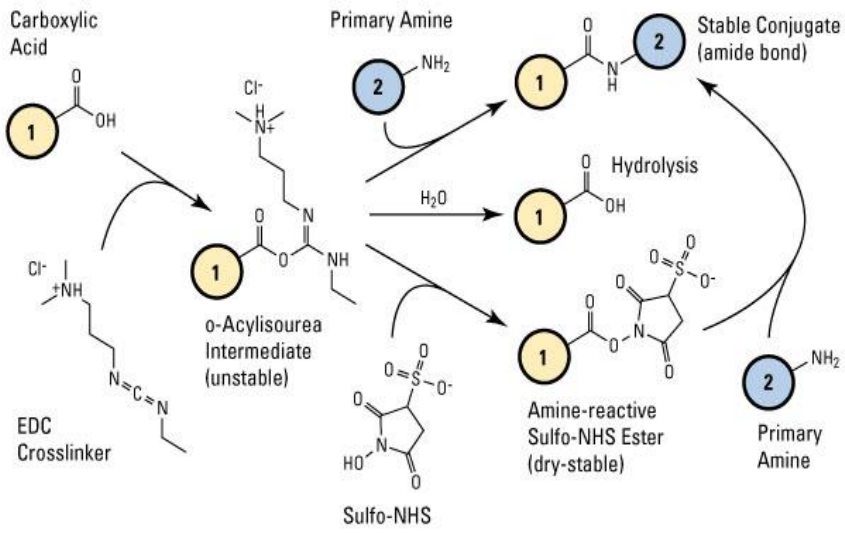

Figure.**1.14.** Diagram illustrating EDC/NHS cross-linking mechanism (adapted from https://www.thermofisher.com/uk/)

1.7.1.2. Glutaraldehyde cross-linking

The aldehyde group of glutaraldehyde reacts with the amino groups of lysine residues in gelatin to form aldimine linkages, as shown in figure.1.15. Even though GA is toxic to the cells, small amounts of GA is found to be nontoxic and proper pre-treatment, and sterilization steps must be done to remove the uncross-linked GA from the scaffolds. Among the chemical cross-linkers, GA is the most efficient method of cross-linking since it can cross-link not only molecules that are close to each other but also the molecules that are separated by a distance. It has been reported that GA cross-linking enhanced the strength of gelatin by two-fold and created a gelatin electrospun membrane which is insoluble in water (146, 147).

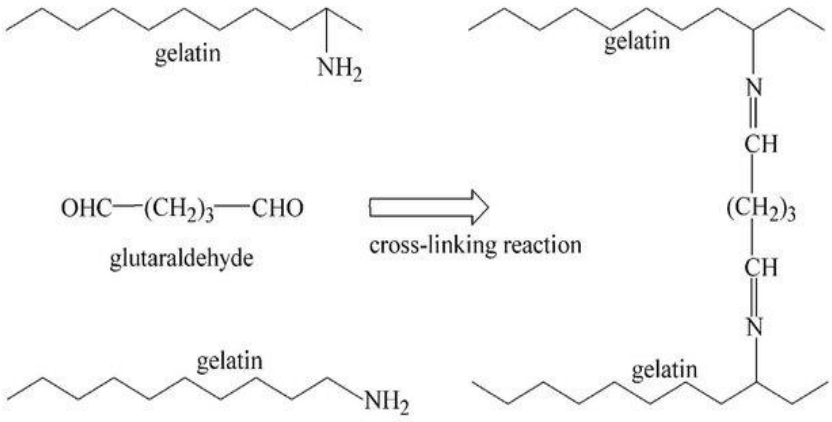

Figure.**1.15**. Cross-linking mechanism of glutaraldehyde (148)

In 2010, R.Juthamas *et al*. reported that the structure and cross-linking degrees were different for physical and chemical cross-linked gelatin nanofibers. The DHT or plasma treated gelatin nanofibers showed a low cross-linking degree but retained the original structure of fiber mats. When the mats were cross-linked with DHT method followed by EDC/NHS, the cross-linking degrees were high, but the fibers were interconnected with swollen morphology. The DHT and GA vapour treated nanofibers were merged without interconnected pores. This result shows the importance of choosing the correct cross-linking method and the effects of these methods in controlling the structure, morphology and degradation of the material (149).

1.7.2. *In situ* cross-linking method

Previous works have reported the inefficiency of DHT and EDC/NHS treatment methods in maintaining the nanofibrous structure. This could preclude the use of scaffolds for tissue/cell engineering applications in the wet condition (150). So, a different cross-linking methodology was introduced recently with the aim of cross-linking nanofibers internally during electrospinning. This process is called *in situ* cross-linking by which the fibers can be cross-linked internally and results in high cross-linking degree with an adequate amount of cross-linker (151).

There were studies which utilized *in situ* cross-linking methods to fabricate nanofibers such as PVA, gelatin, alginate/PVA, PNIPAM/gelatin etc. (151-153). But all these works were done by the direct mixing of polymer solution with a cross-linking agent just before the time of spinning. In this work, a recently modified technique of electrospinning with a double-barrel syringe so that the amount of cross-linking agent added can be minimized with an efficient cross-linking degree is used. In 2015, A. P. Kishan *et al*., first studied the *in situ* cross-linking of gelatin using double-barrel syringe to produce electrospun fibers with improved fiber morphology, stability and tunable degradation rates (97).

This study employs both *in situ* cross-linking, and external crosslinking with Glu vapour with the aim of retaining the fibrous structure of gelatin nanofibers for the stem cell adhesion, proliferation and differentiation.

1.8. AIM AND OBJECTIVES OF THIS WORK

The first objective of the work in this thesis was, to use an *in situ* electrospinning technique to fabricate non-woven and internally cross-linked nanofibrous materials consisting of gelatin, in aqueous solution with varying matrix stiffness.

The second objective of this work was to examine the CPs viability, antigenic profile, proliferation, morphology, angiocrine activity and differentiation potential by incorporating CPs on scaffolds with different matrix stiffness.

2. MATERIALS AND METHODS

All solutions were prepared in the laboratory conditions at a temperature of 19-25°C and relative humidity of 35-70%. The details of the gelatin polymer used for the preparation of gelatin solutions are mentioned below. Gelatin was used as supplied by the manufacturers (Sigma Aldrich, Cat. no. - G2500).

2.1. FABRICATION OF GELATIN NANOFIBROUS SCAFFOLD

2.1.1. Gelatin solution preparation

The gelatin solution for electrospinning was prepared by dissolving 10% and 15% of gelatin in distilled water. The solution was heated above 35°C and was stirred continuously for the homogeneous mixing of gelatin in water. Gelatin from porcine skin (Type A) with a bloom number of 300 which denotes the gel strength of the polymer was purchased from Sigma Life Sciences UK and was used for the entire study.

2.1.2. Electrospinning of gelatin nanofibers

The gelatin nanofibers were fabricated using the electrospinning technique in a controlled temperature and humidity. The details of the electrospinning equipment are listed in Table 3.1. The electrospinning setup consisted of a high voltage supply, spinneret and a grounded collector. In addition to this, a hot plate, and an ultrasonic nebuliser were also used to control the temperature above 40°C and humidity above 60% respectively. The whole setup was placed in a closed incubator to which a thermostat is attached for maintaining the heat and humidity. The image of the electrospinning setup used in the fabrication of gelatin nanofibrous scaffold is shown in figure 2.1.

Table **2.1.** Details of apparatus used in the electrospinning technique.

Label	Equipment	Details	Supplier/Manufacturer
1	Power Supply	EL Series (1-30 kV)	Glassman High Voltage Inc.
2	Syringe Pump	PHD 2000 Infusion pump	Harvard Apparatus
3	Syringes	10 ml Plastipak™	Becton Dickinson
4	Needles	Flat-ended stainless steel	Becton Dickinson
5	Hot Plate	IKA™ RH basic 2	Fisher Scientific
6	Thermostat Incubator	Stuart thermostat incubator	Stuart
7	Ultrasonic Nebuliser	Omron NE-U12	Omron

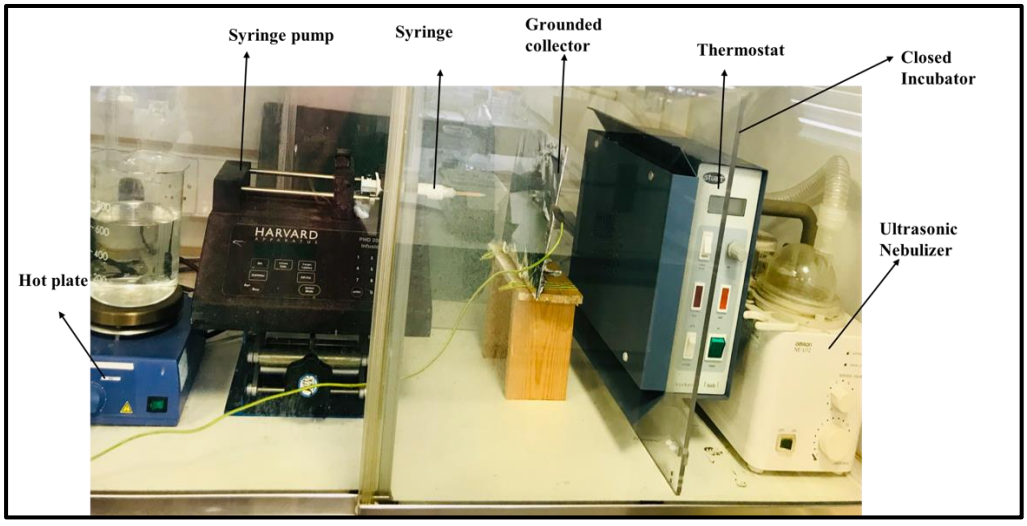

Figure **2.1**. Electrospinning set-up used for producing gelatin nanofibers.

The gelatin solution was taken in a syringe (10 ml) fitted with a needle (21G) and was mounted on the spinneret. Initially, electrospinning was carried out with different concentrations of gelatin, and the electrospinning parameters were varied according to the concentration of solutions being spun. The duration of electrospinning was dependent on the requirements of the investigation. The solutions were electrospun for 4 hours, in order to obtain a sufficient thickness to peel off the nanofibrous membranes from the aluminium foil. For SEM analysis, the gelatin solution was electrospun for 30 minutes. AFM preparation only required the electrospinning of fibres for less than 1 minute. The fabricated nanofibrous scaffolds were stored in a desiccator until they were used and were cut into the needed shapes using a scalpel.

2.2 FABRICATION OF *IN SITU* CROSS-LINKED GELATIN NANOFIBERS (CLGS)

2.2.1. Solution preparation for the fabrication of CLGS

All solutions were prepared in the laboratory conditions at a temperature of 19-25°C and relative humidity of 35-70%. The details of the gelatin polymer used for the preparation of gelatin solutions and EDC/NHS are mentioned below. Gelatin (Sigma Aldrich, Cat. no. - G2500) and EDC/NHS (Thermo Fischer Scientific UK Ltd. Cat. no. - NHS-2451 and EDC-22980) was used as supplied by the manufacturers.

The optimised gelatin concentration of 15% (wt/vol) was used in the fabrication of CLGS. EDC/NHS solution was used for the *in situ* cross-linking of gelatin nanofibers. The concentrations of 14mM EDC and 5.5mM NHS were prepared in absolute ethanol (139). The final pH of the prepared solution was 6.5. Both EDC and NHS were obtained from Life Technologies Ltd, UK and absolute ethanol were supplied by Fisher Scientific UK Ltd.

2.2.2. Solution characterisation

The rheological characterisation of gelatin solution and gelatin solutions with different cross-linking concentrations (2X, 5X and 8X (X=14mM EDC and 5.5mM NHS)) were performed by using a Bohlin Gemini Rheometer (Malvern Instruments Ltd.). Viscosity measurements were performed by using a cone-plate configuration. Details of the parameters used for the investigation are given in table 2.2.

The solutions were loaded on the base plate of the rheometer by avoiding the incorporation of bubbles, and the geometry was lowered. A solvent trap was also used, and the excess solution was wiped out before starting the test.

Table **2.2.** Details of the parameters used in viscometry measurements of gelatin and gelatin solutions with different cross-linking densities.

Viscometry Parameters	**Details**
Geometry	CP/40:4° cone angle, 40 mm in diameter
Shear rates	0.1 – 10 s^{-1}
Mode of measurement	Controlled rate

2.2.3. Electrospinning of CLGS

The *in situ* cross-linking of gelatin nanofibers were achieved by using a double-barrel syringe (10:1) which was purchased from Sulzer Chemtech UK Ltd. Initially, electrospinning was executed with four different cross-linking densities of EDC/NHS (denoted as 2X, 5X, 8X and

10X, X= 14mM of EDC and 5.5mM of NHS) to fabricate gelatin nanofibrous scaffolds with different matrix stiffness. The electrospinning was accomplished by maintaining the concentration of gelatin and distance between the needle and collector constant. The other parameters, such as voltage and flow rate of the solution, were changed accordingly to get nanofibers without any beads.

The gelatin solution was loaded in the largest barrel, and the second barrel was filled with EDC/NHS cross-linking solution. Both were fed at a fixed rate so that they reach the needle at the same time and mix inside the needle before getting ejected to the collector. The mixing was attained with the help of mixing heads attached to the syringe, and a high voltage was applied to the solution. The polymer jet formation was achieved when the surface tension of the solution overcome the applied voltage. Thus, randomly oriented, internally cross-linked, gelatin nanofibers were deposited on the grounded collector, which was kept at a fixed distance from the needle tip. The schematic representation of electrospinning set up is shown in figure.2.2. The fabricated nanofibrous scaffolds were stored in a desiccator until they were used and were cut into the required shapes using a scalpel for further studies.

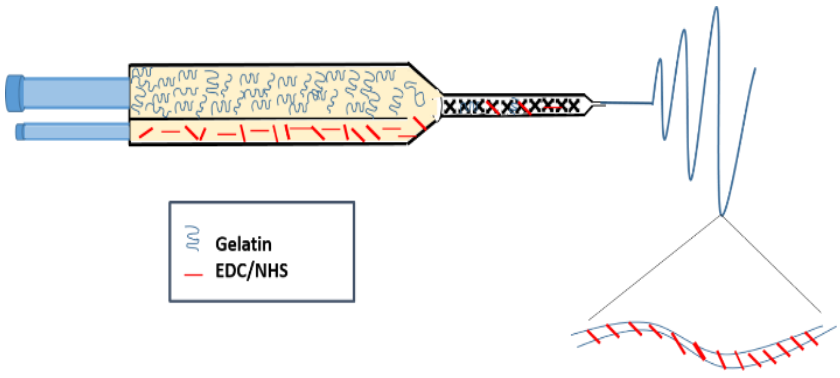

Figure.**2.2**. Schematic representation of double-barrel syringe for *in situ* cross-linked gelatin nanofibers during electrospinning.

2.3 CHARACTERISATION OF CLGS

2.3.1. Scanning electron microscope (SEM) analysis

The structural morphology of gelatin nanofibers was analysed using SEM (JEOL IT300). The nanofibers were spun on an aluminium foil for 30 minutes and were cut into small pieces. They were fixed on aluminium stubs (12mm) with sticky carbon tapes for observation. All the samples were sputter coated with the silver of thickness 15nm using the sputter coater (SC7620, Quorum Technologies, East Grinstead, UK), and were imaged at various magnifications. After SEM analysis, the measurement of electrospun fibre diameters was performed by using Image J, and the average fiber diameter of each scaffold was quantified.

2.3.2. Atomic force microscopy (AFM) analysis

The 3D morphological analysis of the scaffolds was also carried out by using a Multi-mode VIII AFM with Nanoscope V controller. The fibers were spun on an aluminium foil for few seconds to make the fibres less dense and were cut into small pieces using an 8 mm diameter sterile biopsy punch. The microscope uses a non-resonant, Peak Force feedback control mechanism. In Peak Force control, an approach force curve was collected as the AFM tip interacts with the sample. From this, the force applied to the sample by the tip was measured. A force level was selected as a set-point value for the feedback; this is the level of force that will always be applied to the sample. A curve is taken over each pixel of the image, and the approach halted when the set-point value is reached. In this way, the amount of force applied to the sample remains constant across the entire image. An additional benefit to this is that the force curve can be used to measure specific properties of the sample, which is more common tapping mode is just inferred from phase changes in the resonant cantilever. In these experiments, cantilevers with typical spring constants in the range of 40 N/m, namely SCOUT

cantilevers [NuNano, Bristol, UK] and RTESPA cantilevers [Bruker, CA, USA] were utilized. The tip width was less than 5nm, and the scanning speed very slow at a rate of 0.25 Hz.

2.3.3. Degradation test

The CLGS were cut into small pieces (2cmx2cm) using a scalpel. Each of these scaffolds was then placed in a Petri-plate containing 5 ml of Phosphate Buffer Saline (PBS). A pH of 7.4 was used to mimic the human body conditions. The solubility of the samples was measured after two weeks and three weeks of immersion. The samples were taken out at different time points (14 days and 21 days) and were air-dried before imaging.

Later, the SEM images were taken to analyse the stability of nanofibrous scaffolds after immersed in PBS for two weeks and three weeks. All the samples were fixed on aluminium stubs with sticky carbon tapes and were silver coated (15 nm) before performing the SEM imaging. The fiber diameter of the hydrated nanofibers was also measured using Image J.

The CLGS were further chemically cross-linked in the glutaraldehyde (5%) vapour at room temperature by placing the scaffolds in a desiccator. The glutaraldehyde solution (5ml) was poured at the bottom of the desiccator and kept for 24 hrs at room temperature to occur cross-linking. After cross-linking, the samples were exposed in a fume hood for 2 hrs and heat treated at 100°C for 1 hr to remove the residuals of glutaraldehyde and to partially enhance the cross-linking (154).

2.3.4. Fourier transform infrared (FTIR) spectroscopy analysis

FTIR analysis was carried out to confirm the cross-linking ability of EDC/NHS and Glu. For this, the electrospun nanofibrous scaffolds were peeled off from the aluminium substrate, and

2mg of all the samples (pure gelatin, Glu alone treated gelatin and Glu and EDC/NHS cross-linked gelatin nanofibers) were weighed. The spectrum analysis was measured in the frequency range of 500 to 4000 cm^{-1}

2.3.5. Ninhydrin assay

The cross-linking degree of the CLGS was measured by using a UV-Visible Spectrophotometer (U-1900: Hitachi, Tokyo, Japan). Each scaffold with different cross-linking densities of EDC/NHS (2X, 5X, 8X) and Glu/EDC/NHS cross-linked gelatin scaffolds, were cut into small pieces without the aluminium foil. All samples were weighed 10mg before starting the experiment. Later, 2 ml of the ninhydrin solution (0.3M) was taken in four test tubes, and each of the samples was added to the test tubes. The test tubes were heat-treated at 95 °C for 5 minutes (155, 156). Afterwards, 100µl of ninhydrin solution from each test tubes were taken to measure the absorbance. Ethanol was added to these solutions before measurements, and the absorbance was taken at 570nm. The degree of cross-linking was calculated by the formula,

$$\text{Cross-linking index (\%)} = (Cb\text{-}Ca)/Cb \times 100$$

where Ca – Absorbance after cross-linking and Cb – Absorbance before cross-linking

Glycine at various known concentrations was used as standard (157). All the samples were triplicated for the experiment.

2.3.6. Mechanical testing

All scaffolds (pure gelatin, 2X, 5X and 8X CLGS, cross-linked with both EDC/NHS and Glu) were mechanically tested using an Instron testing machine (Cat. no.-2752 006). The mechanical testing was performed at two different conditions, i.e., at the dry and wet state of the scaffolds. The samples were cut into rectangular pieces of dimensions 10±5 mm in length,

5±3 mm in width and 100±50 µm in thickness, respectively. The length, breadth and thickness measurements were acquired by using Vernier callipers. Since the wet samples were difficult to handle, they were placed on an aluminium foil for measuring the thickness. Later, the thickness of the aluminium foil was subtracted from the total thickness to get the width of wet samples. All samples were triplicated, and measurements were taken without aluminium foil substrate. Six measurements were taken at different positions of the scaffolds and mean averages were calculated.

The instrument consisted of a pressure pump, a chamber to fill the water and a thermostat to set the temperature. It was also equipped with a gripping system to which the scaffolds were held for testing. The testing machine was connected to the data acquisition software called 'Bluehill-3'. The chamber was filled with tap water, and the temperature was set at 37°C. Both ends of the samples were attached to a custom-made gripping system which was connected to the mechanical testing device (Figure 2.3). A strain rate of 1mm/min was applied to the scaffolds until failure, and the stress-strain curves were derived from the force-displacement data. The elastic modulus/stiffness of the fibers was evaluated from the slope of the first linear portion of the stress-strain curve. The mechanical testing of the scaffolds under wet conditions was performed by immersing the samples in a chamber containing water at 37ºC. The tensile strength of the scaffolds was also measured from the obtained values.

Figure.**2.3.** Images of dry and wet scaffolds held between the grips of a mechanical testing machine.

2.4. *IN VITRO* CELL STUDIES

2.4.1. Ethics

Studies comply with the principles stated in the Declaration of Helsinki. The protocol for collection of cardiac leftovers from patients undergoing corrective surgery of congenital heart disease was approved by the North Somerset and South Bristol Research Ethics Committee (REC reference 15/LO/1064). Paediatric patients' custodians gave written informed consent for inclusion in the study. The pathology and characteristics of tissue donors used in this work are listed in table.2.3.

Table **2.3.** Clinical characteristics of tissue donors used in the study. The numbers 10, 11, 12 and 32 represents different donors.

Cells Used	Age	Source	Pathology
CP10	17 months	Right Ventricle	Tetralogy of Fallot (TOF)
CP11	Three years	Right Atrium	Atrioventricular Canal Septal Defect
CP12	Three years	Right Ventricle	Atrioventricular Canal Septal Defect
CP32	Three years	Right Atrium	Mitral Valve Defect

To investigate the effect of matrix stiffness on stem cell fate, the CPs were seeded on scaffolds with different cross-linking densities. Various assays such as viability, immunocytochemistry, cell attachment, proliferation, ELISA and differentiation assays were performed to analyse, how the cells are behaving on these substrates in terms of its adhesion, proliferation and differentiation into cardiac specific lineages.

All scaffolds were cut into round pieces of 8mm diameter using accupuch and sterilised before cell seeding. The accupunch is a skin biopsy punch supplied by Schuco International (London) Limited. All experiments were carried out in 48 well plates (CELLSTAR®) except the ELISA test. For ELISA, 96 well plates (R&D Systems) specially designed for ELISA test was used. All scaffolds were immobilised in 48 well plates using Cell Crowns (Sigma Aldrich) before the sterilisation process. The sterilisation was achieved by soaking the scaffolds in ethanol (70%) for 20 minutes and washing with PBS twice. Later the scaffolds were placed under UV light for 30 minutes. After drying, the scaffolds were immersed in ECGM2 media (Promocell) supplemented with 2% FBS for overnight to pre-condition the scaffolds. Pre-conditioning also helps to remove the uncross-linked glutaraldehyde residues from the scaffolds. Next day, each

well was seeded with 20,000 cells. The CPs three donors were used in all the following *in vitro* assays except the viability assay, and all the scaffolds were duplicated for this study. Cells from four donors were used for performing viability assay to attain a statistical significance. The four cell lines used were denoted as CP10, CP11, CP12 and CP32.

2.4.2. Isolation and expansion of CPs and cell culture

The isolation of CPs was accomplished, as described by Avolio *et al.* (21). Briefly, the surgical leftovers of atrium or ventricle specimens from children having congenital heart defects were taken and washed with PBS. All the specimens were 3 to 5 mm in length and <100 mg in weight. After PBS wash, they were manually minced, and the tissue suspension was incubated for 30 minutes with 0.45 WU/mL/g Liberase 2 (Roche Technologies, UK). The minced cell suspension was passed through 70, 40, and 30 μm cell strainers subsequently to obtain a single cell suspension. Endothelial cells were separated using anti-CD31 (Miltenyi Biotech) conjugated beads, following the manufacturer's instructions. From the remaining cells, CD34+ cells were separated by anti-CD34 beads (Miltenyi Biotech). Hence, these obtained cells were cultured in the presence of ECGM2 medium supplemented with 2% fetal bovine serum (FBS). When the cells were 80% confluent, they were passaged to new culture dishes, and frozen stocks were generated for the experiments. The frozen vials were stored initially in -80°C and later they were transferred to liquid nitrogen. Trypsin-EDTA (Life Technologies, UK) was utilised to detach cells from the growth substrate.

As required, the frozen cryovials were taken from liquid nitrogen, and the cells were thawed. For this, the cell suspension was kept in a water bath at 37°C for 1 min. They were then transferred immediately to pre-warmed 5ml of ECGM2 media taken in a 15 ml falcon tube. The centrifugation was carried out at 400xg for 10 min. After this, the cells were resuspended with 1 ml of ECGM2 media without any cell aggregates. They were then seeded to 2 T25 flasks

by adding 5ml of media in each T25. The T25 flasks were incubated at 37°C until they become confluent. When they are confluent, the cells were split and used for further cell studies.

The 80% confluent T25 flasks were taken out of the incubator, and the media was removed. A PBS wash was done, and 2 ml of trypsin (1X trypsin in PBS) was added to detach the cells. After incubation at 37°C for a few mins, the flask was viewed under a microscope to check the detachment of cells. After ensuring all cells were detached, the trypsinisation process was stopped by adding the blocking solution. The blocking solution was prepared by adding 5% of FBS in PBS. This media, along with the cells, were transferred to a falcon tube and centrifuged at 400xg for 10 min. After centrifugation, the cells were resuspended, and the cells were counted. Usually, there should be 700,000-1million CP cells in a confluent T25 flask.

Cell counting was performed using a Burker Counting Chamber. Briefly, 10 µl of cell suspension was diluted with 10 µl of Trypan Blue (Life Technologies). Trypan blue can stain the dead cells in blue colour. The cells were counted in all the four squares, excluding Trypan blue positive cells. The average number of cells was calculated, and the required number of cells/ml was also calculated by the formula,

$$\text{Number of cell/ml} = \text{Average number of cell} \times 10000 \times 2$$

(2 is the dilution factor with Trypan Blue).

Each well was added 500 µl of media and the scaffolds were seeded with 20,000 cells/well. For this, according to the number of scaffolds, the media required was also calculated and added to each well accordingly.

2.4.3. Characterisation of CPs

The isolated CPs were characterised by immunocytochemistry (ICC) assay to assess the cells are expressing their characteristics features. For this, the CPs were seeded on eight-chamber slides at a density of 8,000 cells/cm^2 . The primary antibodies Vimentin, neural/glial antigen 2 (NG2) and octamer-binding transcription factor 4 (OCT4) were used for the ICC assay. The details of dilution factor, primary and secondary antibodies etc. are listed in table.2.4. All three cell cultures (CP10, CP11 and CP12) were stained with each marker to do ICC assay.

Table **2.4.** The details of antibodies used for the ICC assay.

Primary Antibody	TritonX	Supplier	Dilution	Secondary Antibody
Vimentin	Yes	Abcam	1:400	Alexa Fluor 647 Goat anti-Rb
NG2	Yes	Abcam	1:100	Alexa Fluor 647 Goat anti-Rb
OCT4	Yes	Abcam	1:400	Alexa Fluor 647 Goat anti-Rb

To perform ICC, the cells seeded on eight-chamber slides were taken after two days of incubation, and they were fixed and permeabilised. The cell fixation was done by treating the cells with 4% paraformaldehyde (PFA) for 15 min at room temperature after a PBS wash. This was done under a chemical hood to avoid the possible hazards of using toxic PFA. Later, PFA was removed, and the cells were washed with PBS twice. They were stored at 4°C until the ICC staining is done, but not more than five days as the cells may detach from the scaffolds. The cells were maintained in a wet condition, and when required, the cells were taken out of the fridge, and permeabilisation was carried out. Permeabilisation was carried out by treating the cells with 0.1% Triton (Sigma Aldrich) in PBS for 10 min at room temperature. After two times of PBS wash, the cells were blocked by adding the blocking solution for 30 min at room

temperature. By this time, the primary antibodies were prepared according to the dilution factor in blocking solution. Later, the cells were incubated with primary antibodies for overnight at 4°C. On the next day, secondary antibodies were added to cells after washing with PBS twice. After this, the cells were incubated at room temperature for 1 hour protected from light. The nucleus staining was carried out with Hoechst (1:10000) (Sigma Aldrich) for two min incubation in the dark. Later several PBS and distilled water wash, the cells were mounted with Fluoromount G (Biotium UK) until the imaging was done. Imaging was performed by fluorescent microscopy at 20X magnification.

2.4.4. Viability assay

The viability of CPs on CLGS was analysed by performing the live-dead assay. The scaffolds were first sterilised before seeding the cells as described above. After sterilisation, the scaffolds were seeded with 20,000 cells and incubated at 37°C. After two days, the confluency was checked, and staining was performed as per the manufacturer's protocol. For this, 2 ml of the media was added with 1µl of Calcein AM and 1 µl of Hoechst along with 4 µl of Ethidium homodimer III (EthDIII). This was followed by vortex, and 500 µl of the media was added to each well. Then it was incubated at 37°C for 30 min and viewed under Fluorescence microscope (Zeiss, model- AxioVert 200M). The viability assay kit was supplied by (Biotium, UK). For performing the assay, ECGM-2 basal media was used.

2.4.5. Immunocytochemistry (ICC) assay of CPs on scaffolds

Immunocytochemistry assay was performed to investigate whether CPs are maintaining their phenotypic characteristics and stemness when seeded on CLGS. The phenotypic markers Vimentin, NG2 and the stemness marker OCT4, were used for the ICC assay. The details of dilution factor, primary and secondary antibodies etc. are listed in table.2.4.

The scaffolds were cut into 8mm diameter using accupunch and were sterilised as described above. For each scaffold, duplicates were taken, and the same staining protocol for CPs characterisation was used. CPs seeded on 8 chamber slides were taken as a control for each cell line. The cell seeding density was 20,000 cells/well.

2.4.6. Cell adhesion studies

The cell attachment studies were carried out to compare the CPs shapes and morphology when they were seeded on CLGS with different matrix stiffness. For this, SEM was used to observe the morphologies of CPs on scaffolds after 7 days of incubation. The CPs seeded on plastic were used as the control.

The scaffolds were cut into small pieces of 8 mm in diameter and were sterilised. CPs were then seeded onto the scaffolds at a cell density of 20,000 cell/well. Media change was given in two days of the time interval to keep the cells alive. After 7 days of incubation, the CPs were fixed with 4 % PFA and dehydrated through a series of graded-ethanol solutions and air-dried. After that, they were fixed on aluminium stubs with sticky carbon tapes on it. They were silver coated in the vacuum with a thickness of 15nm and were examined under SEM. Backscattered electron detector was used for SEM analysis for better imaging.

2.4.7. Proliferation studies

The ability of the cells to proliferate on the CLGS were evaluated by using Click-iT® EdU (5-ethynyl-2´-deoxyuridine) Imaging Kits. The assay kit was supplied by Invitrogen. The scaffolds were cut into 8mm diameter, and sterilisation was done. The scaffolds were later seeded with 20,000 cells and incubated at 37°C. After two days, the cells were treated with EdU (Component A) along with the media. EdU stock solution was prepared by adding 2 ml of Dimethyl sulfoxide (DMSO, Component C). From this stock 1 µl was taken and mixed with

1ml of the ECGM2 media to prepare the working solution. The cells treated with Edu on plastic was considered as the positive control and the cells not treated with EdU on scaffolds were recognised as the negative control.

After four days of incubation, the media was removed, and the cells were fixed with 4% PFA and incubated at room temperature for 15 min. The cells were washed twice with 3% BSA (Bovine Serum Albumin) in PBS, and the permeabilisation step was carried out. For this, 0.5% Triton in PBS was added to each well and incubated at room temperature for 20 min. The permeabilisation buffer was removed, and the cells were again washed with 3% BSA in PBS. The EdU detection was performed by incubating the scaffolds with a reaction cocktail for 30 min at room temperature, protected from light. The reaction cocktail was prepared according to the manufacturer's instructions. The details of the ingredients added to make the reaction cocktail are listed in Table 2.5. The components were added in the same order as listed in the table, and the volume of each reagent was changed according to the number of wells.

Table **2.5.** Preparation of Click-iT® reaction cocktail for EdU detection.

Reaction Components	**Number of coverslips (10)**
1X Click-iT® reaction buffer (Component D)	4.3 ml
$CuSO_4$ (Component E)	200 µl
Alexa Fluor® azide (Component B)	12.5 µl
1X Reaction buffer additive (Component F)	500 µl
Total volume	5 ml

The working solution of Component D was prepared by transferring all the solution (4 ml) in the Component D bottle to 36 ml of deionised water. The Component F reaction additive buffer (1X) was attained by diluting the 10X additive reaction buffer in the ratio of 1: 10 in deionised water. This solution was made fresh and used on the same day. The 10X additive reaction buffer was obtained by adding 2 ml of deionised water to the vial and mixed well until it gets fully dissolved. The stock solution was stored at -20°C.

After 30 min of incubation, the reaction cocktail was removed, and the cells were washed twice with 3% BSA in PBS. For nuclear staining, Hoechst (Component G) (1:10000) in PBS was added to the scaffolds and incubated for two min followed by PBS wash and distilled water wash. Later, they were stored by adding glycerol until the imaging was done. Imaging was done in the Fluorescent microscopy at 20X magnification. The number of proliferating cells were found out using Image J software.

2.4.8. Enzyme-linked immunosorbent assay (ELISA) test

Protein secretion of CPs was analysed using ELISA by collecting the media after 48 hours of incubating the CPs on 2X, 5X and 8X CLGS. The quantities of Angiopoietin-1 (ANG-1), Angiopoietin-2 (ANG-2) and human vascular endothelial growth factor-A (VEGF-A) (R&D Systems, UK) were determined when CPs on scaffolds were exposed to the ECGM2 media. The scaffolds were cut into 8mm diameter using accupunch, and sterilisation was done. The scaffolds were later seeded with 20,000 cells and incubated at 37°C. After 48 hours, the cell culture media was collected and frozen for performing ELISA. The same protocol was used for performing ELISA for all proteins. The concentration of capture antibody, detection antibody and standard were changed accordingly for each protein based on the manufacturer's

protocol. Different concentrations of each protein were used as the standard according to the manufacturer's protocol. R&D Systems supplied the DuoSet Ancillary Reagent Kit for ELISA. Each kit contained 96 well microplates, plate sealers, substrate solution, stop solution and Reagent Diluent Concentrate 2.

For ANG-1, the standard graph was plotted with different concentrations of ANG-1. The concentrations used for this were 10,000, 5000, 2500, 1250, 625, 313,156 and 0 pg/ml. The higher concentration was prepared from the standard stock solution, and the other concentrations were made by serial dilution. Each concentration of protein was prepared in reagent diluent (1X). After obtaining the standard graph, the plate preparation was carried out. The concentration of each antibody used for the preparation of the stock solution and working solution of ANG-1are mentioned in table.2.6.

Table. **2.6.** Details of the antibodies used for the detection of ANG-1.

Description	**Stock Concentration**	**Working Concentration**
ANG-1 Capture Antibody	720 μg/ml	4 μg/ml
ANG-1 Detection Antibody	36 μg/ml	200 ng/ml
ANG-1 Standard	330 μg/ml	10,000 pg/ml

Firstly, the ELISA plate was prepared by adding 100 μl/well of the diluted capture antibody in PBS. The pate was sealed and incubated overnight at room temperature. Next day, the washing step was performed by adding 300 μl of wash buffer. The wash buffer was prepared by adding 0.05% Tween® 20 in PBS (pH 7.2-7.4). Three washes were done for each well, and the washing was done by using an auto washer (Thermo scientific). After the last wash, the

remaining wash buffer was removed by inverting the plate and blotting it against clean paper towels. It is because complete removal of the liquid at each step is essential for the proper performance of the assay. The plate was then blocked by adding 300 µl of Reagent Diluent to each well and incubated at room temperature for an hour. After the washing step, the sample addition was done. For this, 100 µl of each sample (culture media from 2X, 5X, 8X CLGS and plastic) and standards in Reagent Diluent was added to each well. The plate was then covered with an adhesive strip and incubated at room temperature for 2 hours, followed by the washing step. After this, 100 µl of detection antibody diluted in Reagent Diluent was added to the wells and kept at room temperature for 2 hours. The washing step was repeated after the incubation. The working solution of 100 µl Streptavidin-HRP (1:200) was added to each well and incubated at room temperature for 20 min in the dark, followed by the washing step.

Later, 100 µl of substrate solution was added to each well and incubated for 20 min at room temperature without placing the plate in direct sunlight. The substrate solution was prepared by adding 1:1 mixture of Colour Reagent A (H_2O_2) and Colour Reagent B (Tetramethyl Benzidine). This reaction was then stopped by adding 50 µl of stop solution to each well by gently tapping the plate to ensure thorough mixing. The optical density of each well was determined immediately by using a microplate reader (Opsys MR, DYNEX Technologies) set to 450nm and 570 nm. The readings obtained at 570 nm is subtracted from the readings obtained at 450nm to do the wavelength correction. This subtraction is done to correct the optical imperfections in the plate. The data were normalised for the number of cells at the end of the collection time.

The same procedure was used for performing the ELISA for ANG-2 and VEGF but with different concentrations of reagents. The standard graph for ANG-2 was plotted with the

different concentrations (6000 pg/ml, 3000 pg/ml, 1500 pg/ml, 750 pg/ml, 375 pg/ml, 188 pg/ml and 93.8 pg/ml) of ANG-2. The standard graph for VEGF was plotted with different concentrations (10000 pg/ml, 5000 pg/ml, 2500 pg/ml, 1250 pg/ml, 625 pg/ml, 313 pg/ml and 156pg/ml) of VEGF. The concentrations of capture antibody, detection antibody and standards used for ANG-2 and VEGF are given in table.2.7. and table.2.8. respectively.

Table. **2.7.** Details of the antibodies used for the detection of ANG-2.

Description	Stock Concentration	Working Concentration
ANG-2 Capture Antibody	180 μg/ml	1 μg/ml
ANG-2 Detection Antibody	90 μg/ml	500 ng/ml
ANG-2 Standard	170 ng/ml	6000 pg/ml

Table. **2.8.** Details of the antibodies used for the detection of VEGF-A.

Description	Stock Concentration	Working Concentration
VEGF Capture Antibody	120 μg/ml	1 μg/ml
VEGF Detection Antibody	6 μg/ml	100 ng/ml
VEGF Standard	120 ng/ml	2000 pg/ml

2.4.9. Differentiation Assay

In differentiation assay, CPs were exposed to inductive media to promote differentiation into vascular smooth muscle cells (VSMCs). The CPs on CLGS cultured in ECGM2 media was

used as the negative control. The CLGS were cut into 8mm diameter using accupunch, and sterilisation was done. The CPs (20,000/well) were seeded on the scaffolds and cultured in the ECGM2 media. After 48 hours, ECGM2 medium was substituted with ECGM2 medium added with 2ng/mL human Transforming growth factor beta 1 (TGF-β1, Pepro-Tech). The differentiation assay was performed at two different time points (7^{th} day and 14^{th} day) after adding the differentiation media. This media was replaced with fresh media every two days of the time interval.

At each time points, the scaffolds were taken, and the cells were fixed by treating the scaffolds with 4% paraformaldehyde (PFA) for 15 min at room temperature after a PBS wash. Later, PFA was removed, and the scaffolds were washed with PBS twice. The cells were permeabilised with 0.1% Triton (Sigma Aldrich) in PBS for 10 min at room temperature. After two times of PBS wash, the cells were blocked by adding the blocking solution for 30 min at room temperature. The staining was performed as same as for ICC and the primary antibodies Smooth Muscle (SM)-Calponin and Smooth Muscle alpha Actin (α-SMA) were used. The details of the antibodies used for the staining are listed in table.2.9.

Table**. 2.9.** The details of antibodies used for the differentiation assay.

Primary Antibody	**TritonX**	**Supplier**	**Dilution**	**Secondary Antibody**
Calponin	Yes	Abcam	1:100	Alexa Fluor 647 Goat anti-Rb
α-SMA	Yes	DAKO	1:100	Alexa Fluor 647 Goat anti-ms

After staining the scaffolds were stored in glycerol until the imaging was performed using Fluorescence microscopy at 20X magnification. To quantitatively assess the stress fibers formed by CPs on the scaffolds, the mean intensity of the stained images was measured using

Image J. For this, all stained images were converted into grey scale images and were white balanced for standardisation. The mean stress fiber intensity per cell was calculated by selecting different regions in the image and dividing the obtained intensity by the number of nuclei counted.

2.5. Statistical analysis

Each characterisation experiment was completed in triplicate. For cell studies, each scaffolds were duplicated and evaluated with CPs isolated from three different donors except for viability assay. For viability assay, the cells from four different donors were used. GraphPad Prism was used to perform the statistical analysis. The statistical significance was determined by the one-way ANOVA test, and a p-value of < 0.05 was considered as statistically significant. Data are expressed as the mean ± standard error of the mean (SEM).

3. RESULTS AND DISCUSSIONS I: FABRICATION AND CHARACTERISATION OF *IN SITU* CROSS-LINKED GELATIN NANOFIBROUS SCAFFOLDS (CLGS)

Nanofibrous scaffolds have been widely used for a variety of biomedical applications such as wound dressings, tissue engineering and drug delivery applications, because of their high surface-to-volume ratio, tunable physical and mechanical properties and their structural similarity to the ECM. Electrospinning is the most common method used for the fabrication of nanofibers. It has been used for decades for the synthesis of nanofibers using both natural and synthetic polymers (119). In this work, gelatin was used for electrospinning to obtain non-woven nanofibers.

As discussed in section 2.7, naturally derived gelatin has indicated to have potential applications in the field of tissue engineering and regenerative medicine. Its biological origin, biocompatibility and commercial availability make gelatin an ideal polymer for the tissue engineering applications (158). However, the electrospinnability of gelatin is poor due to the polyelectrolytic nature of gelatin. In addition, gelatin forms strong hydrogen bonds at room temperature, which in turn reduces the mobility of polymer chains (14). Hence for the successful electrospinning of gelatin, it is essential to have a suitable solvent to aid the process of electrospinning as electrospinnability is strongly dependent on polymer chain confirmations and entanglements (159).

In most of the studies, researchers have used high-polarity solvents such as 2,2,2, -trifluoroethanol (TFE), acetic acid and hexafluoroisopropanol (HFIP) for the electrospinning of gelatin polymer nanofibers (160-162). For example, in 2004, Huang *et al.* reported the use of TFE for the successful electrospinning of gelatin for the first time. They used gelatin solution

concentrations of 5 to 12.5% and successfully electrospun gelatin nanofibers of diameter ranging from 100 to 340 nm (162). Since the first report, there have been several other studies, where they used alternative organic solvents for electrospinning gelatin. These high-polarity solvents are required to break the cross-links between the polymer chains (139). But they are often expensive or toxic which adversely affect the biocompatibility of electrospun gelatin nanofibers. For this reason, the incorporation of organic solvents for the nanofiber synthesis is completely evaded as one of the objectives of this study was to fabricate biomimetic and biocompatible gelatin nanofibers. Therefore, an alternative cheap and biocompatible water solvent system is used for the electrospinning of gelatin nanofibers.

3.1. ELECTROSPINNING OF GELATIN NANOFIBERS IN AQUEOUS SOLUTION

A solvent has to perform two crucial roles in the process of electrospinning. Firstly, to dissolve the polymer molecules and secondly to carry those dissolved polymer molecules to the collector. From the literature, it has been found that it is impossible to spin gelatin in pure water solvent at room temperature, despite the fact that gelatin is water soluble. This is because of its polyelectrolytic characteristics and gelatin results in ionizable groups when it is dissolved in water [3-6]. Gelatin also exhibits a semi-solid gel at a temperature <40°C due to the formation of strong hydrogen bonds. This means the aqueous gelatin solution forms a gel at room temperature, which makes gelatin difficult to electrospin. Moreover, the slow evaporation rate of water adversely affects the electrospinning process by hindering the conversion of solution into dry nanofibers during the travel between the needle and collector (139). It is hypothesised that heating will inhibit the formation of gel and allows the gelatin solution to be electrospun at elevated temperature (119). In this work, the challenge of electrospinning gelatin in aqueous solution was accomplished by raising the temperature and humidity, and by keeping the whole

electrospinning setup in an enclosed incubator. The temperature was set above 40°C using a hot plate and humidity was maintained above 50% using an ultrasound nebuliser. This made the favourable conditions for electrospinning gelatin nanofibers in water solvent.

Temperature and humidity are the two environmental factors that significantly influence the electrospinnability of gelatin, particularly in aqueous solution. High temperature and humidity are crucial to prevent the gelation and successful formation of the spinning jet. There are also works stating the dependence of humidity in fiber morphology. In 2014, Li et al. studied the influence of relative humidity on the morphology of gelatin nanofibers when electrospun in aqueous solution. They obtained curled nanofibers at a lower humidity below 50% and converted into helical structures as the humidity is further increased (163). In another study, a relatively lower humidity (<50%) resulted in fiber breakage due to decreased electrostatic discharge from the jet, whereas high humidity resulted in the loss of fiber morphology as a result of increased water absorption (164).

Hence, to achieve electrospinning, in addition to the optimization of various standard parameters such as the concentration of the polymer, the flow rate at which the polymer solution is ejected from the needle, applied voltage and the distance between the needle and the collector, the non-conventional parameters such as temperature and humidity are necessary. The influences of these parameters on the electrospinnability of gelatin in aqueous solutions were investigated and are discussed below.

In the process of electrospinning, an optimum concentration of polymer solution is needed for the formation of nanofibers without beads. Other solution parameters that play an essential role in electrospinning are molecular weight and viscosity. All these factors can change the

rheological properties of the polymer solution, which in turn affects the forces acting on the spinning jet.

From the literature, it has been found that at lower concentrations of solutions, the electrospun scaffolds produced a mixture of fibers and beads, whereas when the concentration is increased, the shape of the beads changed from spherical to spindle-like and finally resulted in the formation of uniform fibers without any beads (165). High polymer concentrations are often not spinnable because of their high viscosity. Since viscosity is directly proportional to the concentration of polymer solution, an increase in polymer concentration results in a higher number of polymer chain entanglements and can hinder the formation of a spinning jet. At lower concentrations, the viscosity of the solution will be lower, and below a particular concentration, the deposition of droplets occurs rather than fibers. Hence, the study started with a lower concentration of 10% (wt/vol) and increased to 15% (wt/vol) of gelatin solution to perform electrospinning.

Initially, when a lower concentration of gelatin (10% wt/vol) with different flow rates (3 μl/min and 5 μl/min) were used, the obtained fibers were with beads. Table 3.1 shows the parameters used for the electrospinning of 10% (wt/vol) gelatin solution and the SEM images of obtained fibers are shown in figure.3.1.

Table.**3.1**. Parameters used for spinning 10% (wt/vol) gelatin solution

Parameters	**Values used**
Concentration of gelatin	10%
Flow rate	3 μl/min and 5 μl/min
Distance between the needle and collector	10 cm
Applied voltage	20 kV
Temperature	Above 40°C
Humidity	Above 50%

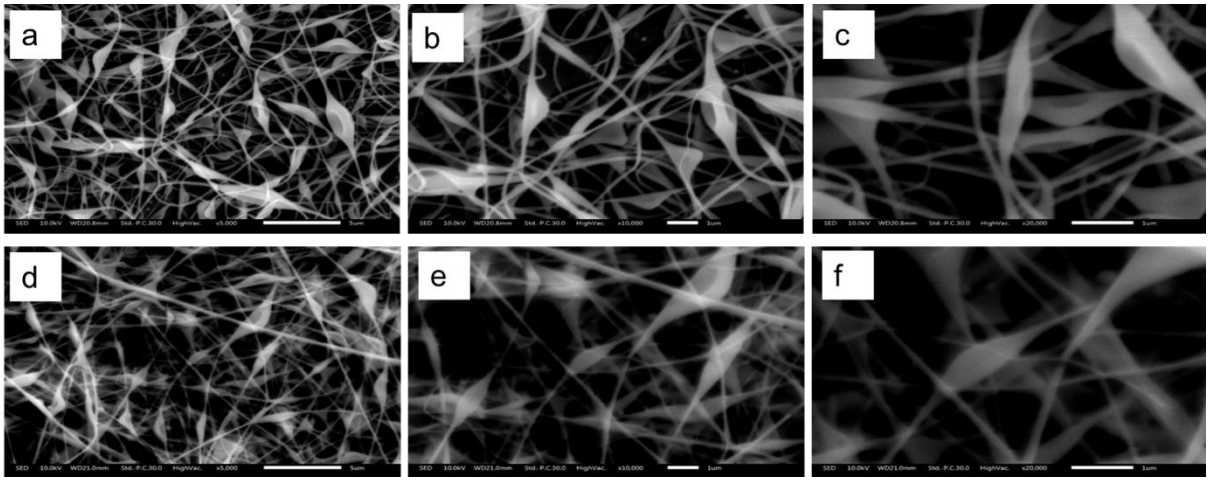

Figure **3.1.** SEM images of 10% (wt/vol) gelatin fibers electrospun at different flow rates. The first row represents the images of electrospun gelatin fibers at a flow rate of 3 μl/min (a, b and c) and second row represent the images of electrospun gelatin fibers at a flow rate of 5μl/min (d, e and f). The applied voltage was set to 20 kV. Images (b),(c), (e) and (f) are the higher magnification images to show the beads.

From the SEM images, it was apparent that both the flow rates created fibers with beads and were not suitable for further studies. There was not much difference in the size of the beads when the flow rate was increased. This indicates that the solution properties are not appropriate for the formation of gelatin nanofibers.

Next, a higher concentration of gelatin (15% wt/vol) was attempted to get a better morphology of fibers. When the gelatin solution of 15% (wt/vol) was electrospun, the obtained fibers were still with beads but with reduced size. Table 3.2. shows the parameters used for electrospinning 15% (wt/vol) gelatin solution and the SEM images of obtained fibers are shown in figure.3.2.

Table.**3.2**. Parameters used for spinning 15% (wt/vol) gelatin solution

Parameters	**Values**
Concentration of gelatin	15%
Flow rate	3 μl/min
Distance between the needle and collector	10 cm
Applied voltage	10 kV
Temperature	Above 40°C
Humidity	Above 50%

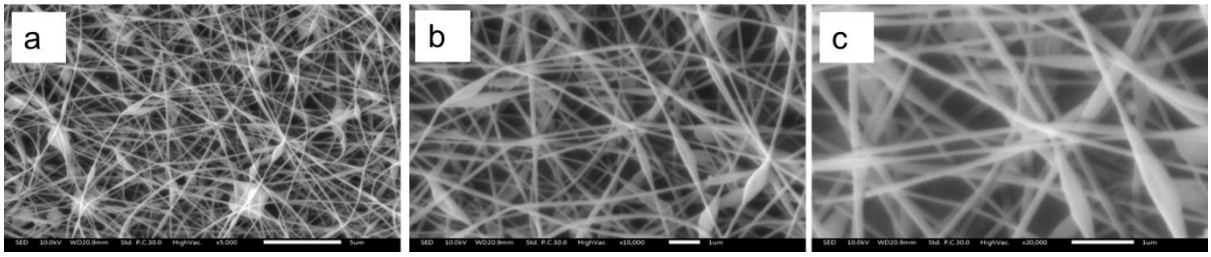

Figure **3.2.** SEM images of 15% electrospun gelatin fibers at a flow rate of 3 µl/min and 10 kV applied voltage. Images (b) and (c) represents the higher magnification images of image (a).

As the concentration increased to 15% (wt/vol),, the fibers formed were of better morphology compared to 10% (wt/vol), electrospun gelatin fibers. From the images, it was evident that the size of the beads was reduced, and the shape of the beads changed from spherical to spindle-like. Hence it was found that 15% (wt/vol), will be the optimum gelatin concentration for electrospinning gelatin in aqueous solution. Also, it was found that changing the other parameters such as applied voltage or flow rate slightly by maintaining the gelatin concentration to 15% (wt/vol),, will result in the creation of nonwoven ultra-thin nanofibers without beads.

When the polymer concentration was increased to 15% (wt/vol),, the applied voltage was 10 kV, as it was the first instance where the fibers were deposited on the collector. According to the literature, the fibers are produced when the electrostatic force of repulsion overcomes the surface tension of the solution. When the concentration is higher, the viscosity increases and the solution carries more charges because of the higher solution conductivity (165). The polymer solution carries the same charges, and under the influence of an electric field, they experience an electrostatic force of repulsion. To overcome this electrostatic force of repulsion, and for the successful formation of the Taylor cone, there should be sufficient applied voltage.

Therefore, from the results, it was assumed that even though fibers were formed at an applied voltage of 10 kV, it was not adequate to produce nanofibers with proper morphology.

The next trial was performed by increasing the applied voltage to 20 kV, while other parameters such as the concentration of gelatin polymer, distance and flow rate were kept constant. The higher concentration of gelatin helped the solution to get viscous enough to form a Taylor cone and the increase in voltage aided the solution to overcome the surface tension and to eject from the needle to the collector. The SEM images of the obtained fibers are shown in figure.3.3.

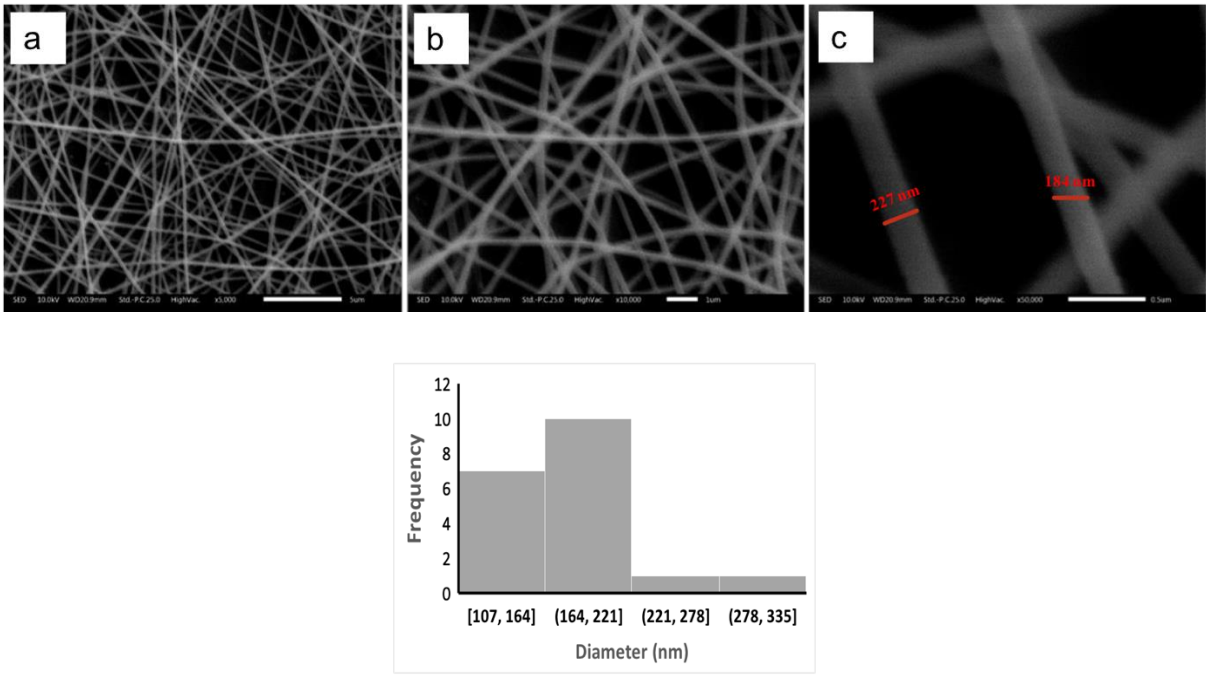

Figure **3.3.** SEM images of optimised gelatin nanofibers at a flow rate of 3 µl/min and 20 kV applied voltage. Images (b) and (c) represents the higher magnification images of (a). In image (c), the diameters of nanofibers measured by Image J software are shown.The histogram represents the average fiber diameter was 190±30 nm.

From the SEM images, the attained nanofibers were beads-free and randomly oriented ultra-thin nonwoven nanofibers. The fibers were continuous with a three-dimensional network structure having interconnected pores which resemble the ECM (**Figure.3.3. a&b**). The nanofibers were found to have an average diameter of 190±30 nm (**Figure.3.3. c**). Hence these parameters were found to be desired parameters for electrospinning gelatin in aqueous solution. The optimised conditions for spinning gelatin nanofibers in pure water solvent are listed in table 3.3. and the photographs of gelatin nanofibrous scaffolds are shown in figure 3.4.

Table **3.3.** Optimised conditions for electrospinning gelatin nanofibers in aqueous solution

Parameters	**Optimised values**
Concentration of gelatin	15%
Flow rate	3 μl/min
Distance between the needle and collector	10 cm
Applied voltage	20 kV
Temperature	Above 40°C
Humidity	Above 50%

Figure **3.4.** Photographs of gelatin nanofibrous scaffolds peeled off from the aluminium foil.

From the SEM images, it was evident that the electrospinning is dependent highly on the concentration of the gelatin. When the concentration of gelatin increased from 10% to 15%, the number of beads formed was reduced, and the fiber morphology of beads on a string was obtained (Figure. 3.2). The effect of polymer concentration on electrospinning nanofibers has been reported in several studies (165-170). In 2013, Oraby *et al*. reported that an increase in the concentration of gelatin solution from 30% to 50% w/v produced beads or smooth fibers depending on the concentration range. Acetic acid was used as the solvent for preparing the gelatin solution, and the electrospinning was carried out at 20 kV applied voltage and a distance of 18 cm. At 30% gelatin concentration, no fibers were observed, but when the concentration was increased to 40%, the fibers were found bonded at their contact sites. It is assumed that this can be due to the incomplete evaporation of the solvent. A further increase in the concentration of gelatin polymer to 50% resulted in fibers with proper morphology. In this article, they have also reported the dependence of fiber diameter on gelatin polymer concentration. When the gelatin concentration was increased from 40% to 50%, the fiber diameter also increased (165). This result was in agreement with the result obtained by Huang *et al.* in 2004 (161).

Another parameter investigated during the process of electrospinning gelatin was the applied voltage. It was found that when the voltage is increased from 15 kV to 20 kV, by keeping all other processing parameters and solution concentration constant, the morphology of the fibers also changed from beads on a string to ultra-fine fibers without any beads. It has been already reported that attainment of a threshold voltage is essential for the initiating drop to stretch enough to form a Taylor cone along with an electric field to start the electrospinning process (165). The applied voltage can induce necessary charges on the polymer solution and helps to

overcome the surface tension under the influence of the electric field. It has also been reported that the increase in applied voltage, increases the electrostatic force of repulsion on the polymer solution and hence results in the easy breakage of the initiating drop to enhance the process of electrospinning and thereby to narrow the fiber diameter (166). But higher voltage is not always recommended as there is an increased probability of occurring beads (166, 167). Hence the optimum applied voltage should be chosen carefully while considering other factors such as the concentration and conductivity of the polymer.

Therefore, the parameters for electrospinning gelatin nanofibers were optimised by maintaining the temperature and humidity above 40°C and 50% respectively. Since one of the aims of this study was to investigate stem cell responses to ECM-like scaffolds with different matrix stiffness, an *in situ* cross-linking electrospinning technique was opted to obtain gelatin nanofibrous scaffolds with tunable mechanical properties.

3.2. ELECTROSPINNING OF CLGS

The gelatin nanofibers should be well cross-linked to be used as a promising material for tissue engineering and regenerative medicine applications. This is because it is of utmost importance that these nanofibers should maintain their structural integrity in aqueous environments. Moreover, since our study was based on how the material's matrix stiffness is affecting the stem cell fate, it was crucial that the nanofibers should retain its structure at least for three weeks to facilitate the stem cell adhesion, proliferation and differentiation.

As discussed in section 2.7.1, there are different cross-linking methods available to make gelatin suitable for tissue engineering applications. The most commonly used cross-linking

method is the external cross-linking in which the cross-linking is done externally after performing the electrospinning. This is usually carried out by soaking the electrospun nanofibrous scaffolds in the cross-linking reagent for a desired period of time. Among the cross-linking reagents, EDC/NHS is the widely used carbodiimide for cross-linking gelatin. The schematic representation of chemical cross-linking with EDC/NHS is explained in the Materials and Methods chapter. There are many studies where EDC/NHS were used for the successful cross-linking of gelatin nanofibers (144, 145, 156, 171). For example, Mota *et al.* reported the use of EDC/NHS as an efficient cross-linking method for cross-linking a peptide modified PCL/gelatin nanofibrous scaffolds. These scaffolds were used for investigating the behaviours of human bone marrow-derived Mesenchymal Stem Cells (MSCs) when cultured on EDC/NHS cross-linked PCL/gelatin nanofibrous scaffolds (156). There are some other studies in which the researchers compared the crosslinking abilities of EDC/NHS and genipin and have found that EDC/NHS is superior to genipin in terms of its cross-linking strength and biocompatibility [15-17]. In a study conducted by R. Yao *et al.*, they analysed the cross-linking efficacy of EDC/NHS and genipin by treating PCL/gelatin nanofibrous scaffolds with 1% genipin, 2% genipin and EDC/NHS respectively. After cross-linking, the genipin cross-linked PCL/gelatin nanofibers were found to be merged and fused together at the junctions. However, the EDC/NHS cross-linked PCL/gelatin nanofibers were less merged and showed no significant difference in the fiber morphology and dimensions. Additionally, they showed enhanced MSCs attachment on the scaffolds, demonstrating their biocompatibility (144). For this reason, EDC/NHS was selected as the cross-linking agent for effectively cross-linking gelatin nanofibers in our study.

Since the objective of this study was to fabricate gelatin nanofibrous scaffolds with different mechanical stiffness, which is dependent on cross-linking densities, an alternative method

named '*in situ* cross-linking electrospinning' was preferred. One of the main advantages of using this method is that the amount of cross-linking agent incorporated into the polymer solution can be controlled internally. The homogeneity of the cross-linking should be improved compared to externally cross-linked nanofibers. In the case of conventional external cross-linking methods, the cross-linking agent is introduced into electrospun nanofibers through diffusion. Also, the cross-linking is not as efficient because increased cross-linking on the surface leads to the reduced diffusion hence decreased chemical bonding inside the nanofibers. There are chances for these weakly cross-linked bonds to disrupt in an aqueous environment, which results in the loss of fiber morphology and structural integrity. Moreover, the external cross-linking requires additional post-processing steps to remove the unreacted residues in order to reduce cytotoxicity. Hence, an *in situ* cross-linking electrospinning method was opted to produce gelatin nanofibers with EDC/NHS as the internal cross-linking agent.

In situ cross-linking is usually achieved by mixing the polymer solution with the cross-linking agent vigorously for an extended period of time to attain homogeneous mixing. For example, in 2016, Takeda *et al.* fabricated nanofibrous collagen scaffolds by an *in situ* cross-linking method. In that work, they used HFIP as the solvent for collagen solution preparation, and this solution was homogeneously mixed with 25% of glutaraldehyde solution to achieve *in situ* cross-linking (172). Although *in situ* cross-linking was effectively accomplished, the method described by Takeda *et al.* does have some drawbacks. Firstly, the cross-linking agent glutaraldehyde is toxic to the cells, and when it is internally cross-linked, there are chances for the unreacted glutaraldehyde residues to remain in the scaffold itself. This will be directly taken up by the cells during the degradation of scaffolds and results in apoptosis of cells in *in vitro* (173-175). Glutaraldehyde cross-linking can also cause calcification in *vivo* (176). Another limitation of this method is that 100% of cross-linking degree cannot be achieved through

mixing and the amount of cross-linking agent that to be incorporated cannot be fine-tuned. Hence, another work done by Kishan *et.al*, was followed, where they used a double-barrel syringe setup to carry out the *in situ* cross-linking of gelatin nanofibers. They used TFE as the solvent for mixing gelatin molecules, and a catalyst 1,4-diazabicyclo [2,2,2] octane (DABCO) was also added to the 5% gelatin solution before electrospinning. A solution of hexamethylene diisocyanate (HDI) was used as the cross-linker, and the barrel ratio used for *in situ* cross-linking was 1:1 with attachable mixing heads (97).

This study also adopted the same method of synthesis as of Kishan *et al*., but with a small difference in the barrel ratio. The aim was to totally minimise the use of any organic solvents during the fabrication process; hence a double barrel syringe of barrel ratio 10:1 was used, and the EDC/NHS was introduced into the smaller barrel. This facilitated in the blending of EDC/NHS with gelatin polymer solution in the required amount for the cross-linking to occur. It is possible to spin conventionally mixed gelatin-EDC/NHS solution with a normal syringe (21G), but the electrospinning was not continuous and resulted in 80% of solution wastage as the viscosity increases with increasing cross-linking density. Therefore double-barrel syringe was utilized to aid electrospinning by mixing the gelatin and EDC/NHS just before it is ejected from the needle and this reduced the chances of clogging. This resulted in the formation of uniform scaffolds and increased the reproducibility.

Thus, gelatin nanofibrous scaffolds with different cross-linking densities (denoted as 2X, 5X and 8X) were developed, and the 10X solution was not spinnable because of the high viscosity of the solution. This made the gelatin solution to get stuck inside the needle and inhibited the formation of a spinning jet. Hence it was worth examining the rheology of gelatin solution with different cross-linking density to find out at what viscosity the solution is not spinnable and to

understand the flow behaviour. The rheological behaviour of gelatin solution with different cross-linking concentrations is discussed below.

3.2.1. Solution characterisation

The solution rheology was analysed to find out the viscosity at which the solution is not spannable and to assess the flow behaviour. The most noticeable effect of increasing the cross-linking concentrations of EDC/NHS on the gelatin solution was a rise in shear viscosity, shown in figure 3.5. This can be explained as the effect of increased cross-linking between the gelatin solution and EDC/NHS. As the concentration of EDC/NHS increased, more overlapping of polymer chains and cross-linker in the solution occurred, and this created a greater opportunity for the chains to interact. Therefore, as the cross-linking concentration is increased, new bonds are formed by resisting the flow of gelatin solution, which in turn resulted in higher viscosity. According to the literature, as the concentration is increased, more dynamic polymer chains entangling and disentangling occurs. This requires tremendous energy, and hence, more of the kinetic energy introduced by the shearing force is dissipated during the process of chain entanglements (177). This results in the resistance of the solution to flow and thereby an increase in viscosity.

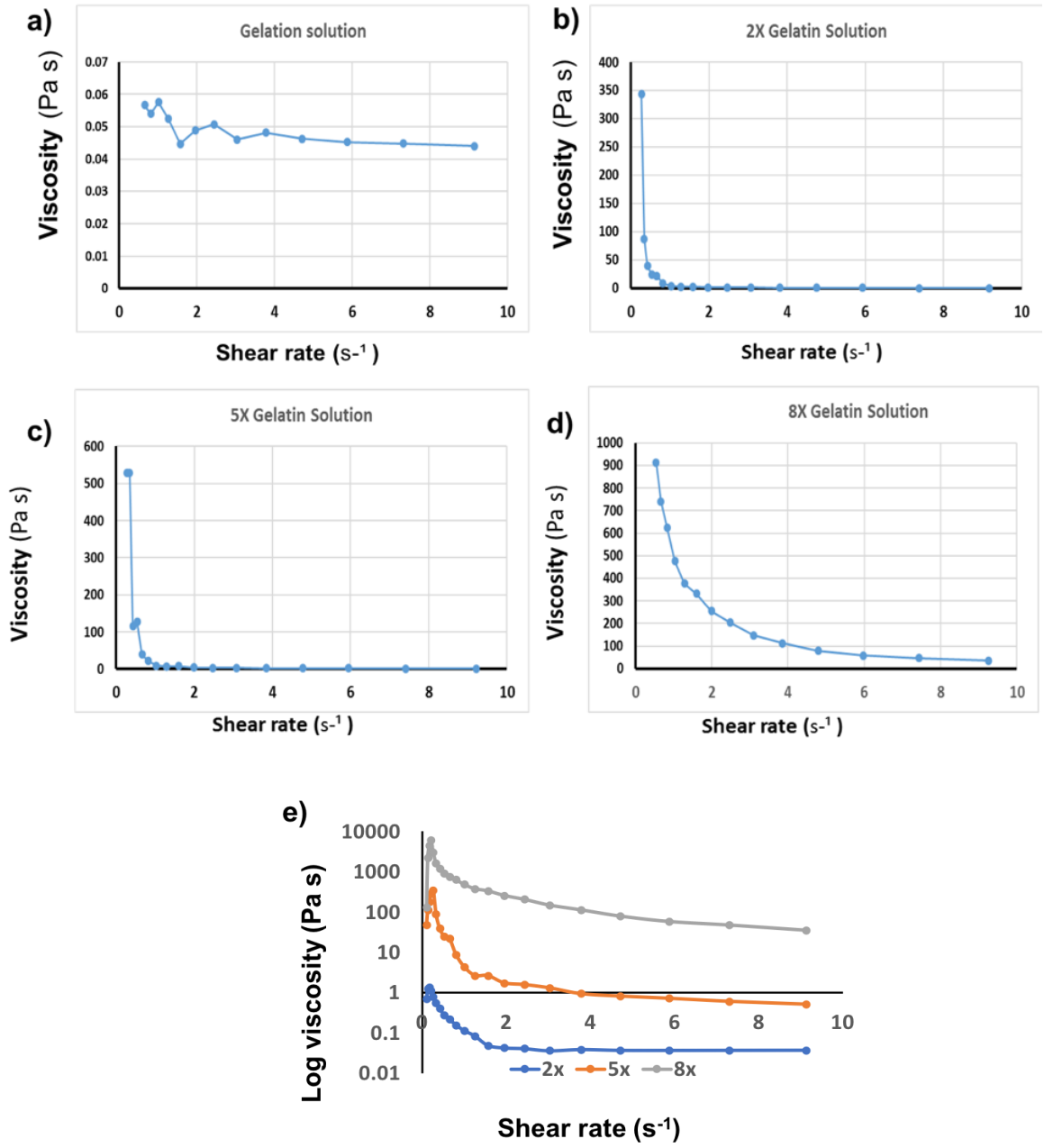

Figure.**3.5.** Graph showing the viscosity vs shear rate characteristics of gelatin solution (a), flow behaviour of 2X gelatin solution (b), flow behaviour of 5X gelatin solution (c) and flow behaviour of 8X gelatin solution (d). The log viscosity vs shear rate graph of 2X, 5X and 8X solutions shows the increase in viscosity as the cross-linking concentration of EDC/NHS is increased (e). The concentration of gelatin is 15%, and X represents 14mM EDC and 5.5mM NHS.

From figure.3.5, it was evident that as the cross-linking density increased not only the viscosity, but the shape of the viscosity vs shear rate curves also differs. The pure gelatin solution followed almost a Newtonian curve at shear rates up to 9 reciprocal seconds (**Figure.3.5. a)**, means the viscosity of gelatin solution is independent of the shear rate. Most of the polymer solution shows a linear, Newtonian region in the viscosity vs shear rate curve. For Newtonian fluids, the viscosity remains constant even though different forces are applied to make the solution flow. For gelatin solutions incorporated with varying concentrations of EDC/NHS, the viscosity vs shear rate curves exhibited a Non-Newtonian shear-thinning behaviour (**Figure 3.5. b), c) and d)**. The viscosity of 47.55 Pa.s was obtained for a 2X solution and was increased to 64.35 Pa.s and 129.6 Pa.s for 5X and 8X solutions respectively at a shear rate of $0.11s^{-1}$. Therefore, as the cross-linking density is increased, the viscosity also increased (**Figure 3.5. e)**. For 2X, 5X and 8X solutions, the viscosity decreased with an increase in the shear rate. A rapid decrease in the viscosity was found for 2X, 5X, and 8X solutions at low shear rates compared to high shear rates. For example, a 2X solution exhibited a rapid decrease in the viscosity from 350 Pa.s to 50 Pa.s. at a lower shear rate (less than 1 s^{-1}) (**Figure 3.5. b)**. This is because of the shear thinning behaviour of the solutions. This shear thinning response is an indication that the polymer solution has more complex molecular chains. The decrease in viscosity with respect to an increase in shear rate could be explained because of the alignment attained by the polymer molecules upon applied shear force. This molecular alignment made the solution to flow more quickly, which reduced the viscosity at increased shear rates. The shear thinning behaviour of the polymer solutions was also investigated by Diego *et. al.* They also found that polymer solutions tested were non-Newtonian pseudo plastic fluids, and the apparent viscosity decreased with increasing shear rate (178).

According to the literature, the viscosity of the polymer solution much depends on various factors such as molecular weight, the shape of the molecules, the interaction between the polymer molecules and the solvent, the concentration of the polymer solution and the hydrophilic nature of the polymer (179). So, the change in viscosity of the polymer solution is due to the synergistic effect of all these factors. In this study, the increase in concentration of the cross-linking agent resulted in more bond formation and made the solution more viscous. It was also found that the gelatin solution is not spinnable above an average viscosity of 900 Pa.s. In 1994, Yasuo *et al.* investigated the rheological behaviour of the ultra-high molecular weight polyethene (UHMWPE) to access its application in the gel spinning technology. In that work, they found that polyethene solutions exhibit a shear thinning behaviour at a shear rate ranging from 10^{-4} to 10^{3} s^{-1}. Furthermore, as the concentration of PE solutions was increased, the non-Newtonian behaviour was more evident (180). Our findings were also similar to this study, which supports the theory.

Hence from the rheology testing, it was found that as the concentration of EDC/NHS increased, the viscosity of the solution also increased, and the solution is not spinnable above an average viscosity of 900 Pa.s. Therefore, the solution characterisation was carried out, and the optimisation of other electrospinning parameters for the fabrication of CLGS are explained in the next section.

3.2.2. Optimisation of CLGS

The CLGS were fabricated by optimising the injection flow rate of the polymer solution from the needle to the collector and applied voltage while keeping constant the distance between the needle and the collector (10 cm) and the gelatin concentration (15%). The optimised

electrospinning conditions for different concentrations of cross-linking agents EDC/NHS (range from 2 times of 14 mM EDC and 5.5 mM NHS to 8 times of 14 mM EDC and 5.5 mM NHS, denoted as 2X, 5X and 8X) is shown in table.3.4.

Table**.3.4.** Optimised electrospinning conditions for CLGS. The temperature was set to above 40°C and humidity above 50% for all the electrospinning process.

Cross-linking density (X=14 mM EDC and 5.5 mM NHS)	**Concentration of gelatin (wt\vol)**	**Flow rate (µl/min)**	**Distance (cm)**	**Voltage (kV)**
2X	15%	25	10	18
5X	15%	10	10	22
8X	15%	7	10	22

The concentration of gelatin was kept constant because, at 15% (wt/vol) gelatin concentration, the fibers formed were beads-free and were with good morphology. So, by following the gelatin concentration to 15% (wt/vol) and distance at 10 cm, the flow rate and applied voltage were adjusted to obtain gelatin nanofibers with different cross-linking densities and therefore different stiffness.

3.3. CHARACTERISATION OF CLGS

To analyse the effect of matrix stiffness on CPs fate, the fabricated gelatin nanofibrous scaffolds should be well cross-linked and structurally stable to be used in the cell culture media for the CPs to adhere, proliferate and differentiate into cardiac specific lineages. Furthermore,

it should be mechanically tested to inspect the effect of increasing cross-linking density in the matrix stiffness.

So, the as-fabricated CLGS were physiochemically characterized by SEM, AFM and FT-IR. The SEM and AFM studies were carried out to investigate the morphological and topographical behaviour of the synthesised gelatin nanofibers. FTIR characterisation was performed to confirm the cross-linking by analysing the characteristics peaks while the ninhydrin assay was conducted to evaluate the efficiency of cross-linking. The stability of the fabricated scaffolds was examined by performing the dissolvability test. The mechanical characterization of the scaffolds was carried out to measure Young's modulus of the scaffolds in both wet and dry conditions.

3.3.1. Morphological characterisation of CLGS

The morphological analysis of the developed CLGS was carried out by using SEM. The SEM images of fabricated gelatin nanofibers with different cross-linking densities are shown in figure.3.6.

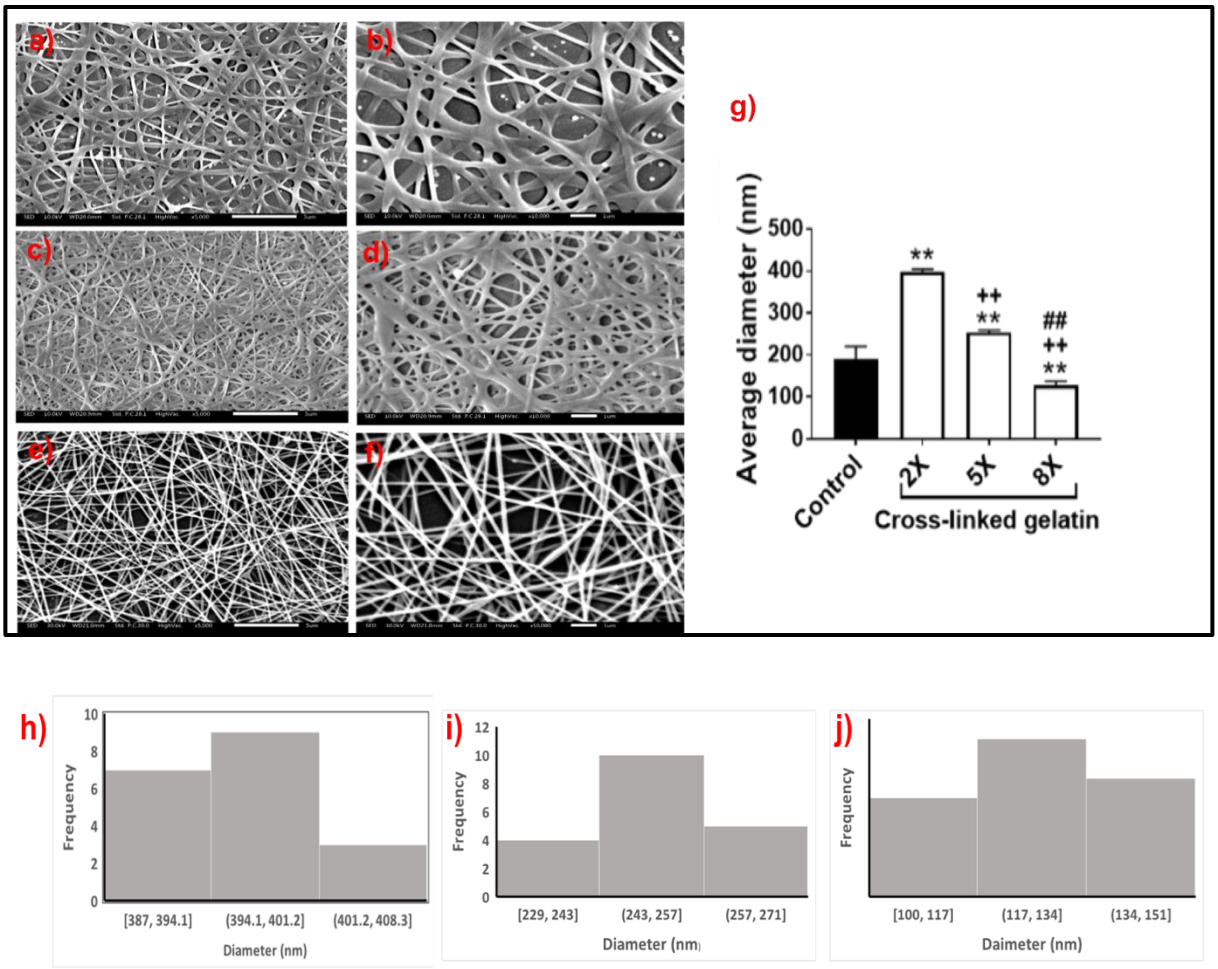

Figure**. 3.6.** SEM images of CLGS. SEM images of 2X CLGS (a & b), 5X CLGS (c & d), and 8X CLGS (e & f). The figures (b), (d) and (f) are the magnified SEM images of (a), (c) and (e), respectively. Bar graph represents the average fiber diameter of each scaffold (uncross-linked gelatin nanofibers were used as the control, and the average fiber diameter is also shown for comparison). The histogram representing the average fiber diameter of 2X (h), 5X (i) and 8X (j) scaffolds are also shown. Values are mean and SE, N=3 repeats. ANOVA, $P<0.01$; Tukey's multiple comparisons test adjusted P values: **$P<0.01$ vs. control, ++$P<0.01$ vs. 2X, ##$P<0.01$ vs 5X.

The SEM images showed that the obtained *in situ* cross-linked nanofibrous structures were beads-free, porous and randomly arranged nonwoven fibers **(Figure.3.6. a)-f).** The 2X and 5X CLGS were appeared to be of webbed morphology rather that intact ultrathin nanofibers and have an average diameter of 398±6 nm and 253±5 nm, respectively **(Figure 3.6. a)- d).** Among the three concentrations of EDC/NHS, the gelatin nanofibers cross-linked with the 8X concentration of EDC/NHS were found to be of uniform structure and good fiber morphology, having an average diameter of 127±10 nm **(Figure 3.6. e) and f).** Hence it was found that as the cross-linking density is increased the fiber diameter reduced significantly (bar graph). This is due to the synergistic influence of electrospinning parameters such as voltage and flow rate. An increase in applied voltage and a decrease in flow rate resulted in nanofibers with reduced fiber diameter. The cross-linking density has also influenced the fiber diameter. An increase in cross-linking density resulted in the new bond formation and shrinkage in fiber dimensions by reducing the fiber diameter significantly. The diameter measurements of individual nanofibers were done by using Image J software.

As discussed in section 4.1.1, many factors such as the concentration of the polymer solution, applied voltage and flow rate can affect the fiber diameter. Here the decrease in fiber diameter can be recognised mainly due to the increase in cross-linking density. When the cross-linking density is increased, new bonds were formed, and the shrinkage of fiber dimensions occurred. There were not many works explaining the effect of cross-linking density on fiber diameter since most of the studies were dealt with external cross-linking in which it was difficult to control the cross-linking density. In work by Kishan *et al*., gelatin scaffolds with different cross-linking densities were fabricated by *in situ* cross-linking with HDI. In this work, they found that the average fiber diameter of the developed 1X mesh was 0.74 ± 0.32 μm, 5X and 10X was 0.77 ± 0.17 μm and 0.72 ± 0.29 μm respectively (where X represents different

concentrations HDI) (97). There was a slight decrease in the fiber diameter when the cross-linking degree was increased, but it was not significant. Hence it is hypothesized that the decrease in gelatin fiber diameter was due to the synergistic effect of increased applied voltage, decreased flow rate and increase in cross-linking density. All these processing parameters collectively contributed to the reduction in gelatin fiber diameter as the cross-linking concentration of EDC/NHS is increased.

Therefore, all the obtained CLGS were morphologically analysed and found that as the cross-linking density is increased, the fiber diameter decreased and the 8X scaffolds have good morphology with randomly oriented ultra-thin fibers compared to other counterparts.

3.3.2. Topographical characterisation of CLGS

The topography of CLGS was tested by using AFM. The 3D surface plot of individual nanofibers is shown in figure.3.7. This shows the topographical behaviour of cross-linked gelatin nanofibers with different concentrations of EDC/NHS. The height information of the individual nanofibers was also obtained from AFM images.

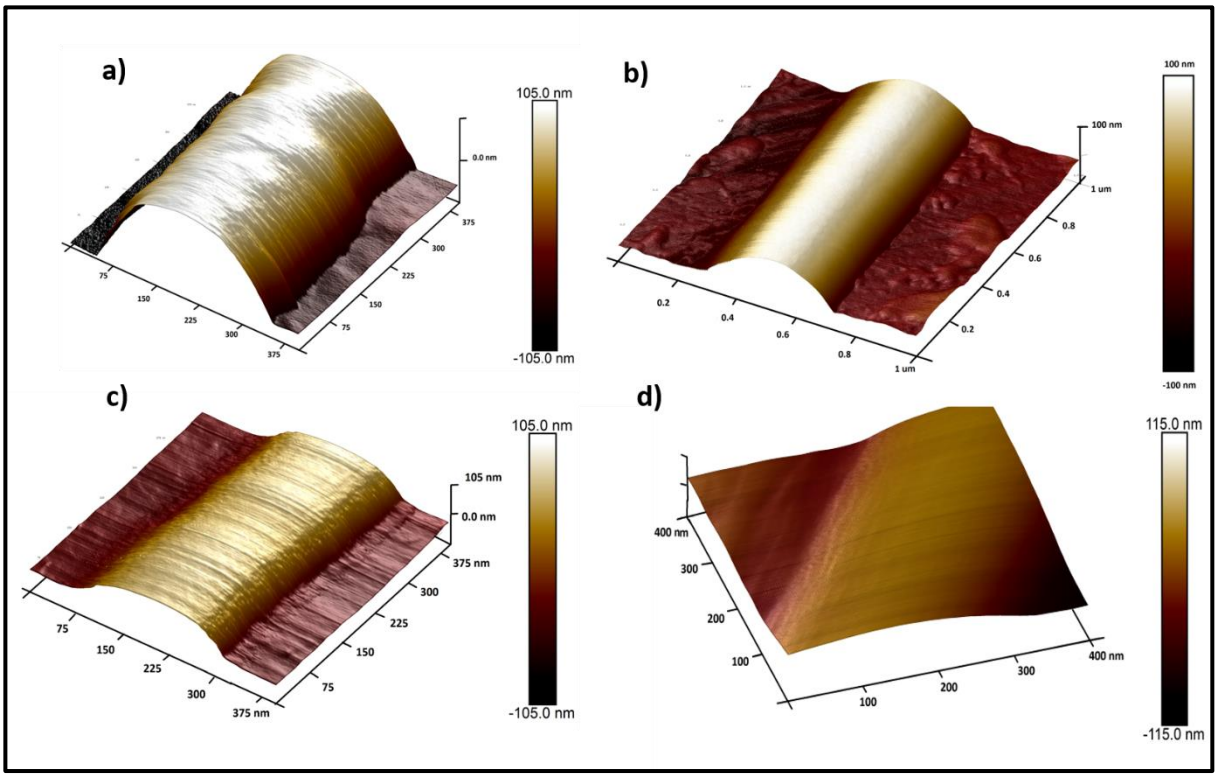

Figure**.3.7.** AFM images of individual nanofibers. The image (a) represents uncross-linked gelatin, (b)-2X cross-linked gelatin, (c)-5X cross-linked gelatin and (d)-8X cross-linked gelatin nanofiber.

All individual fibers were found to have an average height of 106±10 nm. The height information directly reflects the surface roughness of the nanofibers, which is closely related to the aspect ratio (181). In all images, the relative height information is displayed in a colour bar, and the brightest point represents the maximum height of each fiber. In the 3D images, the brightest point shows the nanofiber and dark portion is the substrate, which is aluminium foil. The fiber diameter was also evident from the images. Since they were individual fiber diameters, they could not be correlated with the average fiber diameters obtained by SEM analysis.

From the images, all the individual nanofibers exhibited a smooth surface. The surface topography of uncross-linked gelatin nanofiber and cross-linked gelatin nanofibers were similar. This showed that there was no change in the topography even after the cross-linking of gelatin nanofibers. In work done by Jaiswal *et al.*, they found that when Poly-L-lactic acid PLLA is incorporated with collagen and gelatin is combined with PLLA; the obtained nanofibers showed a higher degree of surface roughness when compared to the pure PLLA and pure gelatin (30). Hence the addition of another polymer resulted in a higher degree of roughness. In this work, the retention of surface topography after cross-linking can be explained as because of the cross-linking occurred between the polymer chains or due to the intermolecular reaction.

It is worth mentioning that the roughness of the material can enhance the cell adhesion and proliferation on nanofibrous scaffolds. In the cell culture study conducted by Jaiswal *et al.*, the scaffolds with a higher degree of roughness (mean root square roughness (Sq) of 1409 nm,) showed improved cell adhesion and spreading compared to other scaffolds (182). They discovered that the blending of PLLA with gelatin increased the surface roughness and reduced the hydrophobicity of PLLA. Since this study was based on the effect of matrix stiffness on the stem cell fate, it was paramount that the surface topography should be smooth to nullify the effect of roughness. Hence from the AFM analysis, it was confirmed that all the obtained nanofibers were smooth which reduced the possibility of occurring alterations in the cellular behaviour that could have happened by surface roughness and all the tested nanofibers were found to have an average height of 106±10 nm.

3.3.3. Structural stability of CLGS

The dissolvability test was performed to check whether the nanofibrous scaffolds are retaining their structural properties when it is immersed in PBS. It was essential for the fibers to maintain their structural integrity at least for three weeks for the cells to adhere, proliferate and differentiate. Cross-linking agents like EDC/NHS, are reportedly less efficient in maintaining structural stability over 3 weeks. This could preclude the use of scaffolds for tissue/cell engineering applications in the wet condition (150). Therefore, the dissolvability property of the EDC/NHS scaffolds were tested and verified if this can be improved by the addition of meagre percentage of Glutaraldehyde (Glu) vapour (5%) which can create stronger aldimine linkages. Reports suggest that glutaraldehyde concentration of up to 8% is non-toxic to cells (183, 184). The SEM images of as-spun scaffolds, EDC/NHS, cross-linked scaffolds after two weeks, and Glu treated EDC/NHS scaffolds after three weeks immersed in PBS are shown in figure. 3.8. The average fiber diameter of hydrated Glu/EDC/NHS cross-linked scaffolds after 3 weeks immersion in aqueous solution was also shown in figure 3.8.

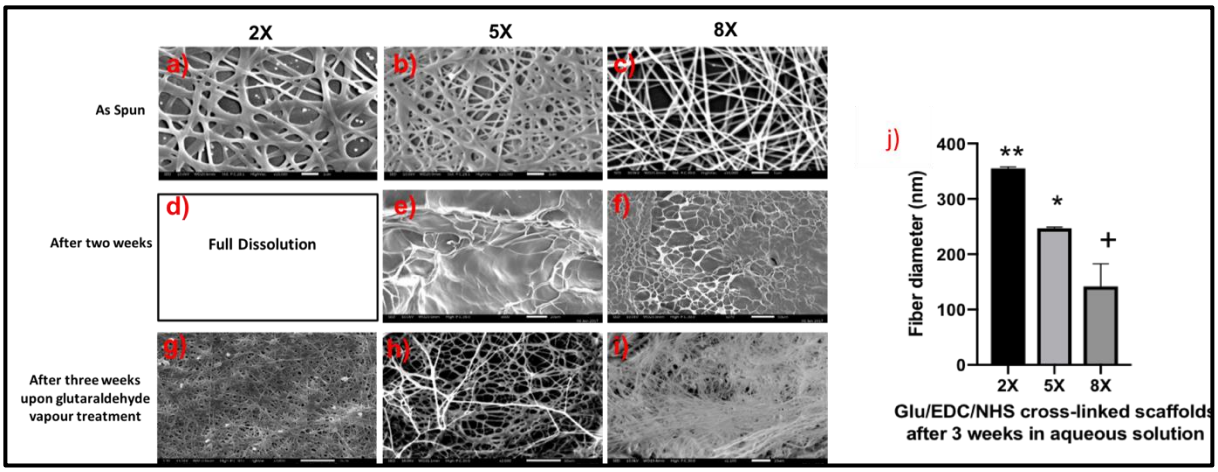

Figure.**3.8.** Degradation test of gelatin nanofibrous scaffolds. The first row represents SEM images of 2X, 5X and 8X EDC/NHS CLGS (a, b and c). The second row represents the SEM images of 2X, 5X and 8X EDC/NHS CLGS after two weeks immersed in PBS (d, e) and f). The third row represents Glu vapour treated EDC/NHS cross-linked 2X, 5X and 8X gelatin nanofibers after 3 weeks immersed in PBS (g, h and i). Image (j) represents the bar diagram showing the average fiber diameter of Glu/EDC/NHS CLGS after 3 weeks in aqueous solution. Values are mean and SE, N=3 repeats. ANOVA, $P<0.01$; Tukey's multiple comparisons test adjusted P values: *$P<0.05$ vs. 2X, +$P<0.05$ vs. 5X, **$P<0.01$ vs 8X.

SEM imaging of as-spun CLGS confirmed the porous and nonwoven fibrous structures of the fabricated scaffolds with different matrix stiffness **(Figure.3.8. (a-c).** The as-spun EDC/NHS cross-linked 2X gelatin nanofibers were fully dissolved, and the material disappeared after two weeks of immersion in PBS **(Figure.3.8. d).** This showed the instability of the gelatin nanofibers when cross-linked with a 2X concentration of EDC/NHS. While 5X and 8X EDC/NHS cross-linked gelatin nanofibers changed its morphology to a film rather than intact nanofibers **(Figure.3.8. e and f)**. As mentioned earlier, since the study was based on the effect of matrix stiffness on stem cell fate, it was important to retain the nanofibrous structure for the

cells to adhere, proliferate and differentiate on the material. So, when an external cross-linking was done with Glu vapour, all scaffolds retained their structure, and a fibrous morphology was obtained even after three weeks immersed in PBS **(Figure.3.8. g, h and i).** This showed the efficiency of the chemical cross-linking method and the stability of the material to be used as a scaffold for tissue engineering and regenerative medicine applications. The diameter of the 2X, 5X and 8X Glu/EDC/NHS cross-linked gelatin nanofibers after 3 weeks immersion in aqueous solution were found to be 338±5 nm, 240±3nm and 110±45nm respectively **(Figure.3.8. j).**

From the quantification analysis of fiber diameter, all scaffolds slightly reduced their fiber dimensions after 3 weeks, and the 8X scaffold displayed ultrathin fibers. Our results were contradictory to the results obtained by Kishen *et.al*. In his work, the gelatin nanofibers were cross-linked with glutaraldehyde, and when immersed in water for a week, the fibers were flattened and formed a webbed morphology (97). Here they have stopped the dissolvability test after a week of immersion in water. If they had continued the experiment until the third week, they would have observed the same morphology of fibers as this work. The reduction in fiber dimensions in this work can be recognized as the effect of partial dissolution of gelatin nanofibers by hydrolysis.

From the dissolvability test, the retention of structural integrity was observed after three weeks, when they are cross-linked both internally (with EDC/NHS) and externally (with Glu). Thus, we obtained well cross-linked and stable CLGS. Therefore, this fabrication process was further assessed for physicochemical characterisation of the scaffolds and studies of tissue engineering with human cells.

3.3.4. FTIR analysis of CLGS

The presence of EDC/NHS and Glu in the CLGS was explored by using FTIR. The FTIR spectra of pure gelatin nanofibers, Glu cross-linked gelatin nanofibers and Glu treated various concentrations of EDC/NHS cross-linked gelatin nanofibers are shown in figure.3.9.

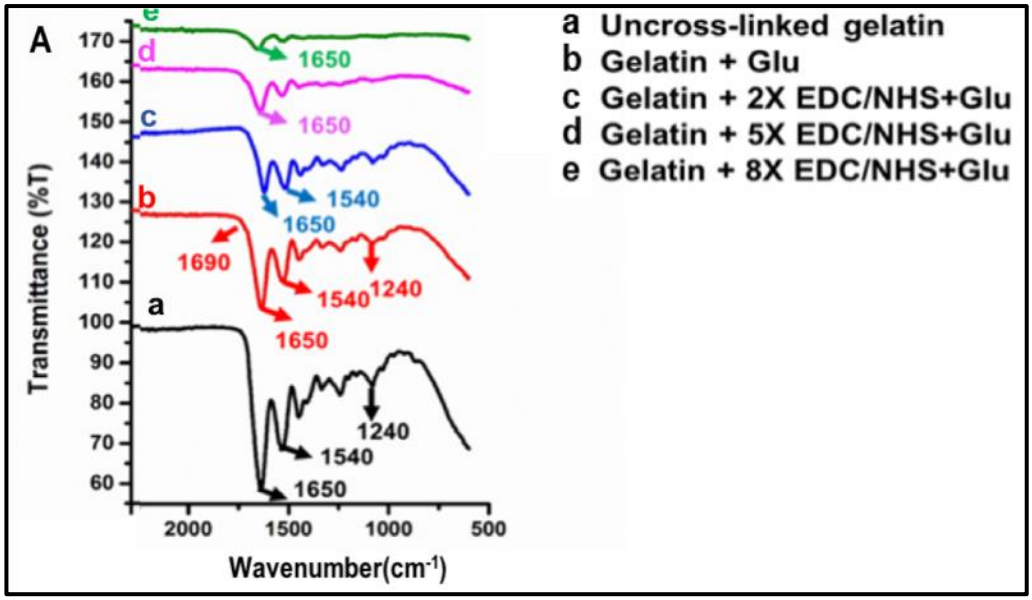

Figure. **3.9.** FTIR spectra of pure gelatin and cross-linked gelatin nanofibers (A). The spectrum (a) denotes uncross-linked gelatin nanofibers, (b) represents Glu alone cross-linked gelatin nanofibers, (c) is the spectrum of Glu treated 2X EDC/NHS cross-linked gelatin nanofibers, (d) is the spectrum of Glu treated 5X EDC/NHS cross-linked gelatin nanofibers and (e) is the spectrum of Glu treated 8X EDC/NHS cross-linked gelatin nanofibers.

The black trace in the figure shows that the characteristic peaks of gelatin were obtained at at 1650 cm^{-1}, which denotes the amide I peak (C=O stretching vibrations), at 1540 cm^{-1}, which corresponds to the amide II peak (N-H bending and C-H stretching vibrations), and at 1240 cm-1, which signifies amide III peak (C-N stretching + N-H in phase bending) **(Figure.3.9. a).**

Similarly, the characteristic absorption peak for aldimine linkage was observed at 1690 cm^{-1} in the Glu crosslinked gelatin nanofibers **(Figure. 3.9. b)**. The peak intensities were much lower for the nanofibers cross-linked with both Glu and EDC/NHS as compared with the Glu alone **(Figure.3.9. c)**, with the decrease in peak intensity, is further enhanced by increasing the concentration of EDC/NHS **(Figure.3.9. d and e)**. This phenomenon can be attributed to the EDC/NHS and Glu capability to reduce the amino groups of gelatin. The structure of gelatin was further disturbed when higher concentrations of EDC/NHS (5X and 8X) were used by eliminating Amide III peaks (1240 cm^{-1}) **(Figure.3.9. d and e)**.

It has been reported that the amide A peaks due to N-H stretching vibrations usually arise at 3400 cm^{-1} to 3340 cm^{-1} (185, 186). In the obtained FTIR spectra, the incidence of amide A peak was at 3300 cm^{-1}. This shift in the amide A band to a lower frequency may be because the N-H groups are involved in the hydrogen bond formation (185, 187). The amide I peak at 1650 cm^{-1} in the spectra of uncross-linked gelatin **(Figure.3.9. a)** and cross-linked gelatin nanofibers **(Figure.3.9. b-e)** have different intensities. In the Glu/EDC/NHS cross-linked gelatin nanofibers, the intensity of amide I peak at 1650 cm^{-1} **(Figure.3.9. c-e)** was much lower when compared to that of uncross-linked gelatin **(Figure.3.9. a)** and Glu alone cross-linked gelatin nanofibers **(Figure.3.9. b)**. This difference in peak intensities upon cross-linking can be justified as because of the weakening of C=O bond in gelatin. As the cross-linking happened, the C=O bond in the gelatin is weakened because of the formation of new bonds between carboxyl groups and amine groups (185, 188). The peak at 1240 cm^{-1}, which denotes the amide III bonds was much weaker for the Glu/2X EDC/NHS cross-linked gelatin nanofibers **[Figure.4.9. (c)]** compared to the uncross-linked gelatin nanofibers **(Figure.3.9. a)**. This showed that the structure of pure gelatin was not disturbed by the cross-linking of Glu and EDC/NHS; however, the peak intensities were reduced. But, when higher concentrations of

EDC/NHS (5X and 8X) were used, the structure of gelatin was further disturbed by eliminating Amide A (3300 cm^{-1}) and Amide III peaks (1240 cm^{-1}), respectively **(Figure.3.9. d and e)**.

These findings were comparable with the results of Zhan *et. al.* (2016). They fabricated glutaraldehyde-gelatin nanofibrous scaffolds by mixing glutaraldehyde along with the gelatin solution to attain *in situ* cross-linking. In the FTIR spectra, amide A band was observed at 3409 cm^{-1}, amide I band was detected at 1644 cm^{-1}, amide II band was observed at 1541 cm^{-1} and amide III bands at 1234 cm^{-1}. All these frequencies were similar to that of the spectra obtained in our study. Another critical observation by Zhan *et al*. was the shift in frequencies of Amide I peaks after cross-linking with different concentrations of glutaraldehyde. As the concentration of glutaraldehyde increased, the amide I peaks shifted to lower frequencies. This is explained as because of the disruption of the helical structure of gelatin by excess glutaraldehyde (147). In the spectra obtained in this work did not show any peak shifts, which shows the incorporation of an exact amount of glutaraldehyde for the gelatin nanofibers to cross-link.

Hence the scaffolds were well cross-linked with EDC/NHS, and Glu and their presence were confirmed by the reduction in the amino group of gelatin. Later, the extent of this cross-linking was investigated by performing the ninhydrin assay.

3.3.5. Cross-linking degree of CLGS

Ninhydrin assay was carried out to estimate the cross-linking degree of gelatin nanofibers after cross-linked with Glu and EDC/NHS. The colour change obtained when the scaffolds are treated with ninhydrin solution, and the quantification of cross-linking degree is shown in figure.3.10.

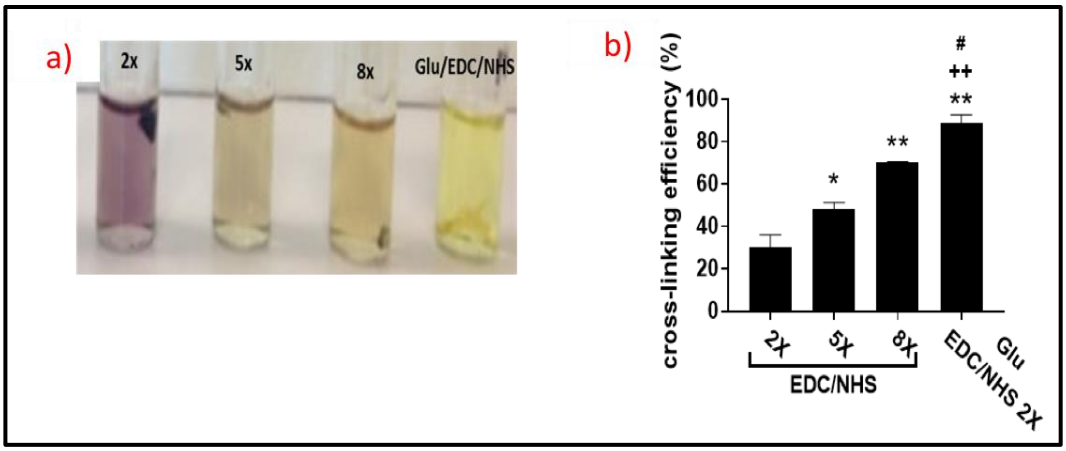

Figure.**3.10.** Ninhydrin assay ofCLGS. (a) Represents the colour change of ninhydrin solution with respect to the cross-linking density. For Glu/EDC/NHS cross-linked gelatin nanofibers, the solution colour remained the same while the nanofibers with lowest cross-linking density changed the ninhydrin solution colour to light blue. (b) Shows the cross-linking degree of gelatin nanofibers. Values are mean and SE, N=3 repeats. ANOVA, $P<0.01$; Tukey's multiple comparisons test adjusted P values: *$P<0.05$ and **$P<0.01$ vs. 2X EDC/NHS, ++$P<0.01$ vs. 5X EDC/NHS, ##$P<0.01$ vs 8X EDC/NHS.

The ninhydrin can react with the free amino groups in lysine residues of gelatin nanofibers upon heating. This caused the 2X nanofibrous scaffolds to change their colour to blue, and as a result, the ninhydrin solution also turned blue **(Figure.3.10. a).** As the cross-linking density is increased, the blue colour of the solution faded and for the Glu/EDC/NHS cross-linked gelatin nanofibers, the ninhydrin solution remained as yellow **(Figure.3.10. a)**. This exhibited the cross-linking ability of Glu and EDC/NHS when cross-linked externally and internally.

The cross-linking degree was also quantified and found that the cross-linking degree of Glu/EDC/NHS cross-linked gelatin nanofibers was significantly higher than the 2X, 5X and

8X EDC/NHS alone cross-linked scaffolds **(Figure.3.10. b)**. Almost 100% of cross-linking was achieved by Glu/EDC/NHS cross-linking whereas EDC/NHS cross-linked 2X, 5X and 8X scaffolds attained 30±9%, 50±5% and 65±2% respectively. Moreover, there was a significant difference in the cross-linking degree obtained among the 2X, 5X and 8XCLGS. The lowest concentration of Glu/EDC/NHS (2X) cross-linked scaffolds were tested in order to understand the effect of cross-linking and to get a significant result. Hence the Glu/EDC/NHS crosslinked scaffolds were found to be more efficient than EDC/NHS alone cross-linked scaffolds.

In internal cross-linking with EDC/NHS, the carboxyl group of EDC/NHS reacts with the amino groups of gelatin to form amide bonds. In external cross-linking with Glu, the aldehyde group in the Glu can react with the amino group in the lysine residues of gelatin to create aldimine linkages. These were the two chemical reactions that occurred when the gelatin nanofibers were cross-linked both internally and externally with EDC/NHS and Glu. As a result of these two reactions, almost 100% cross-linking efficacy was obtained. The lower cross-linking efficiency of 2X, 5X and 8X EDC/NHS alone cross-linked scaffolds demonstrated the existence of free amino groups. This proved the inefficiency of EDC/NHS cross-linking alone compared to EDC/NHS and Glu cross-linking. As the cross-linking concentration of EDC/NHS was increased to 8X, the maximum cross-linking degree achieved was around 70%. When these scaffolds were cross-linked with glutaraldehyde, approximately 100 % of the cross-linking degree was attained.

In work done by Mota *et al*.(2014), they used a ninhydrin test as an indicator to investigate the presence of free amino groups. They fabricated PCL/gelatin nanofibrous scaffolds cross-linked with EDC/NHS and found that the uncross-linked PCL/gelatin scaffolds were blue in colour upon heat treatment, while the cross-linked PCL/gelatin scaffolds remained the same. Here

they have not performed the quantification analysis to assess the degree of cross-linking attained. Hence it was difficult to compare the results with our study and entirely rely on the qualitative result. In another study done by Hui-Kang Ma *et al*.(2010), the amniotic membranes (AM) were cross-linked with different concentrations of EDC/NHS (0.01, 0.05 and 0.25mM EDC/mg AM). In the ninhydrin assay, it was found that the membranes cross-linked with higher concentrations (0.05 and 0.25 mM EDC/mg AM) of EDC/NHS had a significantly higher cross-linking degree when compared to membranes with lower concentrations (0.01 mM EDC/mg AM) (189). Hence the results obtained in this study were in accordance with Hui-Kang Ma *et al*.(2010), that the extent of cross-linking increased with an increase in the concentration of EDC/NHS. Additionally, in their work, the maximum cross-linking index obtained was around 50% for a lower concentration of 0.25 mM EDC/NHS, which was much lower than the concentration used in this study. The highest cross-linking degree of 70% with EDC/NHS in this study can be denoted as the increase in the concentration of EDC/NHS compared to the work of Hui-Kang Ma *et.al*(2010).

The superiority of glutaraldehyde in the cross-linking efficiency compared to other cross-linking agents such as EDC/NHS and genipin has been mentioned in several articles (183, 190, 191). For example, in a review article regarding the cross-linking of biopolymers for biomedical applications by Reddy *et al.*, concluded that glutaraldehyde is the most efficient and practical cross-linking agent despite their limitations and cytotoxicity (183). In 2010, Lai *et al*., evaluated the potential of EDC cross-linked and glutaraldehyde cross-linked gelatin membranes to be used as delivery carriers for retinal sheets. They reported that the cross-linking index of EDC cross-linked gelatin membranes was 55.4 ± 3.2% and that of glutaraldehyde cross-linked gelatin membrane was 72.6 ± 2.7%. This difference between the two groups was statistically significant, as well. But the EDC cross-linked gelatin membranes

exhibited higher cytocompatibility which showed the toxic nature of glutaraldehyde. However, the cytotoxicity of glutaraldehyde depends on the concentration used and exposure time, and it has been reported that up to 8% of glutaraldehyde is non-toxic to cells (183, 184). Therefore, the combined cross-linking effect of EDC/NHS and Glu made the gelatin nanofibers more suitable to be used as a right candidate for further *in vitro* studies.

Thus, it was found out that as the cross-linking density is increased, the cross-linking efficiency of the scaffolds also increased resulting in the new bond formation and Glu/EDC/NHS scaffolds showed highest cross-linking degree. Hence all the scaffolds used for the further *in vitro* studies were both internally and externally cross-linked scaffolds with different matrix stiffness.

3.3.6. Mechanical properties of CLGS

The mechanical properties of the scaffolds were measured by calculating the Young's Modulus (YM) from the stress-strain graphs. The Young's modulus is directly related to the stiffness of the material. The main aim of this work was to assess the effect of matrix stiffness on the stem cell fate; hence, it was very critical to measure the stiffness at both dry and wet conditions. The stiffness of the material will be different in both states, and therefore, the behaviour of the cell will also be altered. Thus, it was imperative to find out the matrix stiffness at the wet condition to evaluate the cell behaviour. The Young's Modulus of uncross-linked gelatin and Glu/EDC/NHS cross-linked gelatin nanofibers in both wet and dry conditions are shown in figure. 3.11.

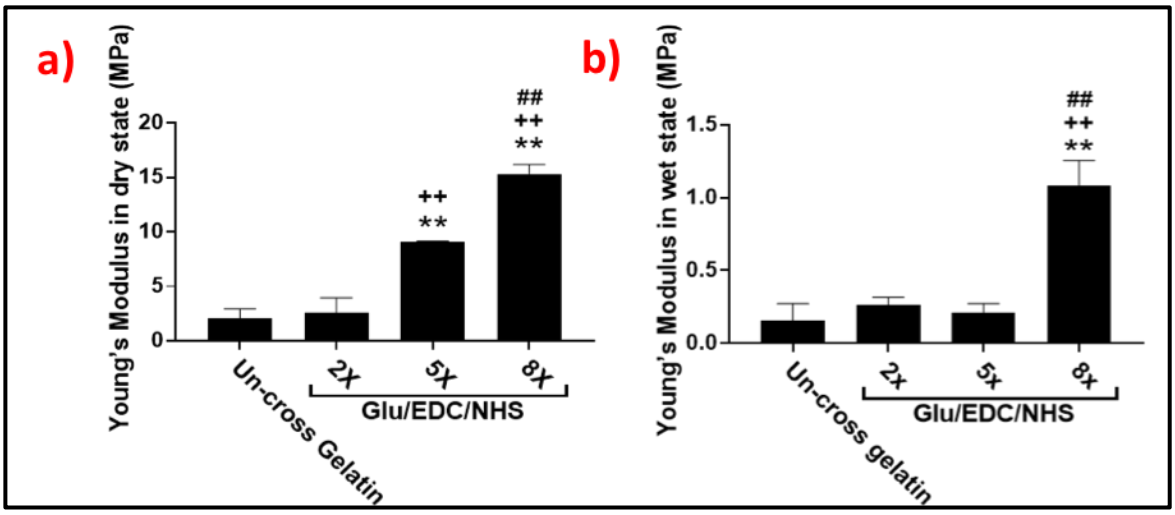

Figure. **3.11.** Mechanical testing of scaffolds. (a) YM of scaffolds in the dry condition, (b) YM of scaffolds in wet condition. Values are mean and SE, N=3 repeats. ANOVA, P<0.01; Tukey's multiple comparisons test adjusted P values: **P<0.01 vs. un-cross gelatin, ++P<0.01 vs. 2X EDC/NHS, ##P<0.01 vs 5X EDC/NHS.

As expected, the scaffolds showed higher YM in the dry state **(Figure.3.11. a)** because of the rigid protein network when compared to the scaffolds in the wet state **(Figure.3.11. b).** This can also be explained as because of the rigid and brittle properties attained by the scaffolds in the absence of water (88). Hence, in the dry state, the scaffolds showed increased YM as the cross-linking density is increased **(Figure.3.11. a)**. When the cross-linking density is higher, the new bonds are formed between the functional groups of the gelatin, which in turn results in the formation of denser and compact structures. This attributed to the increased YM with an increase in cross-linking density. In work done by Vanderhoof *et al.,* they prepared hyaluronan cross-linked gelatin hydrogels and investigated their rheological properties. They found that the gel stiffness was entirely dependent on the concentration and cross-linking density of the cross-linker. When they increased the ratio of thiol-modified gelatin, the effective concentration of the hyaluronan decreased, which in turn reduced the gel stiffness (192). This

result was in accordance with the results in this study, stating that as the cross-linking density is increased, the stiffness of the material also increases.

In both wet and dry conditions, the 8X CLGSshowed a significant difference in the YM when compared to that of pure gelatin, 2X and 5X CLGS. In the dry state, the 8X scaffolds showed an average YM of around 15 MPa, while 2X and 5X CLGS exhibited an average YM of around 4 MPa and 10 MPa **(Figure.3.11. a)**. There was also a significant difference in the YM among 2X and 5X CLGS. The uncross-linked gelatin nanofibers indicated an average YM of around 2 MPa which was very low compared to that of 5X and 8X cross-linked gelatin nanofibers. There was no significant difference in the YM among 2X and uncross-linked gelatin scaffolds. Dias *et al.* recently conducted a study to find out the best composite structures that match closely with the mechanical properties of skin for wound healing applications. They fabricated hybrid electrospun meshes with PCL and gelatin and evaluated its physical, chemical and mechanical properties. In the mechanical testing of scaffolds, they have reported that the gelatin nanofibers exhibited the lowest YM compared to the hybrid and PCL scaffolds. The obtained YM for gelatin scaffolds was less than 1 MPa (193). This result was supplementary to results obtained in this study, as the relative YM of uncross-linked gelatin nanofibers was around 2 MPa. Even though there are numerous works comparing the YM of nanofibrous scaffolds with different polymers, there are only a few works based on the effect of cross-linking density on the YM of nanofibrous scaffolds. In work done by Jiang *et al.*, they synthesised Pullulan/dextran (P/D) nanofibers by *in situ* cross-linking with different concentrations of sodium trimetaphosphate (SMTP) to obtain P/D scaffolds with different matrix stiffness. The YM analysis results were consistent with this study in which they found that as the cross-linking density is increased the YM of the P/D nanofibrous scaffolds also

increased. The YM of P/D scaffolds, when cross-linked with 10% of SMTP, was 7.71 ± 4.58, and the YM value increased 11.08 ± 6.36 kPa for 16% cross-linked P/D scaffolds (194).

In wet condition, the presence of water contributed to a massive difference in the YM of scaffolds **(Figure.3.11. b)**. Usually, the YM of nanofibrous scaffolds is in the range of KPa in the wet conditions. For example, in the previously mentioned work by Jiang *et al.*, when the mechanical testing was done with hydrated samples to obtain the YM, the values were in KPa. The YM for 10 % SMTP cross-linked P/D samples were around 2KPa, whereas that for the 16 % SMTP cross-linked P/D scaffolds were around 3 KPa (194). In this work, the YM of gelatin nanofibers were in the range of MPa. This can be justified as because of the cross-linking effect of EDC/NHS and Glu on the gelatin nanofibrous scaffolds. It is hypothesised that as the cross-linking density is increased, the water absorption capacity of the scaffolds will decrease. Hence the fibers absorb less water as new bonds are formed, and the polymer chains come closer upon cross-linking, which in turn makes the scaffolds to have higher retraction forces (195, 196). The YM of 8X CLGS were found to be around 1 MPa and was significantly higher than all other scaffolds **(Figure 3.11.b).** The difference in the YM of uncross-linked gelatin scaffolds, 2X and 5X CLGS did not show any statistical significance. The lower YM of gelatin, which was less than 0.1 MPa, clearly demonstrates the hydrogel formation in the presence of water (88). In the presence of water, hydrogen bonds are formed with new polymer networks, made the structure more viscoelastic and resulted in reduced YM compared to dry state.

Hence from the mechanical studies, it was detected that the CLGS were stiffer in dry conditions than in the wet state. Additionally, as the cross-linking density is increased, the YM of the scaffolds also increased in the dry state while in the wet state, the YM of uncross-linked gelatin,

2X and 5X CLGS were more or less the same and 8X CLGS showed a significant difference in the YM compared to all other scaffolds in wet condition.

4. RESULTS AND DISCUSSIONS II: *IN VITRO* CELL STUDIES TO ASSESS THE EFFECT OF MATRIX STIFFNESS ON CARDIAC PERICYTES BEHAVIOUR

The stem cell fate is determined by a lot of microenvironmental factors such as biophysical cues, chemical cues and mechanical cues. All these factors play an essential role in deciding stem cell fate. It has been reported that the endothelium and smooth muscle layers can sense the mechanical stimulations such as shear stress and stretching imparted by the pulsated blood flow and thus regulates the normal physiological functions of the cardiovascular system (74, 197-199). Even though there are many works explaining the effect of biophysical cues and chemical cues in affecting the stem cell fate, the impact of mechanical properties, mainly how the matrix stiffness of the material affects the stem cell fate is limited.

This work aims to investigate the effect of matrix stiffness in determining the cardiac pericyte fate. Changes in stiffness occur in the hearts and arterial vessels of patients with congenital heart disease, currently acknowledged as the most common congenital anomaly responsible for 7.5% of all infant deaths and for an increasing heart failure morbidity and mortality (32) As mentioned in the section 2.3.1, CPs are gaining wide-spread attention to be used as one of the potential candidates for tissue repair and regeneration. There are reports showing that pericytes can be effectively used for the repair of infarcted heart, myocardial ischemia, cardiovascular replacement, skeletal muscle tissue engineering etc. (22, 24-28). In work done by Avolio *et al.,* also states the potential use CPs to create stem cell engineered cardiac implants to treat CHDs (21). Exploration is taking place towards this aspect and researchers are finding ways to differentiate CPs into cardiac specific lineages such as vascular smooth muscle cells (VSMCs), endothelial cells and cardiomyocytes.

In order to be used as an implant for treating CHDs, it is really significant to investigate how the matrix stiffness of the substrate material is affecting the CPs fate in terms of its adhesion, proliferation and differentiation into cardiac specific lineages. This information will help the researchers in the design and modelling of prospective cardiac implants to treat CHDs. Therefore, in this work, CPs were isolated from the neonatal cardiac tissues and were incorporated to the fabricated gelatin nanofibrous scaffolds with varying matrix stiffness. These stem cell engineered nanofibrous scaffolds were then examined *in vitro* to analyse the biocompatibility, CPs attachment, proliferation and differentiation as a function of varying matrix stiffness.

In this chapter, the experiments were performed with cells from three different donors except for viability assay (the details of cells used are mentioned in the Materials and Methods section). Firstly, the results of the experiments carried out in each type of cell cultures are reported separately, and later, the cumulative quantification results from all cell cultures are summarized for viability, ICC and differentiation assay.

4.1. Cardiac Pericytes (CPs) Characterisation

To perform cell studies, the CPs were isolated from the surgical leftovers of children who underwent corrective surgery for CHDs. The microscopic image of isolated CPs is shown in figure.4.1. The CPs were found to be healthy, and all were showing the characteristic spindle-shaped morphology of CPs. The results were consistent with the results reported by Avolio *et al.* in their work on the isolation, expansion and characterisation of CPs from neonatal cardiac tissues (31).

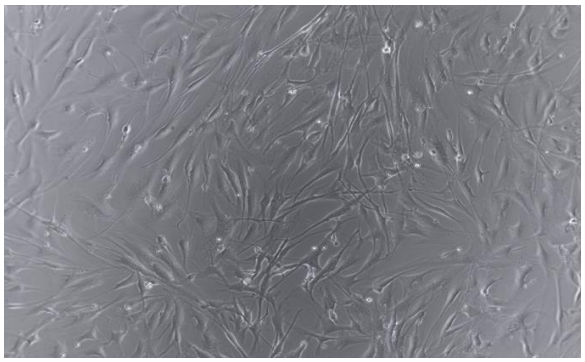

Figure.**4.1.** Phase contrast microscopic image of CPs at Passage 6 of culture (P6). Magnification is 10X.

The isolated CPs were then characterized by ICC assay. The cell expression to each of the pericyte markers and stemness markers are shown in figure.4.2. The blue colour represents the DAPI stained nuclei, and the green represents the positive stains of markers for cytoskeleton/plasma membrane.

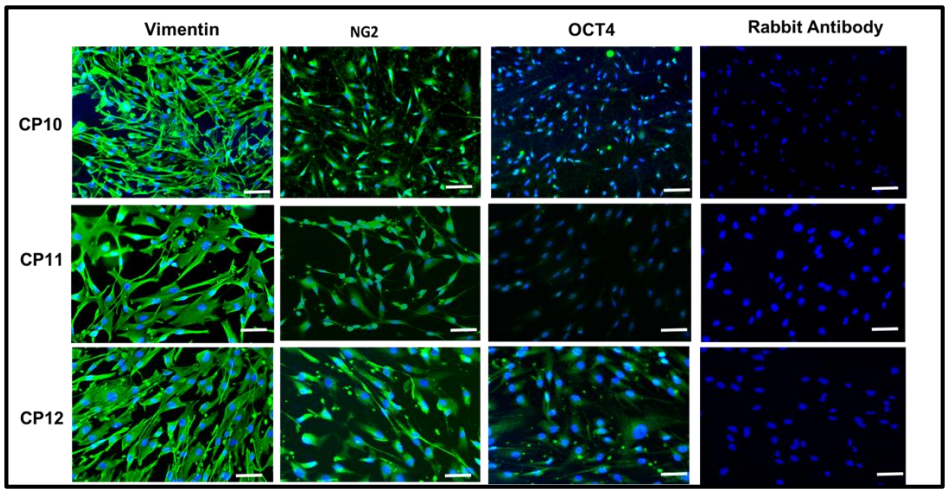

Figure.**4.2.** Immunofluorescence staining for CPs isolated from different donors. . The first column represents the cells stained with Vimentin, the second column shows the cells stained with NG2/CSPG4 (Chondroitin sulphate proteoglycan 4), and the third column displays the cells stained with OCT4 (Octamer-binding protein 4). The fourth column is the rabbit antibody stained nuclei which are the negative control without primary antibodies. CPs were at passage 6 (P6) n=3. Scale bar: 50μm.

The Vimentin can bind to the cytoskeleton, and all the cells stained with an antibody anti-Vimentin expressed strong fluorescence, which confirmed the phenotypic characteristics of isolated CPs at P6 **(Figure.4.2. 1st column).** The cells labelled with an antibody anti-NG2 showed positive expression of the cells, but they were not strong in fluorescence when compared to Vimentin stained CPs. Even though all the cells were positive to the pericyte marker NG2 **(Figure.4.2. 2nd column)**. When the cells were stained with an antibody anti-OCT4, it bound to the nuclei of the cells and showed a positive expression of the marker which means the isolated CPs are maintaining their stemness characteristics **(Figure.4.2. 3rd column).** A small percentage of cells was negative for OCT4, but most of the cells showed a positive expression.

The primary antibodies bind to the specific cell surface receptors (antigens) that are present on the cells. The secondary antibodies labelled with fluorochromes can bind specifically to the epitopes of those primary antibodies, and upon light incidence, they emit fluorescence. The pericyte marker Vimentin bound to the cytoskeleton, NG2 is combined with the plasma membrane and stemness marker OCT4 is incorporated to the nucleus of the CPs and exhibited positive expression to the corresponding markers. The fluorescence intensity is also a factor to determine the extent of CPs expression to each marker. CPs stained with Vimentin, displayed enhanced fluorescence intensity while the CPs stained with NG2 were observed with less fluorescence intensity. Moreover, only a few numbers of cells were expressive for the OCT4 stain, and this can be due to the loss of stemness characteristics of CPs at P6. The quantification of cell density of each cell line is done separately and is given in figure.4.3.

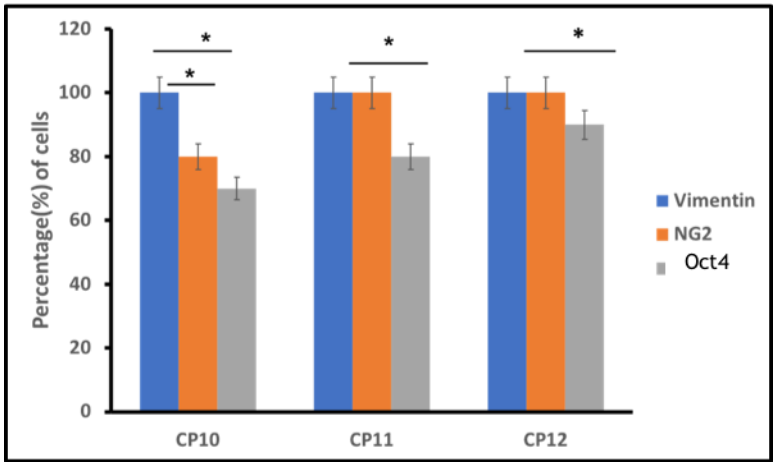

Figure **4.3**. Quantification of ICC on a glass slide. Bar graph represents the percentage of positive cells when CPs are stained with Vimentin, NG2 and OCT4 in CP10, CP11 and CP12 cell types. CPs were at passage 6 (P6) n=3. Scale bar: 50μm. Values are expressed as means±SEM. *P<0.05.

In the quantification analysis, all cell cultures demonstrated 100% positive expression for Vimentin. In CP11 and CP12, 100% of CPs were positive when stained with NG2, however in CP10 cell lines, only 80±3% of the cells were positive, and this difference was significant. The OCT4 represented the lowest percentage of positive cells in all three cell cultures, and this difference was statistically significant when compared to the other counterparts in all three cell cultures **(Figure.4.3)**. Previous studies had reported that when the cells were expanded to several passages, the CPs reduced their positive expression. This means as the cells reach higher passages, they will lose their specific characteristic features (31). For example, in the work of Avolio *et al.*, they observed a substantial reduction in the CP's expression of stemness markers OCT4 and NANOG when they were cultured up to 9 passages (31). Here also we observed the same trend of reduction in the stemness marker expression of OCT4 when CPs were stained at passage 6.

Hence the isolated CPs were characterized and found that they were positive for all the tested markers while a reduced expression for stemness marker at P6. The next step was to study the cytocompatibility of gelatin nanofibrous scaffolds with different matrix stiffness and to find out which scaffold/matrix stiffness is more favourable for the cells to attach.

4.2. Effect of matrix stiffness on CPs viability

The live/dead assay was performed to determine whether stiffness can affect the CPs' viability. After 7 days of incubation in the ECGM2 media, the CPs-seeded scaffolds were stained with Calcein AM and EthD III to image the viable and dead cells. This assay was also performed to understand whether the EDC/NHS and Glu cross-linked gelatin nanofibrous scaffolds are biocompatible to CPs and they are supporting the attachment of CPs. An ideal scaffold should

be well-suited for CPs to support the cell attachment and thereby proliferation and differentiation. The experiments were done in four cell cultures isolated from four different donors to relate the behaviour of CPs isolated from different patients and to obtain a meaningful result. The result of the viability assay carried out in CP10 cell line is given in figure.4.4.

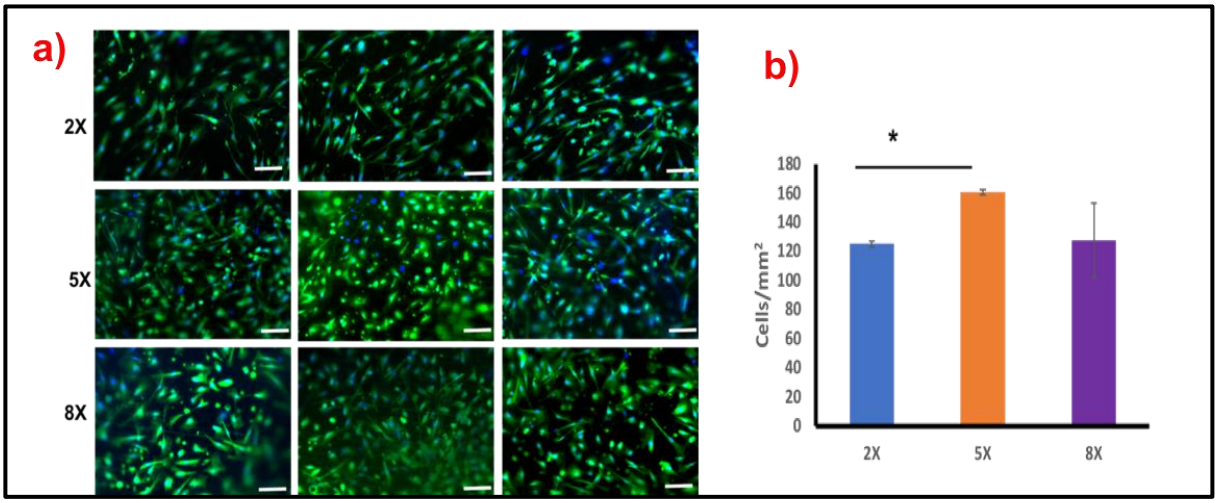

Figure.**4.4.** Viability assay of CP10 (P5) cells on gelatin scaffolds with different cross-linking densities. In the image (a), the first row represents the CPs on 2X CLGS; the second row shows the CPs on 5X CLGS and third row displays the CPs on 8XCLGS. The green colour represents the live cells, and the nuclei are shown in blue colour. The bar diagram (b) denotes the quantification of viable cell density on each scaffold (*$p<0.05$), cells were at passage 5 (P5). Values are expressed as means±SEM. Scale bar: 50µm.

From the images, it was found that none of the cells on the scaffolds were positive to Ethidium III. Consequently, all the cells expressed green fluorescence, which indicated live cells (**Figure.4.4. a)**. Calcein AM is a membrane permeable non-fluorescent esterase substrate, which enters the cytoplasm of live cells and the esterase in live cells cleaves calcein AM into

calcein and yields green fluorescence. EthD III penetrates the dead cells and stains the nucleus with bright red fluorescence. Therefore, almost 100% viability was obtained for all scaffolds irrespective of their matrix stiffness, which means they are non-toxic and support CPs attachment even after 7 days of incubation. It was evident that there was more CPs attachment on the 5X and 8X CLGS when compared to 2X CLGS. The cell density was also quantified to distinguish the number of cells alive and attaching on each scaffold. It was found that the cell density on 5X and 8X CLGS were similar, whereas the cell density on 2X CLGS exhibited a significant difference when compared to 5X CLGS (**Figure.4.4. b)**. The cell density of 2X scaffolds were found to be 120±5 cells/mm^2 . The 5X scaffolds showed an average cell density of 160±10 cells/$mm^{2,}$ while 8X scaffolds revealed a similar trend of 120±30 cells/mm^2 .

Next, the viability assay was performed in the CP11 cell culture, and the results are displayed in figure. 4.5.

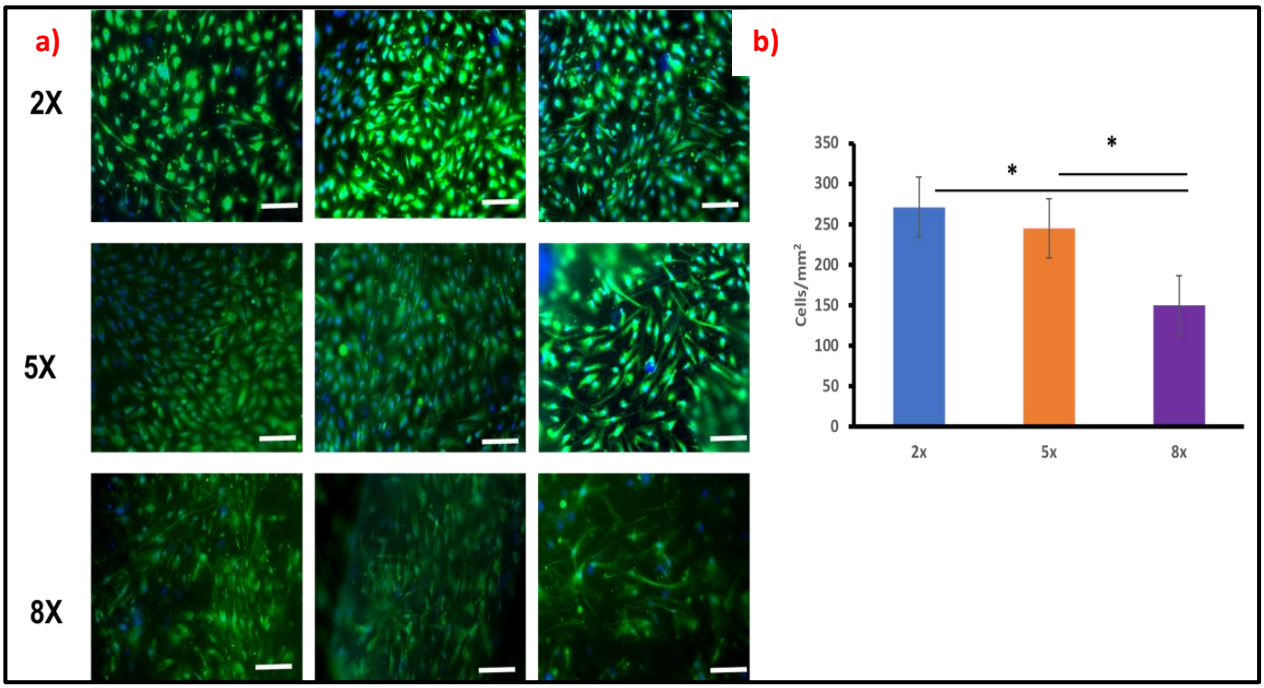

Figure.**4.5.** Viability assay of CP11 (P5) cells on scaffolds with different cross-linking densities. In mage (a), the first row represents the CPs on 2X CLGS; second row shows the CPs on 5X CLGS and third row displays the CPs on 8X CLGS. The green colour represents the live cells, and the nuclei are shown in blue colour. The bar diagram (b) denotes the quantification of cell density on each scaffold (*$p<0.05$), cells were at passage 5 (P5). Values are expressed as means±SEM. Scale bar: 50µm.

Similar to the result obtained from the CP10 cell line, here also CPs were 100% viable on all scaffolds irrespective of their matrix stiffness (**Figure.4.5. a)**. The only difference was in the cell density among the three scaffolds. In CP11cell line, the 2X and 5X CLGS presented the highest cell density compared to 8XCLGS. The difference in the cell density of 8X CLGS was statistically significant with respect to the other two counterparts (**Figure.4.5. b)**. An average cell density of 260±30 cells/mm^2 was exhibited by 2XCLGS, and 5X CLGS were found to be

with 240±40 cell/mm^2. However, the 8X scaffolds showed the lowest cell density of 150±50 cells/mm^2 (**Figure. 4.5. b)**.

Following the viability checks in CP10 and CP11 cell lines, the live-dead assay was performed in CP12 cells cultured on each scaffold. The results of the viability assay examined in the CP12 cells are shown in figure. 4.6.

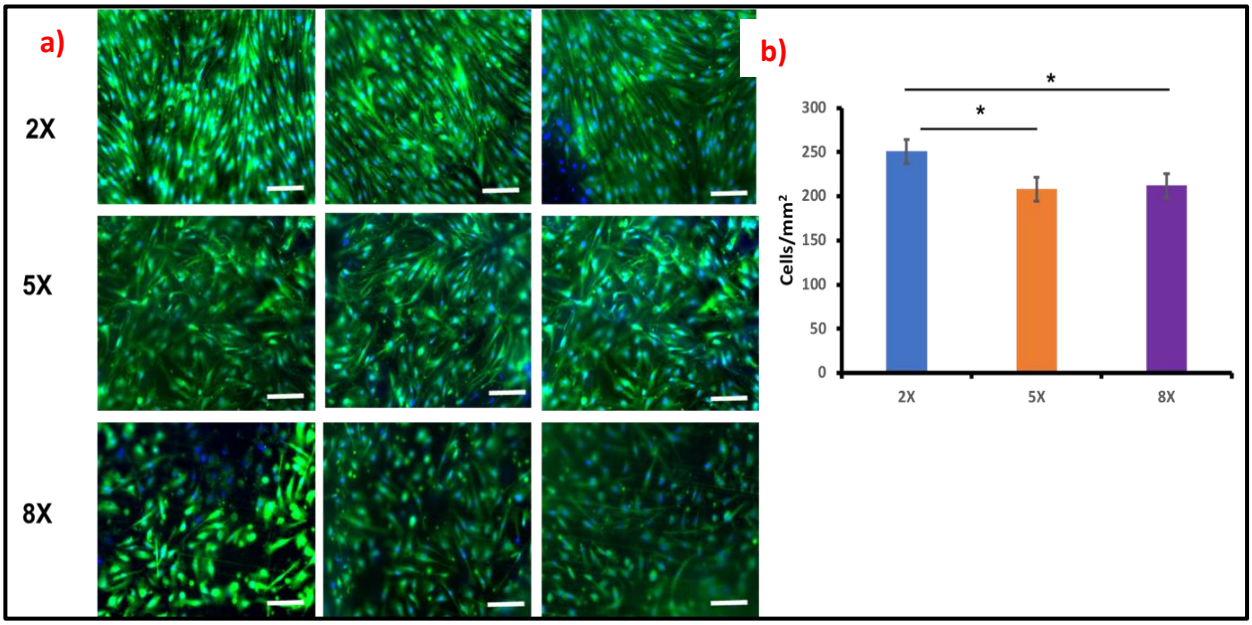

Figure.**4.6.** Viability assay of CP12 (P5) cells on scaffolds with different cross-linking densities. In the image (a), the first row represents the CPs on 2X CLGS; second row shows the CPs on 5X CLGS and third row displays the CPs on 8X CLGS. The green colour represents the live cells, and the nuclei are shown in blue colour. The bar diagram (b) denotes the quantification of cell density on each scaffold (*$p<0.05$), cells were at passage 5 (P5). Values are expressed as means±SEM. Scale bar: 50μm.

From the images, it was clear that the same trend of 100% viability was acquired by all the scaffolds (**Figure.4.6. a)**. As observed in CP11, the 8X CLGS displayed reduced cell density, and this reduction was significant when compared to the 2X CLGS (**Figure.4.6. b)**. The 2X scaffolds denoted highest cell density of 250±20 cells/mm^2 and this showed a considerable increase compared to 5X and 8XCLGS. The 5X and 8X CLGS presented an average cell density of 200±10 cells/mm^2 **(Figure.4.6. b).**

The viability assay was performed in one more cell culture as the results obtained was not sufficient in attaining a substantial outcome. The next cell culture used for the viability assay was CP34, and the results obtained are shown in figure.4.7.

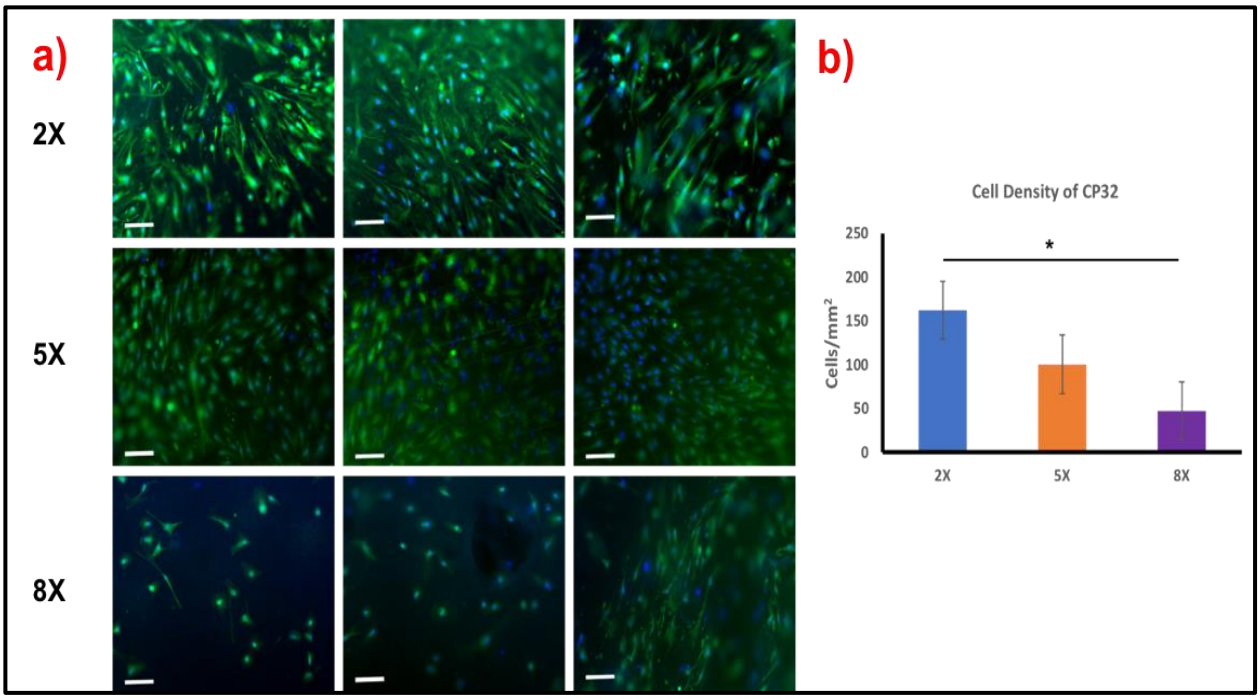

Figure.**4.7.** Viability assay of CP32 (P5) cells on scaffolds with different cross-linking densities. In the image (a), the first row represents the CPs on 2X CLGS; second row shows the CPs on 5X CLGS and third row displays the CPs on 8X CLGS. The green colour represents the live cells, and the nuclei are shown in blue colour. The bar diagram (b) denotes the quantification of cell density on each scaffold (*$p<0.05$), cells were at passage 5 (P5). Values are expressed as means±SEM. Scale bar: 50µm.

In the CP32 cell line, even though all cells were viable, there observed a massive difference in the cell density of CPs on the 8X CLGS with respect to other scaffolds (**Figure.4.7. a)**. The cell density of both 2X and 5X CLGS were found to be 150±30 cells/mm^2 and 100±40 cells/mm^{2,} respectively. The cell density of 8X CLGS were considerably lower and was 30±20 cells/mm^2 (**Figure.4.7. b)**.

All four cell cultures exhibited different cell density on the scaffolds. The CP11 and CP12 cell lines showed similar results in the maximum cells adhered on the scaffolds, while the CP10 and CP32 cell cultures displayed a lower number of cell attachment on scaffolds. This can be explained as because of the effect of matrix stiffness and different confluency rates among the cell cultures. From the images, it was observed that both CP10 and CP32 cells were less confluent on the scaffolds when compared to CP11 and CP12. It is hypothesised that not all cells should acquire the same confluency even if they are in the same passage. The confluency depends on various factors such as the nutrients in the growth medium, temperature, humidity and carbon dioxide supply. Here in this work, all cell cultures were maintained in the same conditions and supplemented with the same ECGM2 media, but CPs exhibited different confluency on the scaffolds. So, the possible reason for this reduced confluency in different cell lines may be due to the effect of matrix stiffness and variance in the characteristic features of the tissue donors. Even though the cells were obtained from the neonatal heart tissues; they were from different donors with different pathology. Another observation in the viability assay was the anisotropic behaviour of CPs on scaffolds with lower stiffness, i.e. 2X CLGS **(Figure.4.5 a).** Nevertheless, this was evident only for CP12 cells. The higher confluency of CP12 would have contributed for this anisotropic behaviour of CPs on 2X CLGS. Further experiments with an increased number of cell cultures and duration are essential to justify this observation.

In order to find out the optimal scaffold for CPs adhesion and to analyse the effect of matrix stiffness on CPs adhesion, a cumulative cell density of all four cell types was calculated, and results are shown in figure.4.8.

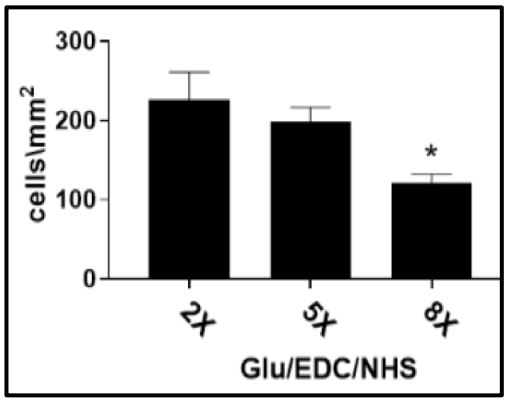

Figure. **4.8.** Bar graph representing cumulative cell density on different types of scaffolds. Values are mean and SE, n=4 cell cultures at passage 5 of culture. ANOVA, $P<0.05$; Tukey's multiple comparisons test adjusted P values: *$P<0.05$ vs 2X.

There observed a substantial difference in the cell density of 8X scaffolds compared to the 2X CLGS, but there was no statistical difference in the cell density between the 5X and 8X CLGS. This suggests that CPs are more likely to attach and flourish on softer substrates that have an average fibre diameter of 400nm. The 2X CLGS exhibited a cumulative cell density of 220±60 cells/mm^2 while 5X and 8X CLGS displayed a cell density of 190±60 cells/mm^2 and 120±10 cells/mm^2 respectively **(Figure.4.8).**

There are many studies associated with the influence of matrix stiffness on cell adhesion and spreading (35, 199-202). As mentioned in section 2.2, the cell-material interactions are aided by a complex network of proteins called integrins, which are the transmembrane proteins bound to the ECM. These adhesion proteins bind the ECM and cytoskeleton of the cells. As a result, the cell experiences forces that are exerted by the ECM and the cells adapt to these microenvironmental forces by adjusting their cytoskeletal contractility. In response to this cytoskeletal contractility, substrates with different matrix stiffness generate different types of

adhesion (203-205). Hence the matrix stiffness plays a vital role in creating the focal adhesions, which are essential for tissue formation (205). From the results, it was evident that CPs are happier to adhere either on softer substrates or substrates with a higher magnitude of fiber diameter (2X scaffolds). The softer substrates with larger fiber diameter would have created more focal adhesions for the CPs to attach. Hence the coupled effect of scaffold elasticity and morphology generated more adhesion sites by altering the cytoskeletal contractility.

Pelham and Wang in 1997, reported that cell attachment and spreading is the first cell function that is influenced by the matrix stiffness/elasticity (206). Subsequent studies have explained the cell-material interactions as a function of matrix elasticity by culturing different cell types on gels or scaffolds with varying matrix stiffness (207-212). For example, when smooth muscle cells (SMCs) were cultured on substrates with different matrix elasticity, it was found that the SMC's spreading increased with matrix elasticity (80, 207). Similarly, the endothelial cells grown on softer substrates of maleic acid copolymer (MACP)-coated polyacrylamide (PAAm) gel showed enhanced cell attachment and spreading (213). In contrast, the cell spreading of the pre-osteoblast cell line (MC3T3-E1) on type I collagen-modified hydrogels were found to be independent of the matrix stiffness. This shows the difference in the cell-material interaction based on different cell types. These variations in the cell-matrix interactions also suggest the importance of exploring different cell's interactions with the matrix, specifically as different cell types experience different cytoskeletal contractility based on the matrix stiffness.

Furthermore, the CPs adhesion on all scaffolds without any dead cells implicates the cytocompatibility of the scaffolds. An ideal scaffold should be non-toxic, porous, biodegradable and mechanically strong to be used for tissue engineering applications (35, 201, 202). The biomimetic nanofibrous structure, which resembles the native ECM and gelatin's

innate ability to foster cell adhesion and promote proteolytic degradation also would have helped CPs to remain viable on all scaffolds (214, 215).

Hence the live/dead assay demonstrated the CLGS capability to support CPs adhesion and thereby the biocompatibility of scaffolds irrespective of their matrix stiffness. Additionally, the softer substrates with a fiber diameter of ~400nm exhibited increased CPs adhesion compared to other scaffolds. After this, the CPs ability to maintain its characteristic features on scaffolds with different matrix stiffness were analysed by performing immunocytochemistry (ICC) assay.

4.3. Effect of matrix stiffness on CPs expression of typical phenotypic and stemness markers

Using immunocytochemistry (ICC), this study next assessed if variation in stiffness could affect the expression of typical antigenic markers. The CPs seeded on scaffolds were incubated for two days in the ECGM2 media and then permeabilised/fixed for staining with primary antibodies followed by secondary antibody staining. The purpose of this assay was to investigate whether the CPs are maintaining their characteristics features when seeded on CLGS with varying matrix stiffness. This experiment was also performed in three cell cultures in order to establish a substantial result. The result of the ICC assay on CP10 cell culture is displayed in figure.4.9.

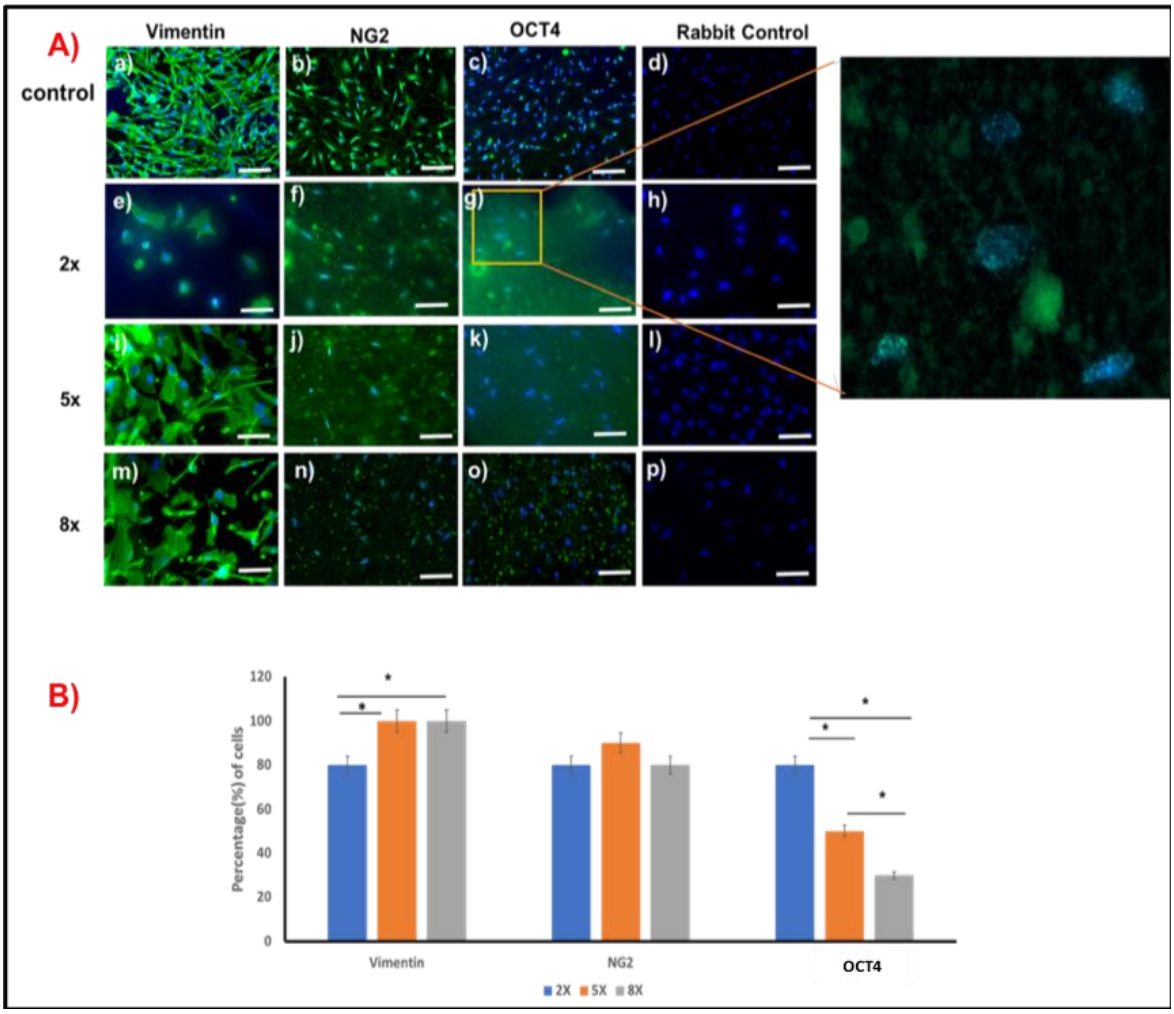

Figure. **4.9.** ICC of CP10 (P6) cells on scaffolds with different matrix stiffness . A) Fluorescent microscopic images of CPs expression on 2X, 5X and 8X CLGS. a-c): CPs expression for the markers Vimentin, NG2 and OCT4 on glass slide (positive control), e-g): CPs expression for the markers Vimentin, NG2 and OCT4 on 2X CLGS, i-k): CPs expression for the markers Vimentin, NG2 and OCT4 on 5X CLGS. m-o): CPs expression for the markers Vimentin, NG2 and OCT4 on 8X CLGS. d), h), i) and p) displays the images of negative control without primary antibody. An enlarged view of the marked section of the image g) is also shown, which represents the positive expression of OCT4 on 2X CLGS. The bar diagram B) displays the quantification of CPs expression on 2X, 5X and 8X CLGS, respectively (*$p<0.05$). Scale bar:

50μm. Values are expressed as means±SEM. Green fluorescence represents the cytoskeleton/plasma membrane and blue represents DAPI stained nuclei.

From the images, it was evident that the number of cells on all scaffolds were lower compared to the control. This result was supporting the report from the viability assay that the CP10 cells were less confluent on scaffolds. The CPs seeded on glass slides were used as the control, and they exhibited positive expression when stained with Vimentin, NG2 and OCT4 **(Figure.4.9. a-c)**. The CPs morphology on 2X CLGS when stained with antibody anti-Vimentin were found to be round, and there were not many cells expressing the Vimentin marker **(Figure.4.9. e)**. This indicates that either CPs were deprived of nutrients essential for their growth or the effect of the matrix would have hindered the formation of their characteristic spindle shape. Whereas both 5X and 8X CLGS exhibited a strong green fluorescence when stained with Vimentin as obtained in control **(Figure 4.9. i&m).** For NG2, only a few numbers of cells exhibited a positive expression on all scaffolds and the fluorescence was not strong compared to the control **(Figure.4.9. f, j&n)**. Nevertheless, more than half of the CPs showed the phenotypic features on each scaffold by expressing NG2 even at the 5^{th} passage of the culture. All the scaffolds expressed a positive signal for OCT4 stained CPs by binding to the nucleus, but they showed a smaller number of positive expressed cells **(Figure.4.9. g, k&o).** As mentioned earlier, it is not necessary that all cells were positive for the same markers. The OCT4 expression of CPs was clearly visible in the enlarged section of the image (g). The appearance of small granules revealed the positive expression of CPs on different scaffolds when stained with OCT4. Hence, we found that CPs demonstrated their characteristic stemness even at the 5^{th} passage of the culture but with a reduced number of positive cell expression.

From the quantification analysis, it was found that 100% of CPs were positive when stained with Vimentin; however, 2X CLGS expressed a noteworthy reduction of 80% when stained with Vimentin. There was no statistical difference in the appearance of CPs on scaffolds with different matrix stiffness when stained with NG2. The OCT4 stained CPs disclosed the lowest percentage of cell expression when compared to the markers Vimentin and NG2. Here as the matrix stiffness of the scaffolds increased, the OCT 4 expression of CPs reduced. Otherwise, as the matrix stiffness of gelatin nanofibrous scaffolds increased the stemness behaviour of CPs decreased. This reduction was substantial among the three scaffolds **(Figure.4.9. B)**. This potential difference can be attributed because of the difference in the matrix stiffness of the scaffolds.

Later, the ICC staining was performed in CP11 cells to analyse the effect of matrix stiffness in maintaining CPs phenotypic characteristics and stemness on scaffolds with different matrix stiffness. The results of the ICC assay on CP11 cells are presented in figure.4.10.

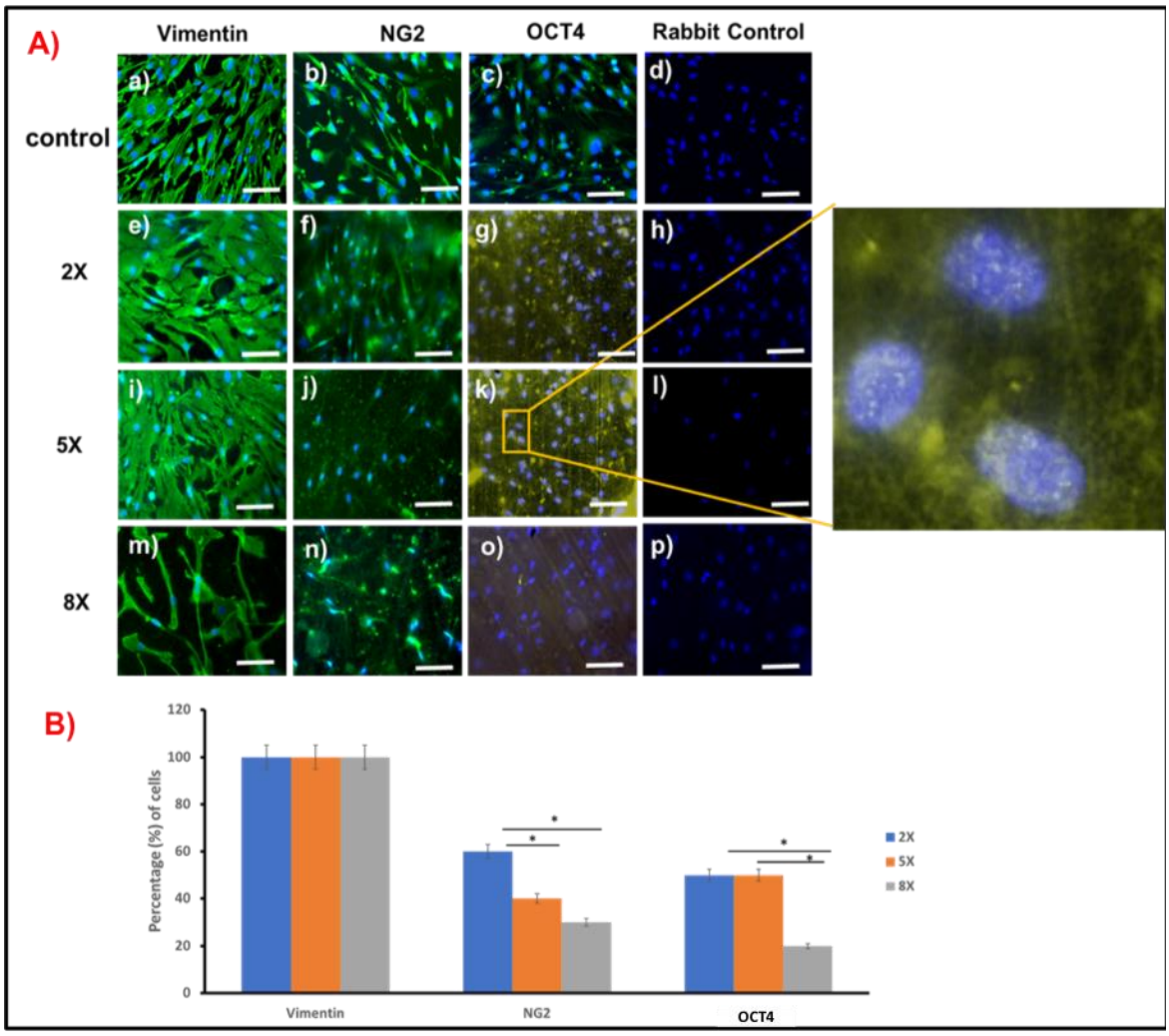

Figure. **4.10.** ICC of CP11 (P6) cells on scaffolds with different matrix stiffness. A) Fluorescent microscopic images of CPs expression on 2X, 5X and 8X CLGS. a-c): CPs expression for the markers Vimentin, NG2 and OCT4 on glass slide (positive control), e-g): CPs expression for the markers Vimentin, NG2 and OCT4 on 2X CLGS, i-k): CPs expression for the markers Vimentin, NG2 and OCT4 on 5X CLGS. m-o): CPs expression for the markers Vimentin, NG2 and OCT4 on 8X CLGS. d), h), l) and p) displays the images of negative control without primary antibody. An enlarged view of the marked section of image k) is also shown, which represents the positive expression of OCT4 on 5X CLGS. The bar diagram B) displays the quantification of CPs expression on 2X, 5X and 8X CLGS, respectively (*$p<0.05$),

Scale bar: 50 µm. Values are expressed as means ± SEM. Green fluorescence represents the cytoskeleton/plasma membrane and blue represents DAPI stained nuclei.

The CPs seeded on glass slides were used as the control, and they exhibited positive expression when stained with Vimentin, NG2 and OCT4 **(Figure.4.10. a-c)**. From the images, it was obvious that the CPs stained with Vimentin showed strong fluorescence on both 2X and 5X CLGS while 8X CLGS exposed light fluorescence with a smaller number of positive cells **(Figure.4.10. e, i&m).** The CPs morphology on 8X CLGS when stained with Vimentin were found to be elongated, and they were stretched so that they lost their spindle-shaped morphology **(Figure.4.10. m).** For NG2, a similar result was obtained as that of CP10 cells. All scaffolds displayed the positive expression of NG2, but the number of positive CPs were less compared to control **(Figure.4.10. f, j&n).** In the case of OCT4 stained cells, a low percentage of CPs exhibited the positive signals **(Figure.4.10. g, k&o),** and the enlarged image of the enclosed section of the image (k) clearly confirmed the positive appearance of OCT4 on 5X CLGS.

From the quantification analysis, it was found that almost 100% of CPs were positive when stained with Vimentin on all scaffolds. However, the number of cells on the 8X CLGS were less compared to the control and other counterparts **(Figure.4.10. B)**. When CPs were stained with NG2, a gradual decrease in the percentage of positive cells was found with increased matrix stiffness. For example, around 60% of CPs were positive for NG2 stained 2X CLGS, whereas 5X and 8X CLGS were measured with an average positive cell of about 40% and 30% respectively **(Figure.4.10. B)**. They exhibited a considerable difference in the percentage of positive CPs when stained with NG2. Furthermore, the OCT4 stained CPs disclosed the lowest

percentage of cell expression when compared to the markers Vimentin and NG2. When the CPs were stained with OCT4, both 2X and 5X CLGS displayed an average of 50 % positive expression, while the 8X CLGS revealed less than 20% of positive cells. This reduction was substantial when compared with 2X and 5X CLGS **(Figure.4.10. B).**

The next step was to analyse the CP12 cell cultures. The results of the ICC assay on CP12 cells are presented in figure.4.11.

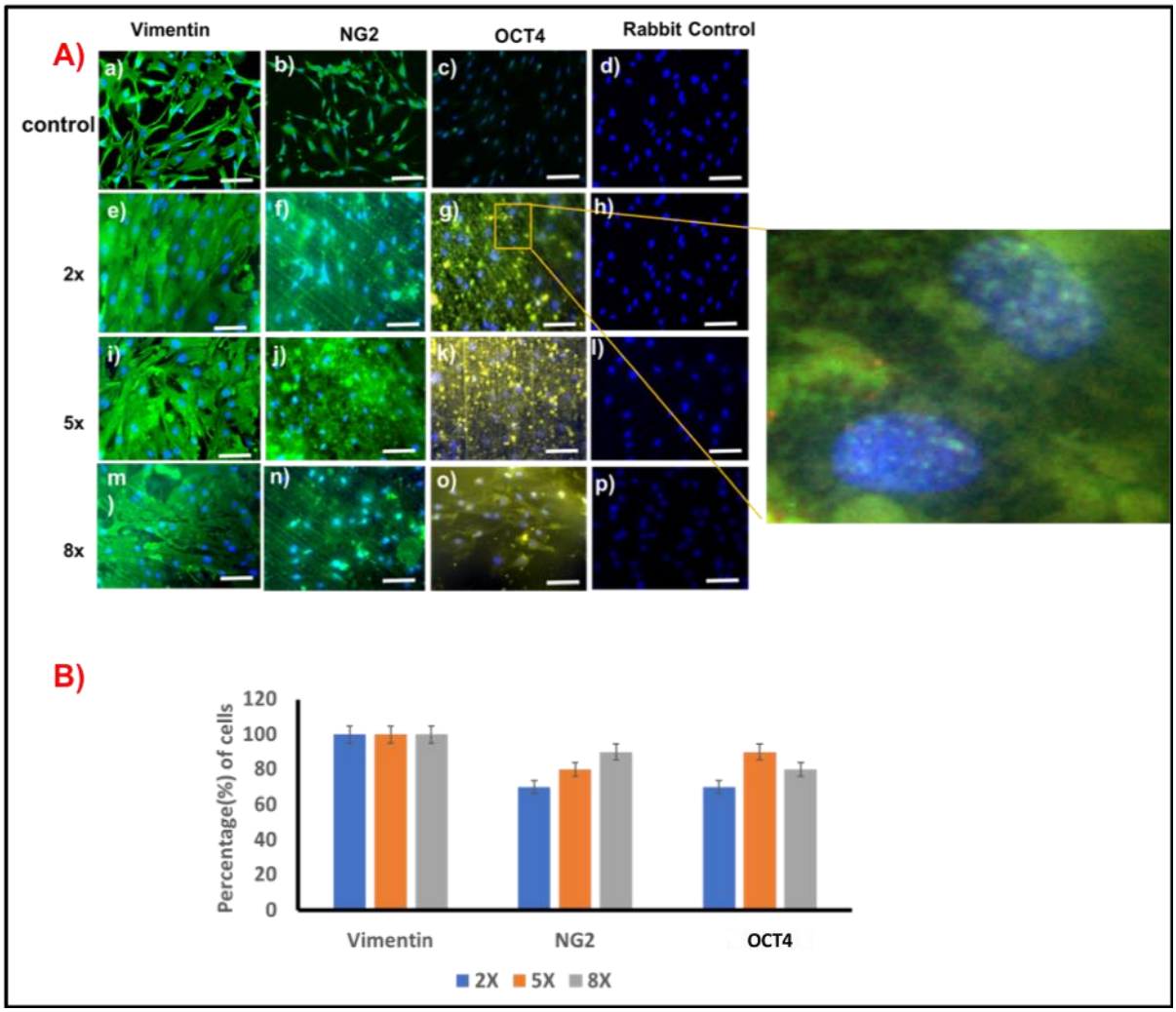

Figure. **4.11.** ICC of CP12 (P6) cells on scaffolds with different matrix stiffness. A) Fluorescent microscopic images of CPs expression on 2X, 5X and 8X CLGS. a)-c): CPs expression for the markers Vimentin, NG2 and OCT4 on glass slide (positive control), e)-g): CPs expression for the markers Vimentin, NG2 and OCT4 on 2X CLGS, i)-k): CPs expression for the markers Vimentin, NG2 and OCT4 on 5X CLGS. m)-o): CPs expression for the markers Vimentin, NG2 and OCT4 on 8X CLGS. d), h), l) and p) displays the images of negative control without primary antibody. An enlarged view of the marked section of the image g) is also shown, which represents the positive expression of OCT4 on 2X CLGS. The bar diagram B) displays the quantification of CPs expression on 2X, 5X and 8X CLGS respectively. Scale bar: 50 µm.

Values are expressed as means ± SEM. Green fluorescence represents the cytoskeleton/plasma membrane and blue represents DAPI stained nuclei.

The CPs seeded on glass slides were used as the control, and they exhibited positive expression when stained with Vimentin, NG2 and OCT4 **(Figure.4.11. a-c)**. From the images, it was noticeable that the CPs stained with Vimentin presented strong fluorescence on all the scaffolds irrespective of their matrix stiffness **(Figure.4.11. e, i&m).** All CLGS demonstrated positive expression of NG2, but the fluorescence intensity was less compared to control **(Figure.4.11. f, j& n).** In OCT4 stained cells, more CPs were found to be positive when compared to the other two cell cultures **(Figure.4.11. g, k & o).** Also, the enlarged image of the enclosed section of the image (g) clearly confirmed the positive appearance of OCT4 on 2X CLGS.

From the quantification analysis, almost all the scaffolds exhibited100% positive signals when stained with Vimentin **(Figure.4.11. B)**. As different from other cell cultures, when CPs were stained with NG2, a gradual increase in the percentage of positive cells were found with increased matrix stiffness, but this difference was not statistically significant. Additionally, the percentage of positive CPs when stained with OCT4 were higher when compared to the other two cell cultures. Also, there was no substantial difference in the percentage of positive cells among each scaffold **(Figure.4.10. B)**.

Hence from the fluorescent images of all three cell cultures, concluded that all CPs were maintaining their phenotype and stemness on all scaffolds irrespective of their stiffness. But in order to get a meaningful quantification result, the cumulative percentage of positive cell expression for each marker in all three cell cultures were calculated and the graph showing these results are displayed in figure.4.12.

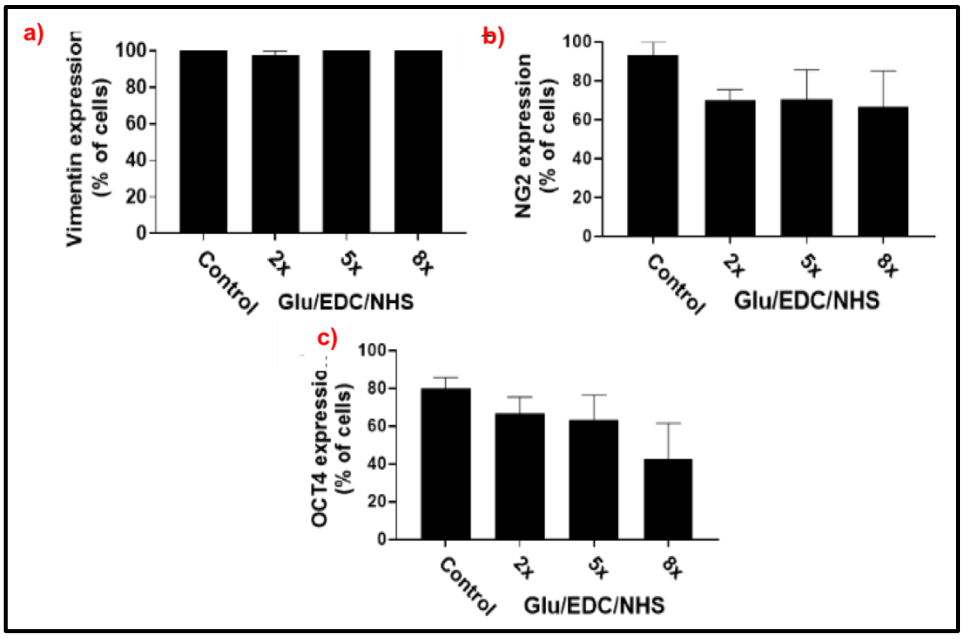

Figure. **4.12**. Cumulative quantification of CPs expression on scaffolds with different matrix stiffness. Bar graphs show the quantification analysis of the positive expression of markers Vimentin (a), NG2 (b) and OCT4 (c) on each scaffold compared to control (glass slide). Values are expressed as means±SEM (n=3 CPs, *p<0.05)

CPs exhibited almost 100% positive signals when stained with Vimentin, which was the same when compared to the control **(Figure.4.12. a).** NG2 stained CPs also showed a similar amount of positive expression compared to the control **(Figure.4.12. b).** Hence from the results of three cell cultures, it was concluded that CPs are maintaining their specific antigenic phenotype in all scaffolds irrespective of their matrix stiffness. Whereas in OCT4, CPs displayed a reduced expression on the 8X CLGS, which was around 45±15%; however, there was no significant difference when compared to the control. All other counterparts revealed a similar percentage of expression when compared to the control **(Figure.5.12. c).** Therefore, it was found that the CPs maintained their unique antigenic properties independent of their matrix stiffness.

In work done by Avolio *et al*., they seeded CPs in a xenograft scaffold called CorMatrix and analysed the possibility of creating CPs-engineered graft for treating CHDs. They also investigated the CPs ability to maintain their phenotypic characteristics by performing the fluorescence staining with Vimentin, NG2 and PDGFR-β. They found that the CPs were able to retain their antigenic properties by showing positive expression for Vimentin, NG2 and PDGFR-β antibodies (31). Our study also supports this finding as all CPs cultured on CLGS exhibited positive signals for Vimentin and NG2 antibodies.

Hence from the results, it was found that CPs seeded on CLGS with different matrix stiffness maintained their antigenic profile. Later, the morphology of CPs when cultured on CLGS were analysed.

4.4. Effect of matrix stiffness on CPs morphology

To further investigate the morphological changes induced by variation in matrix stiffness, CPs were incubated on scaffolds for seven days and then fixed, dried and sputter coated for SEM analysis. The SEM images of cell attachment on plastic, 2X, 5X and 8X CLGS after 7 days of incubation are shown in figure.4.12. Plastic was used as the control to understand the changes in cell shape and morphology compared to CPs attached on scaffolds. The cells used in this experiment was CP12.

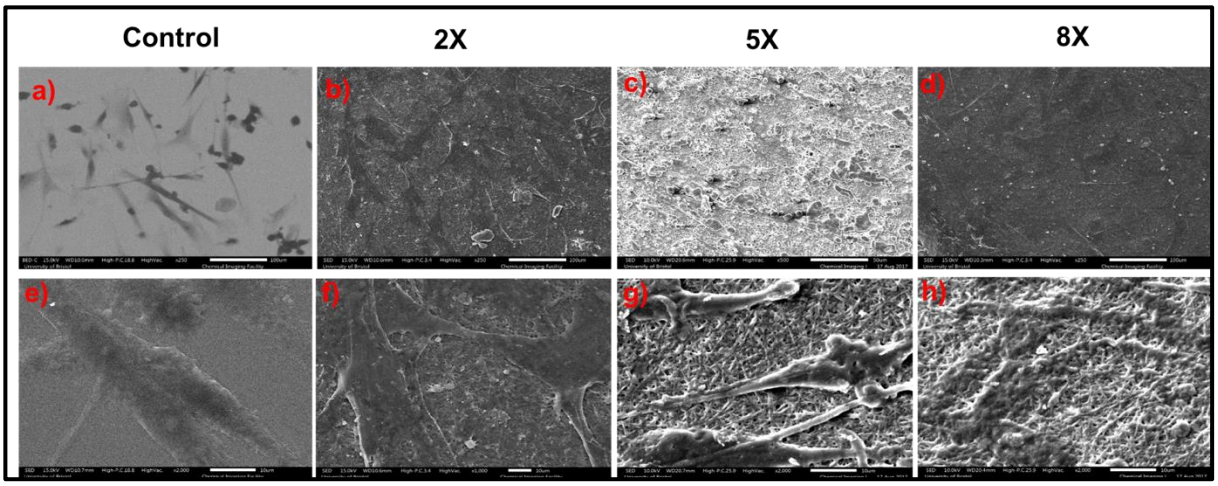

Figure.**4.13**. Figure.**4.13**. SEM images of CPs adhesion on scaffolds with different matrix stiffness. (a-d) displays the CPs attachment on plastic, 2X, 5X and 8X CLGS, respectively. (e-h) Denotes the higher magnification images of CPs attachment on plastic, 2X, 5X and 8X CLGS respectively.

From the SEM images, CPs exhibited a combination of round and spindle-shaped morphology **(Figure.4.13. a).** When seeded on scaffolds, CPs were widespread to generate a 3D cellular network **(Figure.4.13. b-d).** The typical spindle-shape of CPs were well observed in both 2X and 5X scaffolds **(Figure. 4.13. f & g)** while in the 8X CLGS, the cells were elongated, and the spindle shape was not evident **(Figure. 4.13.h).** The cell margins were clearly understood in the SEM images of 2X, and 5X CLGS and the CPs were widespread to generate a cellular network. In contrast, CPs seeded on the 8X CLGS were merged to the nanofibers. Wide spreading of CPs while maintaining their characteristic spindle-shape was witnessed in both 2X and 5X CLGS compared to the control.

The CPs morphological change on the 8X CLGS could be due to several factors. The cell elongation often represents that the cells are deprived of nutrients and are stretching their

structure to find more favourable conditions for their growth. Previous studies have shown that porosity of the scaffolds plays a vital role in cell adhesion and growth by providing essential nutrients and gaseous exchange (216-218). The increased cross-linking density of 8X scaffold might have caused the reduction in pore size and thereby, inadequate nutrient supply to CPs. There are studies suggesting porosity of the graft is crucial for cell migration and deep cell infiltration (219, 220). For example, Druecke *et al.*, evaluated the effect of different pore size of poly (ether ester) block-copolymer scaffolds on vascularization when implanted into the dorsal skinfold chamber of mice. They found that the highest neovascularization was attained by the scaffolds with a pore size of 250-300μm (220). Hence optimum porosity is essential for sufficient nutrient supply for the cells to grow and assist vascularization. So, the morphological behaviour of CPs on 2X and 5X CLGS indicated that they have enough pore size for CPs to maintain their spindle-shape by providing sufficient nutrient supply.

The widespread cellular network formation in both 2X and 5X CLGS can be explained as because of the biocompatible and non-toxic behaviour of the prepared CLGS. There are reports highlighting the excellent properties of gelatin to foster cell adhesion and promote proteolytic degradation, which is fundamental for the cell spreading in a 3D environment (214). The increased cross-linking density of the 8X CLGS can reduce the matrix elasticity and thereby mitigate the focal adhesion points. This would have resulted in the reduced degradation of the scaffolds by cell-secreted matrix metalloproteinase (MMP), which adversely affected the healthy cell spreading. Additionally, the results also proved that the proteolytic degradation products of the gelatin nanofibrous scaffolds are non-toxic for CPs to adhere to the scaffolds.

In a study conducted by Adelow *et al*. (2008), they fabricated peptide functionalised poly (ethylene glycol) hydrogel with different matrix stiffness by altering the ratios of cross-linker

and the polymer-peptide ratios. They then encapsulated Mesenchymal stem cells (MSCs)and SMCs to examine the viability and spreading of cells in different matrix stiffness. They found that the cells were susceptible to gel mechanics, and the softer hydrogels allowed broad cell spreading and viability while the stiffer hydrogels only remained as viable without any cell spreading. This result agrees to our findings, although the scaffolds differed in the range of matrix stiffness (221).

SEM analysis has been widely used to assess the biocompatibility and cell attachment of the fabricated scaffolds (216-218). For example, Sudheesh *et al.* developed chitosan nanofibrin composite hydrogels for skin tissue regeneration and evaluated the adhesion of Human Umbilical Cord Vein Endothelial cells (HUVECs) and Human Dermal Fibroblasts (HDF) on scaffolds with different concentration of nanofibrin. They found that cells changed their morphology and were nicely spread when cells seeded on scaffolds with 2% nanofibrin than the control (217). Hence the SEM analysis also supports the fact that the prepared CLGS are non-toxic and provide physical support as native ECM does *in vivo*. Moreover, flexible and softer substrates were found to be more favourable for the CPs to adhere and grow than the plastic proved the closer resemblance of 2X and 5X CLGS with native proteoglycans (214).

Thus, from the results, it was found that cells are happier to adhere, grow and flourish on softer substrates rather than stiffer substrates. As the cross-linking density increased, the cells changed its shape from spindle to elongated structure and found to be merged entirely to the nanofibers. After cell shape analysis, the effect of matrix stiffness on CPs proliferation rate was investigated.

4.5. Effect of matrix stiffness on CPs proliferation

Next, the proliferation of CPs on 2X, 5X and 8X CLGS using the EdU incorporation assay, which is an indicator of active DNA synthesis was examined (87). The proliferation of CPs on 2X, 5X and 8X CLGS are shown in figure.4.14. The red colour represents the nuclei of the proliferating cells, and blue represents the DAPI stained nuclei of non-proliferating cells.

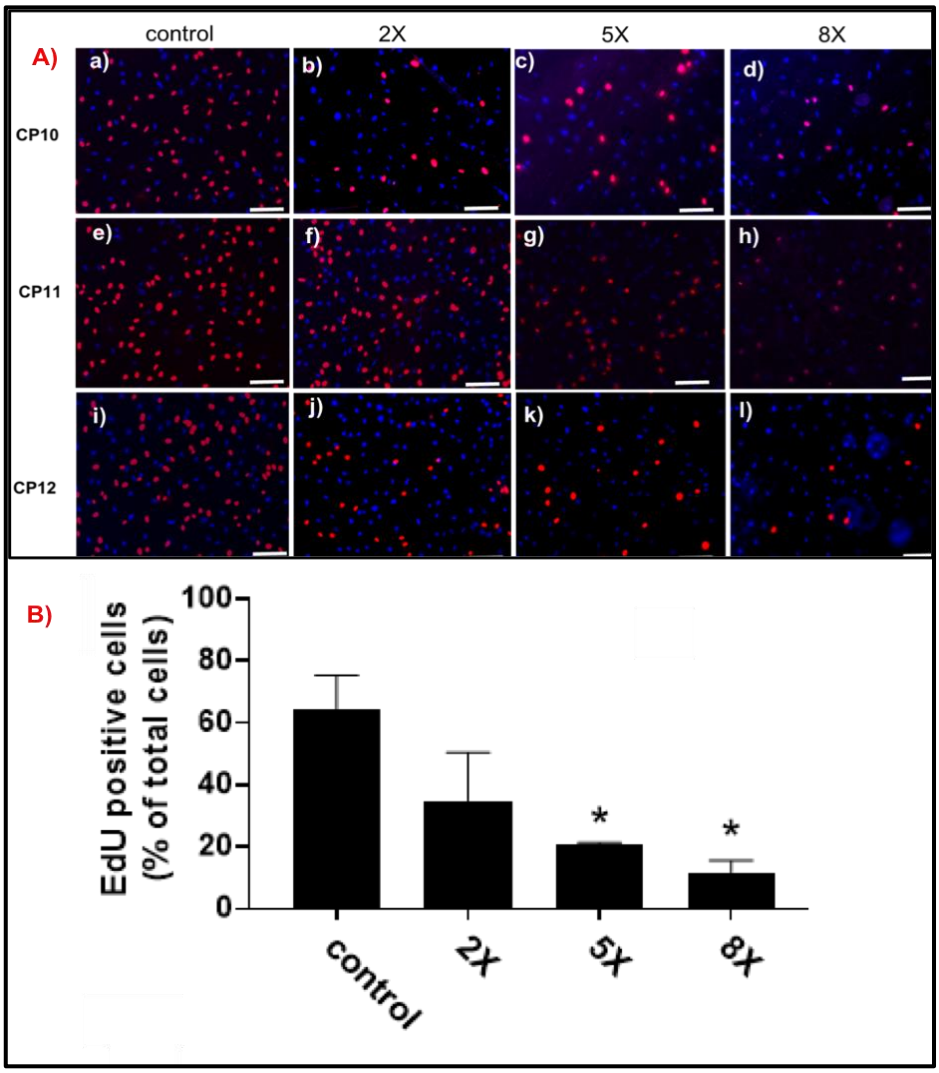

Figure.**4.14**. Proliferation assay by DNA staining on scaffolds with different matrix stiffness. Fluorescent microscopic images of proliferating CPs on plastic (positive control) a), e) & i), 2X CLGS b), f) & j), 5X CLGS c), g) & k) and 8X CLGS d), h) & l). Data expressed as means±SEM. Scale bar: 50µm. (*p<0.05, n=3). Values are mean and SE, N=3 CPs at passage 5 of culture. ANOVA, P<0.05; Tukey's multiple comparisons test adjusted P values. *P<0.05 vs. control.

From the fluorescence microscopy images, it was very evident that the 2X CLGS has a higher number of proliferating cells than 5X and 8X CLGS **(Figure.4.14. A)**. The quantification

analysis also supported this observation as there was a significant reduction in the number of proliferating cells on the 5X and 8X CLGS when compared to the control **(Figure.4.14. B)**. But the percentage of proliferating cells on 2X CLGS were similar to that of control. Merely 12±5 % of CPs were proliferating on 8X CLGS whereas both 5X and 8X CLGS supported the proliferation of around 30±5 % and 38±15% of CPs respectively when seeded on each scaffold. Consequently, it was found that as the matrix stiffness increased, the number of proliferating cells decreased considerably. This shows that CPs prefer to grow and proliferate on a softer substrate than stiffer substrates.

No studies till date have reported the proliferation of CPs on scaffolds. However, there has been reported a study conducted by Qiu *et al.*, where the ovine and murine cardiac side population cells (CSP) were isolated and seeded on polydimethylsiloxane substrates with different elastic modulus to investigate the effect of matrix stiffness on CSP proliferation and differentiation. They found that the stiffening of the microenvironment could lead to the enhanced proliferation of cardiac stem cells than differentiation (222). But the YM range investigated in their study was ranging from 18 to 145 kPa, while the range studied in this study was 263 to 1000 kPA in the wet state. The observation in this work was that proliferation decreases with the increase in stiffness. Hence by combining both the results, it suggests that proliferation of cardiac stromal cells reaches its peak between 140 and 260 KPa (stiffness of fibrotic myocardium) and the fibrotic remodelling of the heart might favour the expansion of the stromal cell compartment. However, more studies are required to confirm this possibility.

There are also studies on the effect of substrate rigidity in the regulation of VSMCs contractility and proliferation (214, 223, 224). Peyton *et al.* found that even though the contractility of the cells was directly dependent on the substrate stiffness, the proliferation of smooth muscle cells

was self-regulating. They combined SMCs into gels made of polyethene glycol (PEG) and fibrinogen with different matrix stiffness ranging from 4448 Pa to 5408 Pa. Their results showed that the SMCs contractile phenotype was regulated by matrix stiffness showing enhanced expression of α-SMA and calponin. Although other groups have demonstrated the dependence of matrix stiffness on SMCs proliferation rate (223). In 2010, Liu *et al*. developed a biomimetic hydrogel made of methacrylated and lysine functionalized dextran-gelatin with different matrix stiffness by changing the degree of methacrylation of polymers and the concentration of the precursor solution. They cultured SMCs on these scaffolds and the cell spreading, proliferation rate and differentiation of SMCs were studied. The proliferation assay was performed by using Bromodeoxyuridine (BrdU), which can bind to the DNA of proliferating cells. In the results, they found an extensive cell spreading, proliferation and widespread cellular network formation in the hydrogels with low mechanical stiffness. This result was in compliance with our results (214). In another study where SMCs were incorporated on polyacrylamide gels, and stiffer surfaces showed increased cell area and proliferation rate (71). From all these reported studies, it is well-defined that even a subtle change in the mechanical properties of the matrix substrate will affect the cell adhesion, spreading and proliferation.

Thus, from the results, it was found that the CPs exhibited enhanced proliferation in softer substrates with large fiber diameter (~400nm) and having a matrix stiffness ranging from 0.2 to 0.3 MPa, whereas the stiffer substrates showed only 12±5 % of proliferating cells. Next, the CPs potential to secrete growth factors to accelerate the differentiation process was assessed.

4.6. Effect of matrix stiffness on CPs secretome

The effect of matrix stiffness of the CP angiocrine secretome was assessed by performing ELISA assays on conditioned media collected after 48 hrs from cell seeding. After two days of incubation on scaffolds the CPs ability to secrete the growth factors such as Angiopoietin-1 (ANG-1), Angiopoietin-2 (ANG-2) and vascular endothelial growth factors A (VEGF-A) were assessed. The absolute concentration in media was normalized for the number of cells to avoid the influence of cell density. The CPs secretome is shown in figure. 4.15. Plastic was used as positive control.

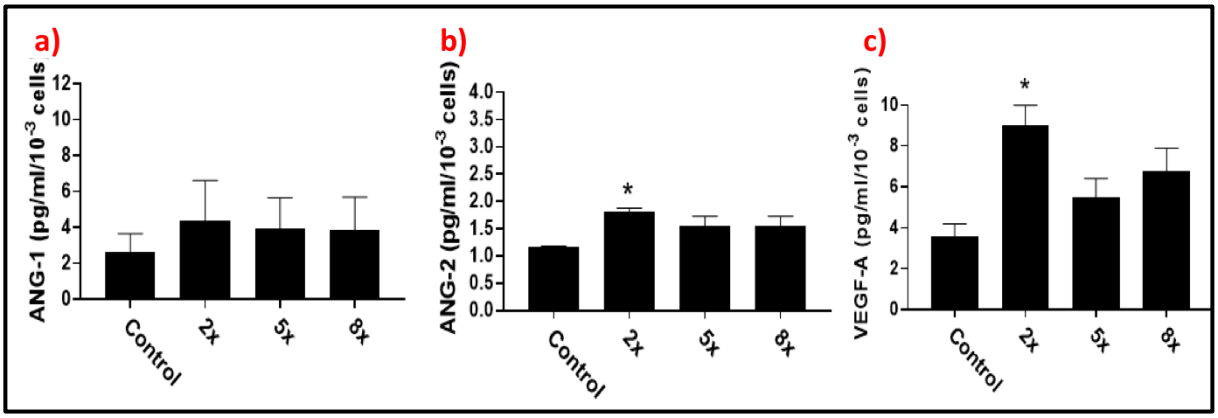

Figure.**4.15.** ELISA test to show the angiogenic growth factor synthesis of CPs on scaffolds with different matrix stiffness. Bar graphs show the concentration of ANG-1 a), ANG-2 b) and VEGF-A c) secreted by CPs on scaffolds with different matrix stiffness. Values are mean and SE, N=3 cell at passage 5 of culture. ANOVA, $P<0.05$; Tukey's multiple comparisons test adjusted P values. *$P<0.05$ vs control.

From the bar diagram, it was found that VEGF is the most abundant secreted growth factor, followed by ANG-1 and ANG-2. For ANG-1, all scaffolds secreted similar concentrations as

of control **(Figure.4.15. a)** whereas the 2X CLGS secreted more ANG-2 and VEGF compared to control **(Figure.4.15. b & c).** In contrast, both 5X and 8X CLGS did not show any statistical significance in the released concentration of ANG-2 and VEGF-A. **(Figure.4.15. b & c).**

In work done by Avolio *et al.,* the CPs secretome were investigated and found that the most abundant secreted growth factor was a hepatocyte growth factor. The other secreted proteins were in the order ANG-1, VEGF-A, ANG-2, stromal cell-derived factor-1α, and fibroblast growth factor-B. They also found that CPs released procollagen type-1, which is an essential constituent of cardiac ECM. Also, they exhibited enhanced secretion of all the above-mentioned proteins than the saphenous vein-derived pericytes (21).

It has been proved that VEGFs, angiopoietins and fibroblast growth factors (FGFs) secreted by stromal cells such as fibroblasts and pericytes or by endothelial cells themselves are essential for sprouting angiogenesis (225, 226). Angiogenesis is the process of formation of new blood vessels from the pre-existing vascular tubes (227). In fact, these growth factors act as angiogenic stimuli to activate endothelial cells by binding to the tyrosine kinase receptor 2(Tie-2). The activated endothelial cells undergo different mechanisms such as vessel destabilization by altering basement membrane proteolytic degradation and this results in the dissociation of pericytes from the capillary. Finally, the endothelial cell migration, proliferation and sprouting occur in the normal physiological angiogenesis (228).

Previous studies have demonstrated the role of angiopoietins and VEGF in blood vessel formation and maturation (229-231). For example, Thurston *et al.* compared the overexpression of these growth factors in the skin of transgenic mice and discovered that the overexpression of Ang-1 in mice resulted in capillaries with increased vessel diameter.

Additionally, these vessels contained an enhanced number of endothelial cells and pericytes, which confirmed the potential of Ang-1 in the endothelial cell maintenance, proliferation and thereby vessel maturation. Although, in transgenic mice overexpressing only VEGF-A, were found to be with leaky blood vessels. But the mice expressing both Ang-1 and VEGF-A resulted in enlarged and highly differentiated blood vessels with an overlay of pericytes and were non-leaky. Hence the vessel sprouting, and growth is initiated by the expression of VEGF while Ang-1 mediates blood vessel remodelling and maturation. Thus, from these findings, they concluded that the co-expression of Ang-1 and VEGF-A is paramount to regulate the process of angiogenesis by performing their unique functions (229). In another work by Augustin *et al*., observed that in mice deficient with Ang-1 and Tie-2 lead to lethality at embryonic day 10.5, because of improper vessel maturation and organization. Also, in mice with overexpression of Ang-2 had no distinct angiogenesis-related phenotype and death occurred in the late gestation period. They also detected an increased level of Ang-2 in diseased conditions associated with vascular dysfunction (230). Hence the same phenotype is observed in the mice deficient of Ang-1 and Tie-2 as well as in mice overexpressed with Ang-2. This made to a conclusion that Ang-2 acts as an antagonist in Tie-2 signalling (232, 233). Therefore, from all these data it was noticeable that Ang/Tie system is essential for maintaining vessel homeostasis in adults and also plays a critical role in mural cell recruitment, vessel remodelling and maturation during embryonic development (231).

It is well-documented that in perivascular cells such as pericytes, VSMCs and fibroblasts, the expression of Ang-1 is predominant (234-236). Ang-1 binds to the Tie-2 receptors on the endothelial cells and activates the phosphoinositide 3- kinase (PI3K) signalling pathways and helps in the endothelial cell survival and quiescent vascularity (237). From our results, it was found that CPs on all scaffolds produced Ang-1same as that of control and is a good sign that

the produced Ang-1 can act as an agonist of Tie-2 signalling which helps in the endothelial cell survival, remodelling and sprouting.

The Ang-2 expression is upregulated during the angiogenic activation of endothelial cells; however, the agonist activity of Ang-2 is much lower than that of Ang-1(238). It has been reported that when endothelial cells treated in specific conditions such as high concentrations of Ang-2, and prolonged stimulations only induced Tie-2 activation (239, 240). In another study, the activation of Tie-2 happened only when endothelial cells were subjected to increased stress (241). Besides, it has been reported that Ang-2 lead to the deterioration of blood vessels in the absence of VEGF and showed enhanced angiogenesis in the presence of VEGF (242). Thus, the data suggests that a fair proportion of both Ang-1 and Ang-2 is essential for regulating Tie-2 assisted signalling pathways and to maintain vascular homeostasis. Moreover, Ang-2 was also found to have an essential role in binding to the integrins and stimulate focal adhesion Kinase (PAK) phosphorylation (243).

VEGF-A can bind to the cell surface receptors such as VEGFR-1 and VEGFR-2 and regulates vascular permeability and angiogenesis (244). Some other functions of VEGF-A include regulating vascular permeability, pro-angiogenic activity and stimulate cell migration (245, 246). The predominant secretion of VEGF-A by CPs on scaffolds than plastic shows the adaptability and favourable conditions of CPs on scaffolds than plastic which is essential for promoting vascular permeability, gene expression, cell migration and angiogenesis (247).

Hence from the results, it was found that CPs are capable of producing ANG-1 and enhanced amount of ANG-2 and VEGF-A when seeded on scaffolds with lower matrix stiffness and fiber diameter of ~400nm, which is essential for activating Tie-2 associated signalling pathways and

thereby endothelial cell migration, proliferation and angiogenesis. Followed by this, the differentiation potential of CPs into VSMCs were investigated when seeded on scaffolds with different matrix stiffness.

4.7. Differentiation Potential of CPs into VSMs on scaffolds with different matrix stiffness

Finally, the CPs were seeded on plastic (control) or scaffolds with increasing concentrations of Glu/EDC/NHS and cultured either in the maintenance ECGM2 media or in differentiation media enriched with TGF-β1 for 7 or 14 days. When CPs on scaffolds were treated with ECGM2 media, none of the cells showed a positive expression towards smooth muscle-calponin and alpha-smooth muscle actin at both time points. But when the CPs were exposed to the differentiation media enriched with TGF-β1, they exhibited positive expression for the markers SM-Calponin and α-SMA irrespective of their matrix stiffness. This shows the mechanical cues alone are inadequate for differentiation and the essentiality of chemical signals for inducing differentiation of CPs. Previous studies from our group have also reported the failure of CPs to differentiate in the absence of inductive media (200). In order to achieve CPs differentiation into VSMCs, differentiation medium added with 20 ng/ml of human PDGF-BB was used previously from our group. In this study, TGF-β1was used as an alternative to PDGF-BB as TGF-β1 has known effects in inducing VSMCs differentiation. For example, in a study Zang *et al*., investigated the differentiation capability of stem cells from human exfoliated deciduous teeth (SHED) into functional VSMCs by utilizing two cytokines of TGF-β family such as transforming growth factor beta 1 (TGF-β1) and bone morphogenetic protein 4 (BMP4). The concluded that TGF-β1regulated SHED differentiation into VSMCs by activating ALK5 signalling pathway. As same as other experiments, the differentiation assay was also performed in 3 cell cultures and at two different time points (7^{th} day and 14^{th} day). The results

obtained after staining the CPs on scaffolds with Calponin and α-SMA are shown in figure.4.16.

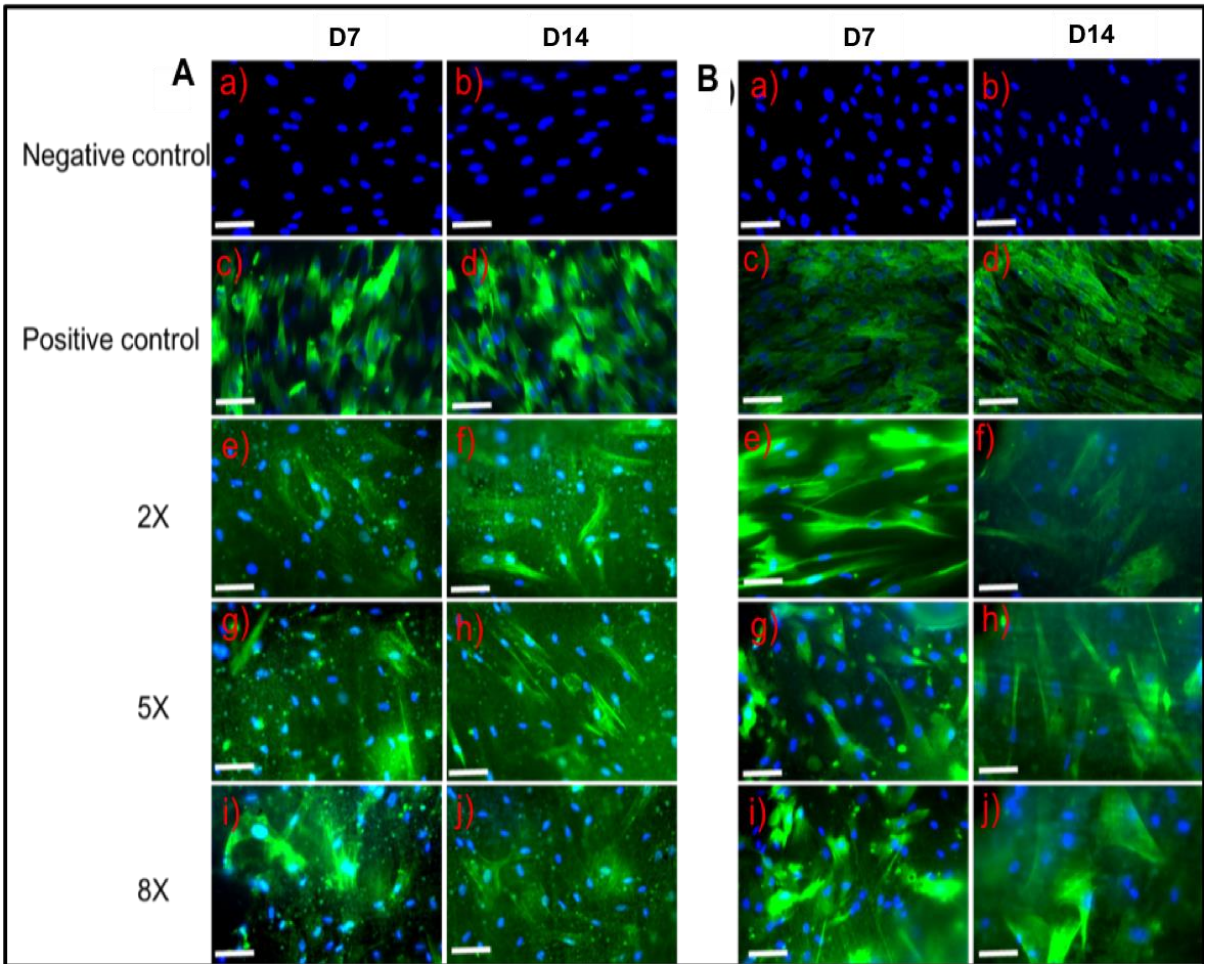

Figure.**4.16**. Differentiation of CP10 (P6) cells on 2X, 5X and 8X CLGS into VSMCs: A) Shows the positive expression of CPs when stained with α-SMA, B) indicates the positive expression of CPs when stained with Calponin. Negative control represents the CPs on scaffolds cultured in ECGM2 media. Positive control is the CPs cultured on glass slides in inductive media. Green colour represents F-actin stained cytoskeleton, and blue colour is DAPI stained nuclei.

From the pictures, it was observed that no differentiation for CPs cultured in the ECGM2 media (**Figure.4.16. a&b)** whereas the CPs treated with inductive media expressed positive signals to both α-SMA (**Figure.4.16. A(c-j)** and calponin (**Figure.4.16. B (c-j)** by staining the actin filaments of CPs. This shows the contractile phenotype of VSMCs and the actin filaments were widespread on the scaffolds. Therefore, the CPs were found to be differentiating into VSMCs independent of their matrix stiffness in CP10 cells. Followed by CP10, CP11 cell lines were also tested, and the results are displayed in figure.4.17.

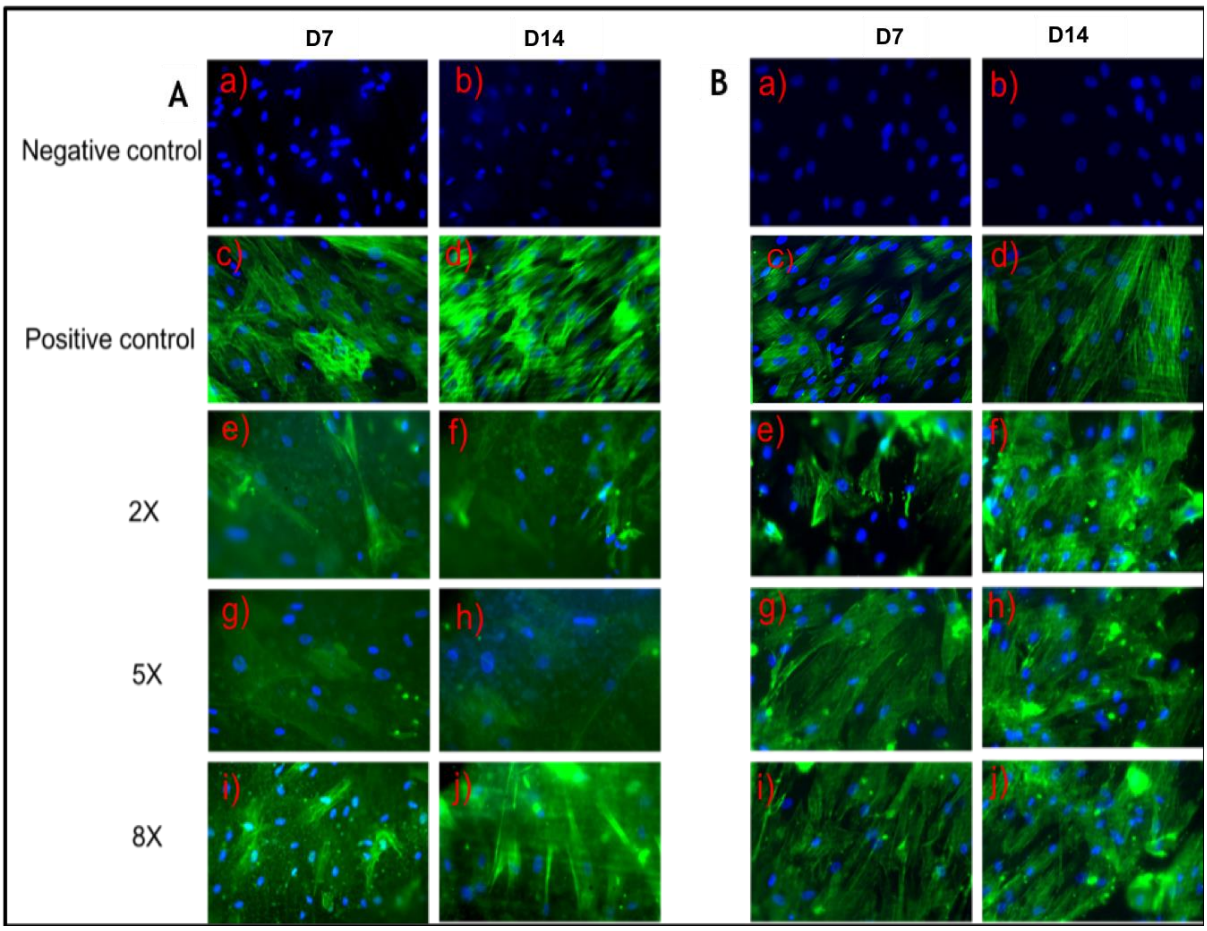

Figure.**4.17**. Differentiation of CP11 (P6) cells on 2X, 5X and 8X CLGS into VSMCs: A) shows the positive expression of CPs when stained with α-SMA, B) indicates the positive expression of CPs when stained with Calponin. Negative control represents the CPs on scaffolds cultured in ECGM2 media. Positive control is the CPs cultured on glass slides in inductive media. Green colour represents F-actin stained cytoskeleton, and blue colour is DAPI stained nuclei.

As of CP10 cells, CP11 cells also showed no differentiation for CPs cultured in the ECGM2 media (**Figure.4.17. a&b)** while the CPs treated with inductive media expressed positive signals to both α-SMA (**Figure.4.17. A(c-j)** and calponin (**Figure.4.17. B (c-j)**. Both calponin and α-SMA stained the actin filaments of CPs and exhibited strong fluorescence **(Figure.4.17. A&B (c-j).** Calponin stained CPs were found to be more expressive compared to the α-SMA

stained CPs. The contractile phenotype of VSMCs was well observed on calponin stained CPs, and the actin filaments were widespread on the scaffolds as that of control **(Figure. 4.17. B (c-j).** Therefore, the CPs were found to be differentiating into VSMCs independent of their matrix stiffness in CP11 cell line. Followed by CP10 and CP11 cell cultures, the differentiation potential of CPs was also tested in CP12 cell cultures, and the results are presented in figure.4.18.

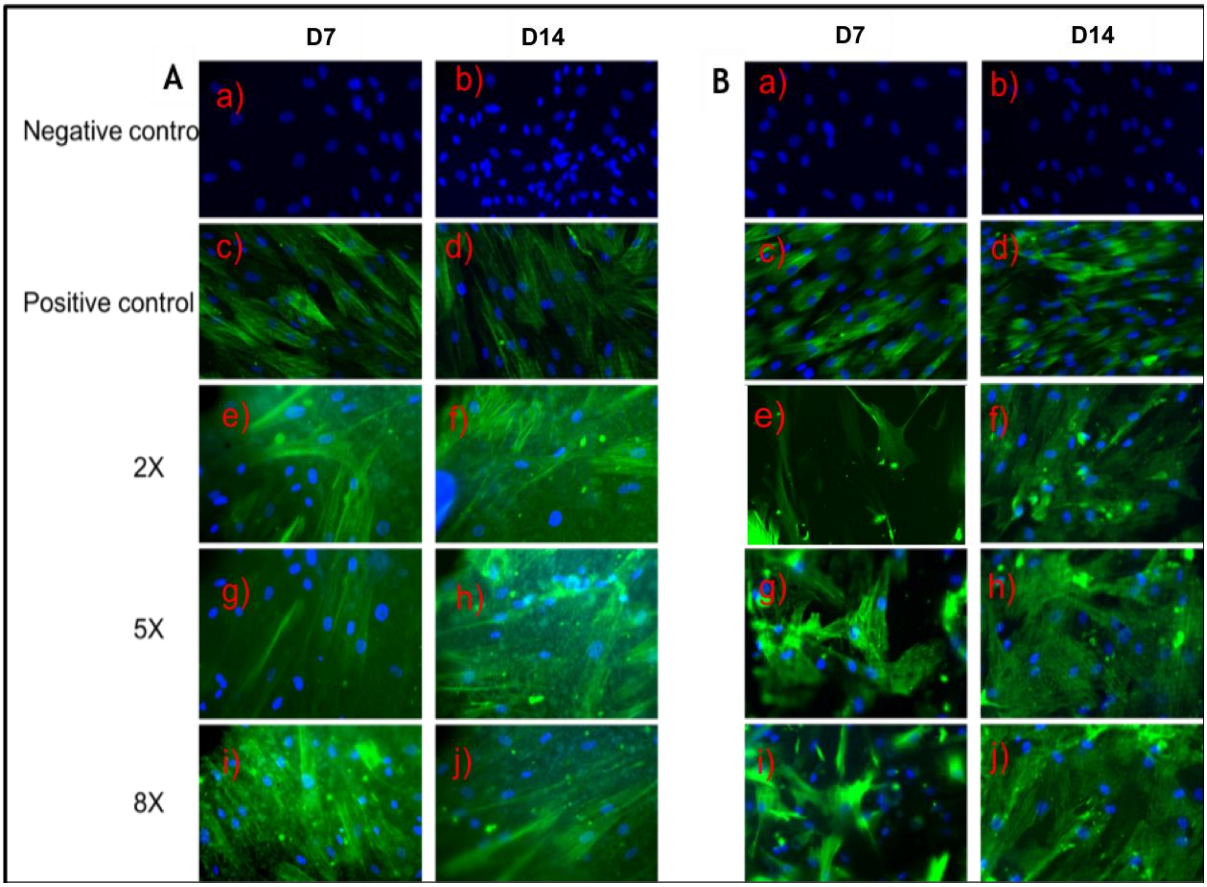

Figure.**4.18**. Differentiation of CP12 (P6) cells on 2X, 5X and 8X CLGS into VSMCs: A) shows the positive expression of CPs when stained with α-SMA, B) indicates the positive expression of CPs when stained with Calponin. Negative control represents the CPs on scaffolds cultured in ECGM2 media. Positive control is the CPs cultured on glass slides in inductive media. Green colour represents F-actin stained cytoskeleton, and blue colour is DAPI stained nuclei.

From the figure, no differentiation was observed for CPs cultured in the ECGM2 media (**Figure.4.18. a&b)**. The contractile phenotype of VSMCs was well observed on both calponin, and α-SMA stained CPs and the actin filaments were widespread on the scaffolds as that of control **(Figure. 4.18. A&B (c-j).** Therefore, the CPs were found to be differentiating into VSMCs independent of their matrix stiffness also in CP12 cell line. In order to attain a meaningful result in the expression of CPs towards the VSMCs differentiation, the actin stress fibers were quantified by measuring the intensity of stress fibers per cell. It was impossible to quantify the number of differentiating cells as the actin filaments were well assembled and widespread on the entire scaffold with the possibility of overlapping of cells. Therefore, the stress fiber intensity was quantified, and the results are shown in figure.4.19.

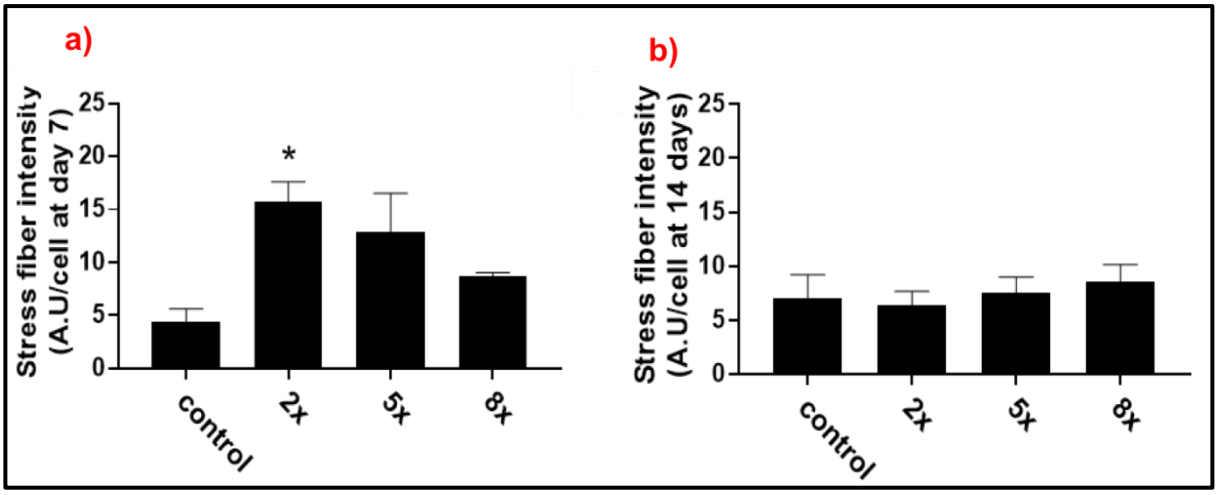

Figure.**4.19**. Stress fiber quantification. (a) Represents the cumulative stress fiber intensity on the 7th day after the addition of inductive media. (b) Shows the cumulative stress fiber intensity on the 14th day after the addition of inductive media. (A.U.-arbitrary unit). Values are mean and SE, N=3 cell cultures at passage 5 of culture. ANOVA, $P<0.05$; Tukey's multiple comparisons test adjusted P values. *$P<0.05$ vs control.

The stress fiber intensity analysis was performed and found that on the 7th day, the CPs cultured on 2X CLGS exhibited higher intensity compared to control and other counterparts **(Figure. 4.19. (a).** However, there was no significant difference in the stress fiber intensity among the scaffolds with respect to the control **(Figure.4.19. (b)** on the 14th day. Furthermore, a substantial accumulation and alignment of F-actin on softer substrates forming extensive stress fibers agrees with the theory that the cells adapt themselves to the 3 D microenvironment and alter their cytoskeletal organisations (248). As explained in section 2.4, the cell experiences various forces from the external microenvironment and the cell surface receptors (integrins) sense these signals and transmit these signals to the nucleus by initiating specific cell signalling pathways (5). Stress fibers are long and aligned contractile actin bundles, which detect and transmit forces to the ECM through focal adhesions (249). These actin bundles can adjust themselves to the external forces from the microenvironments and thus the shape of the cells. Hence the cytoskeletal contractility is much dependent on the elastic modulus (stiffness) of the ECM (67). The higher elasticity fiber diameter of the scaffolds would have provided additional focal adhesion points, which helps in the creation and alignment of F-actin stress fibers and results in the actin polymerisation. Therefore, the cells adapt to these mechanical stimuli by modulating their cytoskeletal contractility and exerts cellular traction forces back to the ECM. Thus, there occurs a tensional homeostasis or force balance between the external forces (from the microenvironment to the cells) and the force exerted by the cells (traction force) due to their endogenous cytoskeletal contractility. This plays an essential role in the basic cellular functions such as adhesion, proliferation, differentiation, survival and apoptosis (5, 66, 67). Hence the increased stress fiber formation on softer substrates shows that matrix has optimum stiffness for CPs to alter their cytoskeletal contractility and thereby differentiation into VSMCs.

The mechanotransduction and the signalling pathways that determine the assembly of stress fibers is yet to be well understood. In 1997, Kaibuchi *et al*. proposed the dependence of Rho-kinase in the formation of actin stress fibers and focal adhesions. The extracellular signals such as lysophosphatidic acid (LPA) stimulates the cells by converting guanosine diphosphate (GDP)-Rho to guanosine triphosphatase (GTP)-Rho and participates in the Rho-mediated signalling pathways which are essential for stress fiber formation and focal adhesions. They proved the influence of Rho-kinase by testing the formation of focal adhesion and stress fibers by injecting the catalytic domain of Rho-kinase to serum-starved Swiss 3T3 cells. They observed the development of focal adhesions and stress fibers in the cells injected with the catalytic domain of Rho-kinase, whereas the cells injected with the inactive domain of Rho-kinase were deprived of stress fibers and focal adhesions (250). In another study, Tojkander *et al.*, recently showed that the Ca^{2+} influxes activate Ca^{2+} calmodulin-dependent kinase 2 (CaMKK2) at focal adhesions and act as an upstream factor for the phosphorylation of 50AMP-activated protein kinase (AMPK) which in turn promotes the maturation of actomyosin bundles (251). Hence, several types of research are still carrying out works towards exploring how cells sense these signals and perform cytoskeletal organisations.

Further investigation is required to identify the exact mechanism involved in the CPs adhesion and interaction with the gelatin nanofibrous scaffolds to proliferate and differentiate into VSMCs. This includes various cell and molecular-based assays to identify the signalling cascades involved in transmitting the forces through focal adhesions and the gene expressions during the differentiation process.

Hence from the differentiation assay, it was found that CPs differentiated into VSMCs when seeded on all scaffolds irrespective of their matrix stiffness, but there was an enhanced stress fiber formation on 2X CLGS after 7 days of adding inductive media.

5 THESIS SUMMARY AND CONCLUSIONS

The objectives of the work described in this thesis were first to fabricate biomimetic gelatin nanofibrous scaffolds with varying matrix stiffness in aqueous solution by *in situ* cross-linking electrospinning technique, and secondly, to investigate the effect of matrix stiffness in regulating Cardiac Pericytes (CPs) behaviour by analysing CPs antigenic profile, morphology, viability, proliferation, angiocrine activity and capacity to differentiate into vascular smooth muscle cells (VSMCs) on gelatin nanofibrous scaffolds with different matrix stiffness.

This chapter will summarise the main studies that were conducted, along with the most relevant findings. Finally, the conclusions of the work will be presented, and suggestions for future work are also mentioned.

5.1 SUMMARY OF FINDINGS

5.1.1 Fabrication and characterization of mechanically tunable gelatin nanofibrous scaffolds

One of the main milestones in our study was the fabrication of a scaffold made of electrospinning gelatin nanofibers in aqueous solution. This study opted an alternative method of electrospinning gelatin in a pure water solvent, approaching this challenge by raising the environmental temperature (40°C) and humidity (above 50%) using a hot plate and ultrasound nebuliser and by keeping the whole setup in an enclosed incubator.

Another accomplishment of this study was the preparation of electrospun gelatin nanofibrous scaffolds with different matrix stiffness by utilizing *in situ* cross-linking technique. This was achieved by employing a double-barrel syringe (10:1-barrel ratio) to introduce cross-linking agents during electrospinning to make uniformly cross-linked gelatin nanofibers with defined morphology and mechanical properties since the cross-linking reaction between gelatin and EDC/NHS occurred as soon as they were mixed (252), the processing window needed to be carefully controlled in order not to compromise the electrospinnability, as the viscosity of the solution increased with the increasing crosslink degree. The 10:1 double-barrel syringe was chosen to serve this purpose. Moreover, to aid electrospinning, the voltage was augmented with a reduced flow rate accordingly.

The morphological and topographical characterisation of gelatin nanofibrous scaffolds revealed a considerable reduction in the fiber dimensions according to the progressive increase in cross-linking density while maintaining the same height. This is due to the synergistic influence of electrospinning parameters, in particular, the increase in applied voltage and the decrease in flow rate being determinants in creating nanofibers with reduced fiber diameter. Moreover, high cross-linking densities can contribute to shrinking the gelatin nanofibers as new bonds are formed between the polymer chains, which in turn can diminish the intermolecular space.

The initial hypothesis was to create the gelatin nanofibrous scaffolds cross-linked internally with different concentrations of EDC/NHS. However, data from the literature indicate that cross-linking agents, like EDC/NHS, which creates amide bonds are less efficient in maintaining the structural stability over 3 weeks in aqueous solution (150); this could preclude the use of scaffold in the wet condition for tissue/cell engineering applications. Therefore, the

dissolvability property of the EDC/NHS cross-linked scaffolds were tested and verified their stability over three weeks. The scaffolds cross-linked with lower concentrations of EDC/NHS were disappeared entirely within two weeks of immersion in the aqueous solution. Hence, it was further assessed if this can be improved by the addition of Glutaraldehyde (Glu) vapour cross-linking, which can create stronger aldimine linkages. As expected, this significantly facilitated to maintain the scaffolds structural stability even after three weeks. Retention of structural stability by cross-linking was an essential requisite for subsequent functional studies on living cells.

The prepared gelatin nanofibrous scaffolds were well-crosslinked as shown in the results, using the Ninhydrin assay and assessing peak intensities, which indicated a reduction in the lysine amine groups through the interaction with the aldehyde group of Glu. In Ninhydrin assay, the intensity of the blue colour faded with increasing concentrations of the EDC/NHS and became yellow in samples cross-linked with Glu\EDC\NHS. Quantification of the data indicated that Glu/EDC/NHS had superior cross-linking activity as compared with the other conditions. In the FTIR analysis, the peak intensities were much lower for the nanofibers cross-linked with both Glu and EDC/NHS as compared with the Glu alone, and the reduction in peak intensity was further enhanced by increasing the concentration of EDC/NHS. Moreover, the structure of the gelatin was also disturbed when higher concentrations of EDC/NHS were used.

The scaffolds showed higher YM values in the dry state as the cross-linking concentration of EDC/NHS increased. This is likely the consequence of the new bonds between the functional groups of the polymer, causing the formation of denser and more compact structures. Ina wet state, the presence of water contributed to the acquisition of viscoelastic properties and reduction in the YM, which also became remarkably different among scaffolds. The Glu and

8X EDC/NHS cross-linked scaffolds exhibited an average YM of 0.9±0.3 MPa, which was higher than the other crosslinked scaffolds, showing values <0.3 MPa, or uncross-linked gelatin, whose YM was <0.1 MPa.

5.1.2 Effect of matrix stiffness on CPs fate in terms of its adhesion, proliferation and differentiation into VSMCs

The *in vitro* cell studies showed that subtle changes in the mechanical properties of the matrix substrate could remarkably influence the behaviour of human cardiac cells. This study focused on CPs because of the increasing evidence these cells modulate cardiovascular repair and remodelling through the interaction with adjacent cells and the surrounding ECM. Birbair *et al*. reported the presence of two pericyte subtypes in mice, type-1 (Nestin-GFP-/NG2-DsRed+) and type-2 (Nestin-GFP+/NG2-DsRed+), surrounding blood vessels in heart, lungs, kidneys, spinal cord, and brain (253). Type-1, but not type-2, pericytes increase and accumulate near the fibrotic tissue in all organs analysed (253). However, it remains unclear whether cardiac microvascular pericytes could lead to cardiac fibrosis following an ischaemic injury (254). Our group have previously identified a clonogenic population of CPs in the heart of patients with CHD and demonstrated that, after exposure to differentiation media, they acquired markers of VSMCs, but failed to differentiate into endothelial cells or cardiomyocytes (255). In a Matrigel assay, CPs form networks and enhance the network capacity of endothelial cells (255). Moreover, they produce collagen-1 and release chemo-attractants that stimulate the migration of c-Kit$^+$ cardiac stromal cells (255). When seeded onto clinically approved xenograft scaffolds and cultured in a bioreactor, CPs showed the ability to penetrate into and colonize the graft (255). Extending these findings, this study shows that CPs are capable of colonizing and remaining viable within gelatin nanofiber scaffolds. They also exhibited enhanced cell density,

proliferation and extensive spreading in the softer substrates with large fiber diameter, while maintaining their antigenic phenotype and stemness features.

The elasticity of the scaffolds would have resulted in more focal adhesion points and hence favoured cell retention. The biomimetic nanofibrous structure, which resembles the native ECM, together with the porous structure favouring essential nutrients and gaseous exchange (218) and the gelatin's ability to support cell adhesion and promote proteolytic degradation, (214) might also have helped CPs to remain viable and proliferate extensively on softer scaffolds. Cell proliferation capacity has been previously found to increase in response to microenvironment stiffening for other non-cardiac progenitor cell populations (256, 257). A study on ovine cardiac stromal cells showed elevated substrate stiffness increased cell proliferation (33). However, the elastic moduli examined in that study ranged from 18 to 145 kPa, while the range studied here was 263 to 1000 kPa in the wet state. It was observed that proliferation decreased with the increase in stiffness. Altogether, this suggests that proliferation of cardiac stromal cells reaches its peak between 140 and 260 KPa. The reported elastic moduli of myocardium range from (7, 27). It is tempting to speculate that fibrotic remodelling of the heart might favour additional expansion of the stromal cell compartment.

It has been reported that the proangiogenic capacity of human CP is associated with the release of a number of angiocrine factors (255). In this study, it was found that seeding CPs on gelatin scaffolds increased their capacity to release VEGF-A into the medium. However, no effect of stiffness on the angiocrine secretome was found, except for an increased Ang-2 release when CPs were seeded in softer scaffolds. The Ang/Tie-2 pathway plays a crucial role in the paracrine cross-talk between the pericytes and endothelial cells. The tie-2 receptor is expressed by endothelial cells and activated by pericytes-secreted Ang-1, resulting in the induction of

survival, proliferation, migration, and anti-inflammatory signals. Ang-2 acts as a partial agonist of Tie-2, inhibiting Tie-2 signalling in the presence of Ang-1, but activating Tie-2 in the absence of Ang-1. Additional experiments allowing larger changes in stiffness are warranted to determine whether the angiogenic activity of CP can be modulated by manipulating the elastic moduli of the matrix.

Changes in stiffness did not alter the differentiation capacity of CPs. However, a substantial accumulation and alignment of F-actin fibers in CPs on softer substrates with increased fiber diameter. This is in keeping with the theory that cells adapt their cytoskeletal organisation to the elastic modulus of the surrounding microenvironment (258, 259). Cytoskeletal contraction transfers traction forces back to the ECM. In this study, the higher elasticity and diameter of softer scaffolds might have provided focal adhesion points aiding the creation and alignment of F-actin stress fibers resulting in the actin polymerisation.

5.2. CONCLUSIONS

This study resulted in the successful production of biomimetic gelatin nanofibrous scaffolds in a water solvent system with different matrix stiffness using an *in situ* cross-linking electrospinning method.

The CLGS with a randomly oriented topography and that combine a matrix stiffness of ≤0.3 MPa and ~400nm diameter, induced better CP adhesion, extensive cell spreading, proliferation and stress fiber formation. These data support the feasibility of modulating the behaviour of human cardiac stromal cells through the manipulation of mechanical characteristics of the substrate. The study has, however, some limitations. This study explored a narrow range of

matrix stiffness and also limited the observation to a relatively short-duration culture. Further studies are warranted to enhance the therapeutic potential of CPs through modulation of the accompanying matrix substrate for the corrective treatments of cardiac defects.

5.3 FUTURE WORK

With regards to continuing the work that has been presented in this thesis, further investigations can be made into the fabrication of scaffolds with other natural polymers (collagen, alginate, chitosan etc.) or synthetic polymers (PCL, PLLA, PEG etc.), or a combination of both, to obtain scaffolds with a wide range of matrix stiffness. In this work, the range studied was 263 to 1000 kPa in the wet state. The reported elastic moduli of myocardium range from 18 to 60 kPa in normal myocardium and 55 to 295 kPa in fibrotic myocardium. Hence, it is worth investigating the effect of comparatively lower matrix stiffness in regulating CPs behaviour as changes in stiffness occur in the hearts, and arterial vessels of patients with congenital heart disease are regarded as one of the most common congenital anomalies in infants.

Another point of research interest would be the characterization of nanofibers using AFM. In this study, an attempt to measure the Young's Modulus of individual nanofiber specimens were made by utilizing the Peak Force Tapping Technology using a Multi-mode VIII AFM with Nanoscope V controller. It was found that the single fibers are accessible by AFM to measure the YM, but the values obtained were in a higher order of magnitude (GPa). The values obtained in the tensile testing of the fibrous scaffolds in this study were in the range of MPs, and hence the values attained for individual fibers using AFM was not reliable in terms of its higher order of magnitude and uniformity. This implies that the experimental design needs to be improved. Hence more AFM measurements with a greater number of samples are required

to justify this observation. Also, the AFM measurements using other probes such as colloidal probes serve as another potential approach to examine the YM of nanofibers.

The anisotropic behaviour of CPs on softer substrates that was observed in one of the most confluent cell cultures is quite interesting to take forward that concept to further investigate the effect of nanofiber orientation on CPs fate. For example, when CP12 cell lines were seeded on scaffolds with low stiffness (2X), the CPs were found to be of highly aligned even if they were cultured on a randomly oriented nanofibrous structure. Hence it is crucial to analyse the effect of nanofiber orientation in stem cell behaviour by producing nanofibrous structures with different orientations.

Further investigations with long-duration cell culture and with a more significant number of cell cultures are requisite for the better understanding of CPs behaviour in order to obtain the accurate knowledge of the therapeutic potential of CPs through modulation of the accompanying matrix substrate for the corrective treatments of cardiac defects. To address this, it may also be possible to target the cellular signalling pathways responsible for the mechanotransduction by utilizing molecular biology techniques and gene expression analysis using Polymer Chain Reactions (PCR). Further investigations can be carried out on how these signals are selectively taken up by CPs and transported to the nucleus for performing the cellular functions.

REFERENCES

1. Frantz C, Stewart KM, Weaver VM. The extracellular matrix at a glance. Journal of Cell Science. 2010;123(24):4195-200.
2. Kim SH, Turnbull J, Guimond S. Extracellular matrix and cell signalling: the dynamic cooperation of integrin, proteoglycan and growth factor receptor. Journal of Endocrinology. 2011;209(2):139-51.
3. Bosman FT, Stamenkovic I. Functional structure and composition of the extracellular matrix. Journal of Pathology. 2003;200(4):423-8.
4. Tsimbouri P, Gadegaard N, Burgess K, White K, Reynolds P, Herzyk P, et al. Nanotopographical Effects on Mesenchymal Stem Cell Morphology and Phenotype. Journal of Cellular Biochemistry. 2014;115(2):380-90.
5. Sun YB, Chen CS, Fu JP. Forcing Stem Cells to Behave: A Biophysical Perspective of the Cellular Microenvironment. In: Rees DC, editor. Annual Review of Biophysics, Vol 41. Annual Review of Biophysics. 412012. p. 519-42.
6. Trappmann B, Chen CS. How cells sense extracellular matrix stiffness: a material's perspective. Current Opinion in Biotechnology. 2013;24(5):948-53.
7. Nava MM, Raimondi MT, Pietrabissa R. Controlling Self-Renewal and Differentiation of StemCells via Mechanical Cues. Journal of Biomedicine and Biotechnology. 2012.
8. Nam J, Johnson J, Lannutti JJ, Agarwal S. Modulation of embryonic mesenchymal progenitor cell differentiation via control over pure mechanical modulus in electrospun nanofibers. Acta Biomaterialia. 2011;7(4):1516-24.
9. Liu L, Yuan QH, Shi J, Li X, Jung DJ, Wang L, et al. Chemically-defined scaffolds created with electrospun synthetic nanofibers to maintain mouse embryonic stem cell culture under feeder-free conditions. Biotechnology Letters. 2012;34(10):1951-7.
10. Gauthaman K, Venugopal JR, Yee FC, Peh GSL, Ramakrishna S, Bongso A. Nanofibrous substrates support colony formation and maintain stemness of human embryonic stem cells. Journal of Cellular and Molecular Medicine. 2009;13(9B):3475-84.
11. Lv HW, Li LS, Sun MY, Zhang Y, Chen L, Rong Y, et al. Mechanism of regulation of stem cell differentiation by matrix stiffness. Stem Cell Research & Therapy. 2015;6.
12. Kuo CK, Smith ML. Biomaterial design motivated by characterization of natural extracellular matrices. Mrs Bulletin. 2014;39(1):18-24.
13. Kohn JC, Zhou DW, Bordeleau FO, Zhou AL, Mason BN, Mitchell MJ, et al. Cooperative Effects of Matrix Stiffness and Fluid Shear Stress on Endothelial Cell Behavior. Biophysical Journal. 2015;108(3):471-8.
14. Zhang YZ, Ouyang HW, Lim CT, Ramakrishna S, Huang ZM. Electrospinning of gelatin fibers and gelatin/PCL composite fibrous scaffolds. Journal of Biomedical Materials Research Part B-Applied Biomaterials. 2005;72B(1):156-65.
15. Mahairaki V, Lim SH, Christopherson GT, Xu LY, Nasonkin I, Yu C, et al. Nanofiber Matrices Promote the Neuronal Differentiation of Human Embryonic Stem Cell-Derived Neural Precursors In Vitro. Tissue Engineering Part A. 2011;17(5-6):855-63.
16. Li WJ, Tuli R, Okafor C, Derfoul A, Danielson KG, Hall DJ, et al. A three-dimensional nanofibrous scaffold for cartilage tissue engineering using human mesenchymal stem cells. Biomaterials. 2005;26(6):599-609.
17. Kang XH, Xie YB, Powell HM, Lee LJ, Belury MA, Lannutti JJ, et al. Adipogenesis of murine embryonic stem cells in a three-dimensional culture system using electrospun polymer scaffolds. Biomaterials. 2007;28(3):450-8.

18. Nur-E-Kamal A, Ahmed I, Kamal J, Schindler M, Meiners S. Three-dimensional nanofibrillar surfaces promote self-renewal in mouse embryonic stem cells. Stem Cells. 2006;24(2):426-33.
19. Xia H, Nho RS, Kahm J, Kleidon J, Henke CA. Focal adhesion kinase is upstream of phosphatidylinositol 3-kinase/Akt in regulating fibroblast survival in response to contraction of type I collagen matrices via a beta(1) integrin viability signaling pathway. Journal of Biological Chemistry. 2004;279(31):33024-34.
20. Wu SC, Chang WH, Dong GC, Chen KY, Chen YS, Yao CH. Cell adhesion and proliferation enhancement by gelatin nanofiber scaffolds. Journal of Bioactive and Compatible Polymers. 2011;26(6):565-77.
21. Avolio E, Rodriguez-Arabaolaza I, Spencer HL, Riu F, Mangialardi G, Slater SC, et al. Expansion and Characterization of Neonatal Cardiac Pericytes Provides a Novel Cellular Option for Tissue Engineering in Congenital Heart Disease. Journal of the American Heart Association. 2015;4(6).
22. Avolio E, Meloni M, Spencer HL, Riu F, Katare R, Mangialardi G, et al. Combined Intramyocardial Delivery of Human Pericytes and Cardiac Stem Cells Additively Improves the Healing of Mouse Infarcted Hearts Through Stimulation of Vascular and Muscular Repair. Circulation Research. 2015;116(10):E81-E94.
23. Gubernator M, Slater SC, Spencer HL, Spiteri I, Sottoriva A, Riu F, et al. Epigenetic Profile of Human Adventitial Progenitor Cells Correlates With Therapeutic Outcomes in a Mouse Model of Limb Ischemia. Arteriosclerosis Thrombosis and Vascular Biology. 2015;35(3):675-88.
24. Fuoco C, Sangalli E, Vono R, Testa S, Sacchetti B, Latronico MVG, et al. 3D hydrogel environment rejuvenates aged pericytes for skeletal muscle tissue engineering. Frontiers in Physiology. 2014;5.
25. Katare RG, Madeddu P. Pericytes from human veins for treatment of myocardial ischemia. Trends in Cardiovascular Medicine. 2013;23(3):66-70.
26. Vono R, Spinetti G, Gubernator M, Madeddu P. What's New in Regenerative Medicine: Split up of the Mesenchymal Stem Cell Family Promises New Hope for Cardiovascular Repair. Journal of Cardiovascular Translational Research. 2012;5(5):689-99.
27. Katare R, Riu F, Mitchell K, Gubernator M, Campagnolo P, Cui YX, et al. Transplantation of Human Pericyte Progenitor Cells Improves the Repair of Infarcted Heart Through Activation of an Angiogenic Program Involving Micro-RNA-132. Circulation Research. 2011;109(8):894-U191.
28. Campagnolo P, Cesselli D, Zen AAH, Beltrami AP, Krankel N, Katare R, et al. Human Adult Vena Saphena Contains Perivascular Progenitor Cells Endowed With Clonogenic and Proangiogenic Potential. Circulation. 2010;121(15):1735-U112.
29. Avolio E, Caputo M, Madeddu P. Stem cell therapy and tissue engineering for correction of congenital heart disease. Front Cell Dev Biol. 2015;3(39).
30. Frank GS, Mark MB, Kak-Chen C, Lilliam V, Richard P. Preliminary experience with cardiac reconstruction using decellularized porcine extracellular matrix scaffold: human applications in congenital heart disease. World Journal for Pediatric and Congenital Heart Surgery. 2010;1:132-6.
31. Bernstein HS, Srivastava D. Stem cell therapy for cardiac disease. Pediatric Research. 2012;71(4):491-9.
32. Stout KK, Broberg CS, Book WM, Cecchin F, Chen JM, Dimopoulos K, et al. Chronic Heart Failure in Congenital Heart Disease: A Scientific Statement From the American Heart Association. Circulation. 2016;133(8):770-801.

33. Qiu Y, Bayomy AF, Gomez MV, Bauer M, Du P, Yang Y, et al. A role for matrix stiffness in the regulation of cardiac side population cell function. Am J Physiol Heart Circ Physiol. 2015;308(9):H990-7.
34. Li RA. Cardiovascular regeneration. Stem Cell Research & Therapy. 2014;5.
35. Hu JA, Smith LA, Feng K, Liu XH, Sun HL, Ma PX. Response of Human Embryonic Stem Cell-Derived Mesenchymal Stem Cells to Osteogenic Factors and Architectures of Materials During In Vitro Osteogenesis. Tissue Engineering Part A. 2010;16(11):3507-14.
36. Smit FE, Dohmen PM. Cardiovascular Tissue Engineering: Where We Come From and Where Are We Now? Medical Science Monitor Basic Research. 2015;21:1-3.
37. Khoshnood B, Lelong N, Houyel L, Thieulin AC, Jouannic JM, Magnier S, et al. Prevalence, timing of diagnosis and mortality of newborns with congenital heart defects: a population-based study. Heart. 2012;98(22):1667-73.
38. Sun RR, Liu M, Lu L, Zheng Y, Zhang PY. Congenital Heart Disease: Causes, Diagnosis, Symptoms, and Treatments. Cell Biochemistry and Biophysics. 2015;72(3):857-60.
39. Woodward CS. Keeping Children With Congenital Heart Disease Healthy. Journal of Pediatric Health Care. 2011;25(6):373-8.
40. Wald RM, Valente AM, Marelli A. Heart failure in adult congenital heart disease: Emerging concepts with a focus on tetralogy of Fallot. Trends in Cardiovascular Medicine. 2015;25(5):422-32.
41. Barron DJ, Kilby MD, Davies B, Wright JG, Jones TJ, and Brawn WJ. Hypoplastic left heart syndrome. Lancet 2009;374:551-64.
42. Said SM, and Burkhart HM, . When repair is not feasible: prosthesis selection in children and adults with congenital heart disease. Semin. Thorac Cardiovasc Surg Pediatr Card Surg Annu. 2014;17:22-9.
43. Razzouk AJ, and Bailey LL. Heart transplantation in children for endstage congenital heart disease. Semin Thorac Cardiovasc Surg Pediatr Card Surg Annu. 2014;17:69-76.
44. Francisco X. Galdos, Yuxuan Guo, Sharon L. Paige, Nathan J. VanDusen, Sean M. Wu, Pu WT. cardiac regeneration. Crculation research. 2017;120(6).
45. Sanganalmath SK, Bolli R. Cell Therapy for Heart Failure A Comprehensive Overview of Experimental and Clinical Studies, Current Challenges, and Future Directions. Circulation Research. 2013;113(6):810-34.
46. Pincott ES, Burch M. Potential for stem cell use in congenital heart disease. Future Cardiol. 2012;8:161-9.
47. Lambert V, Gouadon E, Capderou A, Le Bret E, Ly M, Dinanian S, et al. Right ventricular failure secondary to chronic overload in congenital heart diseases: Benefits of cell therapy using human embryonic stem cell-derived cardiac progenitors. Journal of Thoracic and Cardiovascular Surgery. 2015;149(3):708-15.
48. Burkhart HM, Qureshi MY, Peral SC, O'Leary PW, Olson TM, Cetta F, et al. Regenerative therapy for hypoplastic left heart syndrome: First report of intraoperative intramyocardial injection of autologous umbilical-cord blood-derived cells. Journal of Thoracic and Cardiovascular Surgery. 2015;149(3):E35-E7.
49. Butcher JT, Mahler GJ, Hockaday LA. Aortic valve disease and treatment: The need for naturally engineered solutions. Advanced Drug Delivery Reviews. 2011;63(4-5):242-68.
50. Fallahiarezoudar E, Ahmadipourroudposht M, Idris A, Yusof NM. A review of: Application of synthetic scaffold in tissue engineering heart valves. Materials Science & Engineering C-Materials for Biological Applications. 2015;48:556-65.
51. Dean EW, Udelsman B, Breuer CKY. Current advances in the translation of vascular tissue engineering to the treatment of pediatric congenital heart disease. J Biol Med. 2012;85:229–38.

52. Masuda S, Shimizu T, Yamato M, Okano T. Cell sheet engineering for heart tissue repair. Advanced Drug Delivery Reviews. 2008;60(2):277-85.
53. Moschouris K, Firoozi N, Kang YQ. The application of cell sheet engineering in the vascularization of tissue regeneration. Regenerative Medicine. 2016;11(6):559-70.
54. Kobayashi J, Kikuchi A, Aoyagi T, Okano T. Cell sheet tissue engineering: Cell sheet preparation, harvesting/manipulation, and transplantation. Journal of Biomedical Materials Research Part A. 2019;107(5):955-67.
55. Shinoka T, Breuer CK, Tanel RE, Zund G, Miura T, Ma PX, et al. Tissue engineering heart valves: Valve leaflet replacement study in a lamb model. Annals of Thoracic Surgery. 1995;60(6):S513-S6.
56. Hibino N, McGillicuddy E, Matsumura G, Ichihara Y, Naito Y, Breuer C, et al. Late-term results of tissue-engineered vascular grafts in humans. Journal of Thoracic and Cardiovascular Surgery. 2010;139(2):431-U233.
57. Kalfa D, Bacha E. New technologies for surgery of the congenital cardiac defect. Rambam Maimonides Med J. 2013;4:e0019.
58. Freedman BR, Bade ND, Riggin CN, Zhang SJ, Haines PG, Ong KL, et al. The (dys)functional extracellular matrix. Biochimica Et Biophysica Acta-Molecular Cell Research. 2015;1853(11):3153-64.
59. Biernacka A, Frangogiannis NG. Aging and Cardiac Fibrosis. Aging and Disease. 2011;2(2):158-73.
60. Kapelko VI. Myocardial extracellular matrix and its changes in heart diseases. Kardiologiya. 2000;40(9):78-90.
61. Twomey C. Understanding Stem Cells: An Overview of the Science and Issues from the National Academies. 2006:24p.
62. Spencer HL, Slater SC, Rowlinson J, Morgan T, Culliford LA, Guttridge M, et al. A journey from basic stem cell discovery to clinical application: the case of adventitial progenitor cells. Regenerative Medicine. 2015;10(1):39-47.
63. Leite CF, Almeida TR, Lopes CS, da Silva VJD. Multipotent stem cells of the heart-do they have therapeutic promise? Frontiers in Physiology. 2015;6.
64. Zhang H, Dai S, Bi JX, Liu KK. Biomimetic three-dimensional microenvironment for controlling stem cell fate. Interface Focus. 2011;1(5):792-803.
65. Guilak F, Cohen DM, Estes BT, Gimble JM, Liedtke W, Chen CS. Control of Stem Cell Fate by Physical Interactions with the Extracellular Matrix. Cell Stem Cell. 2009;5(1):17-26.
66. Mammoto T, Ingber DE. Mechanical control of tissue and organ development. Development. 2010;137(9):1407-20.
67. Wozniak MA, Chen CS. Mechanotransduction in development: a growing role for contractility. Nature Reviews Molecular Cell Biology. 2009;10(1):34-43.
68. Butcher DT, Alliston T, Weaver VM. A tense situation: forcing tumour progression. Nature Reviews Cancer. 2009;9(2):108-22.
69. Hahn C, Schwartz MA. Mechanotransduction in vascular physiology and atherogenesis. Nature Reviews Molecular Cell Biology. 2009;10(1):53-62.
70. Ingber DE. Mechanobiology and diseases of mechanotransduction. Annals of Medicine. 2003;35(8):564-77.
71. Murphy WL, McDevitt TC, Engler AJ. Materials as stem cell regulators. Nature Materials. 2014;13(6):547-57.
72. Blank U, Karlsson G, Karlsson S. Signaling pathways governing stem-cell fate. Blood. 2008;111(2):492-503.

73. Chowdhury F, Na S, Li D, Poh YC, Tanaka TS, Wang F, et al. Material properties of the cell dictate stress-induced spreading and differentiation in embryonic stem cells. Nature Materials. 2010;9(1):82-8.
74. Yamamoto K, Sokabe T, Watabe T, Miyazono K, Yamashita JK, Obi S, et al. Fluid shear stress induces differentiation of Flk-1-positive embryonic stem cells into vascular endothelial cells in vitro. American Journal of Physiology-Heart and Circulatory Physiology. 2005;288(4):H1915-H24.
75. Moore KA, Polte T, Huang S, Shi B, Alsberg E, Sunday ME, et al. Control of basement membrane remodeling and epithelial branching morphogenesis in embryonic lung by Rho and cytoskeletal tension. Developmental Dynamics. 2005;232(2):268-81.
76. Young JL, Engler AJ. Hydrogels with time-dependent material properties enhance cardiomyocyte differentiation in vitro. Biomaterials. 2011;32(4):1002-9.
77. Engler AJ, Sen S, Sweeney HL, Discher DE. Matrix elasticity directs stem cell lineage specification. Cell. 2006;126(4):677-89.
78. Zoldan J, Karagiannis ED, Lee CY, Anderson DG, Langer R, Levenberg S. The influence of scaffold elasticity on germ layer specification of human embryonic stem cells. Biomaterials. 2011;32(36):9612-21.
79. Gilbert PM, Havenstrite KL, Magnusson KEG, Sacco A, Leonardi NA, Kraft P, et al. Substrate Elasticity Regulates Skeletal Muscle Stem Cell Self-Renewal in Culture. Science. 2010;329(5995):1078-81.
80. Engler AJ, Griffin MA, Sen S, Bonnetnann CG, Sweeney HL, Discher DE. Myotubes differentiate optimally on substrates with tissue-like stiffness: pathological implications for soft or stiff microenvironments. Journal of Cell Biology. 2004;166(6):877-87.
81. McBeath R, Pirone DM, Nelson CM, Bhadriraju K, Chen CS. Cell shape, cytoskeletal tension, and RhoA regulate stem cell lineage commitment. Developmental Cell. 2004;6(4):483-95.
82. Wingate K, Bonani W, Tan Y, Bryant SJ, Tan W. Compressive elasticity of three-dimensional nanofiber matrix directs mesenchymal stem cell differentiation to vascular cells with endothelial or smooth muscle cell markers. Acta Biomaterialia. 2012;8(4):1440-9.
83. Bian LM, Hou C, Tous E, Rai R, Mauck RL, Burdick JA. The influence of hyaluronic acid hydrogel crosslinking density and macromolecular diffusivity on human MSC chondrogenesis and hypertrophy. Biomaterials. 2013;34(2):413-21.
84. Wang LS, Boulaire J, Chan PPY, Chung JE, Kurisawa M. The role of stiffness of gelatin-hydroxyphenylpropionic acid hydrogels formed by enzyme-mediated crosslinking on the differentiation of human mesenchymal stem cell. Biomaterials. 2010;31(33):8608-16.
85. Naraghi M, Chasiotis I, Kahn H, Wen YK, Dzenis Y. Mechanical deformation and failure of electrospun polyacrylonitrile nanofibers as a function of strain rate. Applied Physics Letters. 2007;91(15).
86. Chew SY, Hufnagel TC, Lim CT, Leong KW. Mechanical properties of single electrospun drug-encapsulated nanofibres. Nanotechnology. 2006;17(15):3880-91.
87. Carrabba M, De Maria C, Oikawa A, Reni C, Rodriguez-Arabaolaza I, Spencer H, et al. Design, fabrication and perivascular implantation of bioactive scaffolds engineered with human adventitial progenitor cells for stimulation of arteriogenesis in peripheral ischemia. Biofabrication. 2016;8(1).
88. Dias JR, Baptista-Silva S, de Oliveira CMT, Sousa A, Oliveira AL, Bartolo PJ, et al. In situ crosslinked electrospun gelatin nanofibers for skin regeneration. European Polymer Journal. 2017;95:161-73.
89. Tan EPS, Lim CT. Novel approach to tensile testing of micro- and nanoscale fibers. Review of Scientific Instruments. 2004;75(8):2581-5.

90. Tan EPS, Lim CT. Nanoindentation study of nanofibers. Applied Physics Letters. 2005;87(12).
91. Tan EPS, Lim CT. Mechanical characterization of nanofibers - A review. Composites Science and Technology. 2006;66(9):1102-11.
92. Mohammadzadehmoghadam S, Dong Y, Davies IJ. Recent Progress in Electrospun Nanofibers: Reinforcement Effect and Mechanical Performance. Journal of Polymer Science Part B-Polymer Physics. 2015;53(17):1171-212.
93. Tan EPS, Lim CT. Physical properties of a single polymeric nanofiber. Applied Physics Letters. 2004;84(9):1603-5.
94. Stevens MM, George JH. Exploring and engineering the cell surface interface. Science. 2005;310(5751):1135-8.
95. Dalby MJ, Gadegaard N, Tare R, Andar A, Riehle MO, Herzyk P, et al. The control of human mesenchymal cell differentiation using nanoscale symmetry and disorder. Nature Materials. 2007;6(12):997-1003.
96. Li WJ, Laurencin CT, Caterson EJ, Tuan RS, Ko FK. Electrospun nanofibrous structure: A novel scaffold for tissue engineering. Journal of Biomedical Materials Research. 2002;60(4):613-21.
97. Kishan AP, Nezarati RM, Radzicki CM, Renfro AL, Robinson JL, Whitely ME, et al. In situ crosslinking of electrospun gelatin for improved fiber morphology retention and tunable degradation. Journal of Materials Chemistry B. 2015;3(40):7930-8.
98. Kraehenbuehl TP, Langer R, Ferreira LS. Three-dimensional biomaterials for the study of human pluripotent stem cells. Nature Methods. 2011;8(9):731-6.
99. Nerurkar NL, Han WJ, Mauck RL, Elliott DM. Homologous structure-function relationships between native fibrocartilage and tissue engineered from MSC-seeded nanofibrous scaffolds. Biomaterials. 2011;32(2):461-8.
100. Benoit DSW, Schwartz MP, Durney AR, Anseth KS. Small functional groups for controlled differentiation of hydrogel-encapsulated human mesenchymal stem cells. Nature Materials. 2008;7(10):816-23.
101. Gerecht S, Burdick JA, Ferreira LS, Townsend SA, Langer R, Vunjak-Novakovic G. Hyaluronic acid hydrogen for controlled self-renewal and differentiation of human embryonic stem cells. Proceedings of the National Academy of Sciences of the United States of America. 2007;104(27):11298-303.
102. Siti-Ismail N, Bishop AE, Polak JM, Mantalaris A. The benefit of human embryonic stem cell encapsulation for prolonged feeder-free maintenance. Biomaterials. 2008;29(29):3946-52.
103. Li ZS, Leung M, Hopper R, Ellenbogen R, Zhang MQ. Feeder-free self-renewal of human embryonic stem cells in 3D porous natural polymer scaffolds. Biomaterials. 2010;31(3):404-12.
104. Chen JL, Yin Z, Shen WLA, Chen XA, Heng BC, Zou XAH, et al. Efficacy of hESC-MSCs in knitted silk-collagen scaffold for tendon tissue engineering and their roles. Biomaterials. 2010;31(36):9438-51.
105. Yang MC, Wang SS, Chou NK, Chi NH, Huang YY, Chang YL, et al. The cardiomyogenic differentiation of rat mesenchymal stem cells on silk fibroin-polysaccharide cardiac patches in vitro. Biomaterials. 2009;30(22):3757-65.
106. Smith LA, Liu XH, Hu J, Wang P, Ma PX. Enhancing Osteogenic Differentiation of Mouse Embryonic Stem Cells by Nanofibers. Tissue Engineering Part A. 2009;15(7):1855-64.
107. Arumugam R, Srinadhu ES, Subramanian B, Nallani S. beta-PVDF based electrospun nanofibers - A promising material for developing cardiac patches. Medical Hypotheses. 2019;122:31-4.

108. Sridhar S, Venugopal JR, Sridhar R, Ramakrishna S. Cardiogenic differentiation of mesenchymal stem cells with gold nanoparticle loaded functionalized nanofibers. Colloids and Surfaces B-Biointerfaces. 2015;134:346-54.
109. Dahlin RL, Kasper FK, Mikos AG. Polymeric Nanofibers in Tissue Engineering. Tissue Engineering Part B-Reviews. 2011;17(5):349-64.
110. Smith LA, Liu XH, Hu J, Ma PX. The influence of three-dimensional nanofibrous scaffolds on the osteogenic differentiation of embryonic stem cells. Biomaterials. 2009;30(13):2516-22.
111. Smith LA, Liu XH, Hu JA, Ma PX. The Enhancement of human embryonic stem cell osteogenic differentiation with nano-fibrous scaffolding. Biomaterials. 2010;31(21):5526-35.
112. Huang ZM, Zhang YZ, Kotaki M, Ramakrishna S. A review on polymer nanofibers by electrospinning and their applications in nanocomposites. Composites Science and Technology. 2003;63(15):2223-53.
113. Khil MS, Cha DI, Kim HY, Kim IS, Bhattarai N. Electrospun nanofibrous polyurethane membrane as wound dressing. Journal of Biomedical Materials Research Part B-Applied Biomaterials. 2003;67B(2):675-9.
114. Kim SH, Nam YS, Lee TS, Park WH. Silk fibroin nanofiber. Electrospinning, properties, and structure. Polymer Journal. 2003;35(2):185-90.
115. Jing Z, Xu XY, Chen XS, Liang QZ, Bian XC, Yang LX, et al. Biodegradable electrospun fibers for drug delivery. Journal of Controlled Release. 2003;92(3):227-31.
116. Verreck G, Chun I, Rosenblatt J, Peeters J, Van Dijck A, Mensch J, et al. Incorporation of drugs in an amorphous state into electrospun nanofibers composed of a water-insoluble, nonbiodegradable polymer. Journal of Controlled Release. 2003;92(3):349-60.
117. Jin HJ, Fridrikh SV, Rutledge GC, Kaplan DL. Electrospinning Bombyx mori silk with poly(ethylene oxide). Biomacromolecules. 2002;3(6):1233-9.
118. Zeleny J. The electrical discharge from liquid points, and a hydrostatic method of measuring the electric intensity at their surfaces. Physical Review. 1914;3(2):69-91.
119. Bhardwaj N, Kundu SC. Electrospinning: A fascinating fiber fabrication technique. Biotechnology Advances. 2010;28(3):325-47.
120. Kidoaki S, Kwon IK, Matsuda T. Mesoscopic spatial designs of nano- and microfiber meshes for tissue-engineering matrix and scaffold based on newly devised multilayering and mixing electrospinning techniques. Biomaterials. 2005;26(1):37-46.
121. Stankus JJ, Guan JJ, Wagner WR. Fabrication of biodegradable elastomeric scaffolds with sub-micron morphologies. Journal of Biomedical Materials Research Part A. 2004;70A(4):603-14.
122. Liang D, Hsiao BS, Chu B. Functional electrospun nanofibrous scaffolds for biomedical applications. Advanced Drug Delivery Reviews. 2007;59(14):1392-412.
123. Sill TJ, von Recum HA. Electro spinning: Applications in drug delivery and tissue engineering. Biomaterials. 2008;29(13):1989-2006.
124. Taylor G. Electrically driven jets. Proceedings of the Royal Society of London Series a-Mathematical and Physical Sciences. 1969;313(1515):453-&.
125. Yarin AL, Koombhongse S, Reneker DH. Bending instability in electrospinning of nanofibers. Journal of Applied Physics. 2001;89(5):3018-26.
126. Adomaviciute E, Milasius R. The influence of applied voltage on poly(vinyl alcohol) (PVA) nanofibre diameter. Fibres & Textiles in Eastern Europe. 2007;15(5-6):69-72.
127. Stankus JJ, Guan JJ, Fujimoto K, Wagner WR. Microintegrating smooth muscle cells into a biodegradable, elastomeric fiber matrix. Biomaterials. 2006;27(5):735-44.
128. Reneker DH, Chun I. Nanometre diameter fibres of polymer, produced by electrospinning. Nanotechnology. 1996;7(3):216-23.

129. Li D, Xia YN. Electrospinning of nanofibers: Reinventing the wheel? Advanced Materials. 2004;16(14):1151-70.
130. Dzenis Y. Spinning continuous fibers for nanotechnology. Science. 2004;304(5679):1917-9.
131. He JH, Wan YQ, Yu MY. Allometric scaling and instability in electrospinning. International Journal of Nonlinear Sciences and Numerical Simulation. 2004;5(3):243-52.
132. Feng JJ. The stretching of an electrified non-Newtonian jet: A model for electrospinning. Physics of Fluids. 2002;14(11):3912-26.
133. Fridrikh SV, Yu JH, Brenner MP, Rutledge GC. Controlling the fiber diameter during electrospinning. Physical Review Letters. 2003;90(14).
134. Chong EJ, Phan TT, Lim IJ, Zhang YZ, Bay BH, Ramakrishna S, et al. Evaluation of electrospun PCL/gelatin nanofibrous scaffold for wound healing and layered dermal reconstitution. Acta Biomaterialia. 2007;3(3):321-30.
135. Levett PA, Melchels FPW, Schrobback K, Hutmacher DW, Malda J, Klein TJ. A biomimetic extracellular matrix for cartilage tissue engineering centered on photocurable gelatin, hyaluronic acid and chondroitin sulfate. Acta Biomaterialia. 2014;10(1):214-23.
136. Ravichandran R, Sundaramurthi D, Gandhi S, Sethuraman S, Krishnan UM. Bioinspired hybrid mesoporous silica-gelatin sandwich construct for bone tissue engineering. Microporous and Mesoporous Materials. 2014;187:53-62.
137. Sell SA, Wolfe PS, Garg K, McCool JM, Rodriguez IA, Bowlin GL. The Use of Natural Polymers in Tissue Engineering: A Focus on Electrospun Extracellular Matrix Analogues. Polymers. 2010;2(4):522-53.
138. Wang X, Niu HT, Wang XG, Lin T. Needleless Electrospinning of Uniform Nanofibers Using Spiral Coil Spinnerets. Journal of Nanomaterials. 2012.
139. Zhang S, Huang YQ, Yang XP, Mei F, Ma Q, Chen GQ, et al. Gelatin nanofibrous membrane fabricated by electrospinning of aqueous gelatin solution for guided tissue regeneration. Journal of Biomedical Materials Research Part A. 2009;90A(3):671-9.
140. Zhao Y, Qiu YH, Wang HH, Chen Y, Jin SH, Chen SS. Preparation of Nanofibers with Renewable Polymers and Their Application in Wound Dressing. International Journal of Polymer Science. 2016.
141. Drexler JW, Powell HM. Dehydrothermal Crosslinking of Electrospun Collagen. Tissue Engineering Part C-Methods. 2011;17(1):9-17.
142. Haugh MG, Murphy CM, McKiernan RC, Altenbuchner C, O'Brien FJ. Crosslinking and Mechanical Properties Significantly Influence Cell Attachment, Proliferation, and Migration Within Collagen Glycosaminoglycan Scaffolds. Tissue Engineering Part A. 2011;17(9-10):1201-8.
143. Weadock KS, Miller EJ, Bellincampi LD, Zawadsky JP, Dunn MG. Physical cross-linking of collagen-fibers - comparison of ultraviolet-irradiation and dehydrothermal treatment. Journal of Biomedical Materials Research. 1995;29(11):1373-9.
144. Yao RJ, He J, Meng GL, Jiang B, Wu F. Electrospun PCL/Gelatin composite fibrous scaffolds: mechanical properties and cellular responses. Journal of Biomaterials Science-Polymer Edition. 2016;27(9):824-38.
145. Torres-Giner S, Gimeno-Alcaniz JV, Ocio MJ, Lagaron JM. Comparative Performance of Electrospun Collagen Nanofibers Cross-linked by Means of Different Methods. Acs Applied Materials & Interfaces. 2009;1(1):218-23.
146. Farris S, Schaich KM, Liu LS, Cooke PH, Piergiovanni L, Yam KL. Gelatin-pectin composite films from polyion-complex hydrogels. Food Hydrocolloids. 2011;25(1):61-70.
147. Zhan JC, Morsi Y, Ei-Hamshary H, Al-Deyab S, Mo XM. In vitro evaluation of electrospun gelatin-glutaraldehyde nanofibers. Frontiers of Materials Science. 2016;10(1):90-100.

148. Chen PR, Kang PL, Su WY, Lin FH, Chena MH. The evaluation of thermal properties and in vitro test of carbodiimide or glutaraldehyde cross-linked gelatin for pc 12 cells culture. Biomedical Engineering-Applications Basis Communications. 2005;17(2):101-7.
149. Ratanavaraporn J, Rangkupan R, Jeeratawatchai H, Kanokpanont S, Damrongsakkul S. Influences of physical and chemical crosslinking techniques on electrospun type A and B gelatin fiber mats. International Journal of Biological Macromolecules. 2010;47(4):431-8.
150. Davidenko N, Schuster CF, Bax DV, Raynal N, Farndale RW, Best SM, et al. Control of crosslinking for tailoring collagen-based scaffolds stability and mechanics. Acta Biomaterialia. 2015;25:131-42.
151. Tang C, Saquing CD, Harding JR, Khan SA. In Situ Cross-Linking of Electrospun Poly(vinyl alcohol) Nanofibers. Macromolecules. 2010;43(2):630-7.
152. Stone SA, Gosavi P, Athauda TJ, Ozer RR. In situ citric acid crosslinking of alginate/polyvinyl alcohol electrospun nanofibers. Materials Letters. 2013;112:32-5.
153. Slemming-Adamsen P, Song J, Dong MD, Besenbacher F, Chen ML. In Situ Cross-Linked PNIPAM/Gelatin Nanofibers for Thermo-Responsive Drug Release. Macromolecular Materials and Engineering. 2015;300(12):1226-31.
154. Zhang YZ, Venugopal J, Huang ZM, Lim CT, Ramakrishna S. Crosslinking of the electrospun gelatin nanofibers. Polymer. 2006;47(8):2911-7.
155. Lai JY, Ma DHK. Glutaraldehyde cross-linking of amniotic membranes affects their nanofibrous structures and limbal epithelial cell culture characteristics. International Journal of Nanomedicine. 2013;8:4157-68.
156. Mota A, Lotfi AS, Barzin J, Hatam M, Adibi B, Khalaj Z, et al. Human Bone Marrow Mesenchymal Stem Cell Behaviors on PCL/Gelatin Nanofibrous Scaffolds Modified with A Collagen IV-Derived RGD-Containing Peptide. Cell Journal. 2014;16(1):1-10.
157. Lai JY, Li YT, Cho CH, Yu TC. Nanoscale modification of porous gelatin scaffolds with chondroitin sulfate for corneal stromal tissue engineering. International Journal of Nanomedicine. 2012;7:1101-14.
158. Asghari F, Samiei M, Adibkia K, Akbarzadeh A, Davaran S. Biodegradable and biocompatible polymers for tissue engineering application: a review. Artificial Cells Nanomedicine and Biotechnology. 2017;45(2):185-92.
159. Kong LY, Ziegler GR. Molecular Entanglement and Electrospinnability of Biopolymers. Jove-Journal of Visualized Experiments. 2014(91).
160. Nguyen TBL, Lee BT. Electrospinning of polyvinyl alcohol/gelatin nanofiber composites and cross-linking for bone tissue engineering application. Journal of Biomaterials Applications. 2012;27(3):255-66.
161. Huang ZM, Zhang YZ, Ramakrishna S, Lim CT. Electrospinning and mechanical characterization of gelatin nanofibers. Polymer. 2004;45(15):5361-8.
162. Mindru TB, Mindru IB, Malutan T, Tura V. Electrospinning of high concentration gelatin solutions. Journal of Optoelectronics and Advanced Materials. 2007;9(11):3633-8.
163. Li WW, Qin XH. Effect of Relative Humidity on the Morphology of Electrospun Gelatin Aqueous Solutions. Advanced Materials Research. 2014;941-944:1225-8.
164. Nezarati RM, Eifert MB, Cosgriff-Hernandez E. Effects of Humidity and Solution Viscosity on Electrospun Fiber Morphology. Tissue Engineering Part C-Methods. 2013;19(10):810-9.
165. Oraby MA, Waley AI, El-Dewany AI, Saad EA, El-Hady BMA. Electrospun Gelatin Nanofibers: Effect of Gelatin Concentration on Morphology and Fiber Diameters. Journal of Applied Sciences Research. 2013;9(1):534-40.
166. Deitzel JM, Kleinmeyer J, Harris D, Tan NCB. The effect of processing variables on the morphology of electrospun nanofibers and textiles. Polymer. 2001;42(1):261-72.

167. Liu HQ, Hsieh YL. Ultrafine fibrous cellulose membranes from electrospinning of cellulose acetate. Journal of Polymer Science Part B-Polymer Physics. 2002;40(18):2119-29.
168. Ryu YJ, Kim HY, Lee KH, Park HC, DR L. Transport properties of electrospun nylon 6 non-woven mats.. . Eur Polym J. 2003;39:1883-9.
169. MG M, LJ, CM, TE L. Phospholipid non-woven electrospun membranes. Science 2006;311:353-5.
170. Haghi AK, Akbari M. Trends in electrospinning of natural nanofibers. Physica Status Solidi a-Applications and Materials Science. 2007;204(6):1830-4.
171. Song E, Kim SY, Chun T, Byun HJ, Lee YM. Collagen scaffolds derived from a marine source and their biocompatibility. Biomaterials. 2006;27(15):2951-61.
172. Takeda N, Tamura K, Mineguchi R, Ishikawa Y, Haraguchi Y, Shimizu T, et al. In situ cross-linked electrospun fiber scaffold of collagen for fabricating cell-dense muscle tissue. Journal of Artificial Organs. 2016;19(2):141-8.
173. Farina A, Fievet MH, Plassart F, Menet MC, Thuillier A. Residual glutaraldehyde levels in fiberoptic endoscopes: measurement and implications for patient toxicity. Journal of Hospital Infection. 1999;43(4):293-7.
174. Vanwachem PB, Vanluyn MJA, Damink L, Dijkstra PJ, Feijen J, Nieuwenhuis P. Biocompatibility and tissue regenerating capacity of cross-linked dermal sheep collagen. Journal of Biomedical Materials Research. 1994;28(3):353-63.
175. L. L. H. Huang-Lee, Cheung DT, M. E. Nimni. Biochemical changes and cytotoxicity associated with the degradation of polymeric glutaraldehyde derived crosslinks. J Biomed Mater Res. 1990;24:1185-201.
176. Schmidt CE, Baier JM. Acellular vascular tissues: natural biomaterials for tissue repair and tissue engineering. Biomaterials. 2000;21(22):2215-31.
177. McKee MG, Wilkes GL, Colby RH, Long TE. Correlations of solution rheology with electrospun fiber formation of linear and branched polyesters. Macromolecules. 2004;37(5):1760-7.
178. Diego GD, Jose´ MN, Lourdes CQ. Influence of concentration and temperature upon rheology of k-carrageen aqueous solutions. EJEAFChe 2006;5(1):1213-20.
179. Krevelen DWV. Properties of Polymers Elsevier (1990). 1990:898.
180. O. Yasuo, M. Hiroki, S. Hiroshige, Hiroshi Y. Short branch effects on the creep properties of the ultra-high strength polyethylene fibers
Journal of Polymer Science, Part B, Polymer Physics, . 1994;32:261-9.
181. Luo C, Li L, Li JR, Yang G, Ding S, Zhi W, et al. Modulating cellular behaviors through surface nanoroughness. Journal of Materials Chemistry. 2012;22(31):15654-64.
182. Jaiswal A. Nanofibrous Scaffolds for Tissue Engineering Applications. Brazilian Archives of Biology and Technology. 2016;59B:1678-4324.
183. Reddy N, Reddy R, Jiang QR. Crosslinking biopolymers for biomedical applications. Trends in Biotechnology. 2015;33(6):362-9.
184. PR U, Mohanan PV, TV K. Glutaraldehyde treatment elicits toxic response compared to decellularization in bovine pericardium. Toxicol Int. 2012;19(1):51-8.
185. Cheng XC, Shao ZY, Li CB, Yu LJ, Raja MA, Liu CG. Isolation, Characterization and Evaluation of Collagen from Jellyfish Rhopilema esculentum Kishinouye for Use in Hemostatic Applications. Plos One. 2017;12(1).
186. Sai KP, Babu M. Studies on Rana tigerina skin collagen. Comparative Biochemistry and Physiology B-Biochemistry & Molecular Biology. 2001;128(1):81-90.
187. Wang L, An XX, Yang FM, Xin ZH, Zhao LY, Hu QH. Isolation and characterisation of collagens from the skin, scale and bone of deep-sea redfish (Sebastes mentella). Food Chemistry. 2008;108(2):616-23.

188. Usha R, Sreeram KJ, Rajaram A. Stabilization of collagen with EDC/NHS in the presence of L-lysine: A comprehensive study. Colloids and Surfaces B-Biointerfaces. 2012;90:83-90.
189. Ma DHK, Lai JY, Cheng HY, Tsai CC, Yeh LK. Carbodiimide cross-linked amniotic membranes for cultivation of limbal epithelial cells. Biomaterials. 2010;31(25):6647-58.
190. Lai JY, Li YT. Evaluation of cross-linked gelatin membranes as delivery carriers for retinal sheets. Materials Science & Engineering C-Materials for Biological Applications. 2010;30(5):677-85.
191. Rault I, Frei V, Herbage D, AbdulMalak N, Huc A. Evaluation of different chemical methods for cross-linking collagen gel, films and sponges. Journal of Materials Science-Materials in Medicine. 1996;7(4):215-21.
192. Vanderhooft JL, Alcoutlabi M, Magda JJ, Prestwich GD. Rheological Properties of Cross-Linked Hyaluronan-Gelatin Hydrogels for Tissue Engineering. Macromolecular Bioscience. 2009;9(1):20-8.
193. Dias JR, Baptista-Silva S, Sousa A, Oliveira AL, Bartolo PJ, Granja PL. Biomechanical performance of hybrid electrospun structures for skin regeneration. Materials Science & Engineering C-Materials for Biological Applications. 2018;93:816-27.
194. Jiang X, Nai MH, Lim CT, Le Visage C, Chan JKY, Chew SY. Polysaccharide nanofibers with variable compliance for directing cell fate. Journal of Biomedical Materials Research Part A. 2015;103(3):959-68.
195. Martucci JF, Espinosa JP, Ruseckaite RA. Physicochemical Properties of Films Based on Bovine Gelatin Cross-linked with 1,4-Butanediol Diglycidyl Ether. Food and Bioprocess Technology. 2015;8(8):1645-56.
196. Vargas G, Acevedo JL, Lopez J, Romero J. Study of cross-linking of gelatin by ethylene glycol diglycidyl ether. Materials Letters. 2008;62(21-22):3656-8.
197. Adamo L, Naveiras O, Wenzel PL, McKinney-Freeman S, Mack PJ, Gracia-Sancho J, et al. Biomechanical forces promote embryonic haematopoiesis. Nature. 2009;459(7250):1131-U120.
198. Lucitti JL, Jones EAV, Huang CQ, Chen J, Fraser SE, Dickinson ME. Vascular remodeling of the mouse yolk sac requires hemodynamic force. Development. 2007;134(18):3317-26.
199. Davies PF. Flow-mediated endothelial mechanotransduction. Physiological Reviews. 1995;75(3):519-60.
200. Wang N, Butler JP, Ingber DE. Mechanotransduction across the cell-surface and through the cytoskeleton. Science. 1993;260(5111):1124-7.
201. Ingber DE. Cellular tensegrity - defining new rules of biological design that govern the cytoskeleton. Journal of Cell Science. 1993;104:613-27.
202. Choquet D, Felsenfeld DP, Sheetz MP. Extracellular matrix rigidity causes strengthening of integrin-cytoskeleton linkages. Cell. 1997;88(1):39-48.
203. Katz BZ, Zamir E, Bershadsky A, Kam Z, Yamada KM, Geiger B. Physical state of the extracellular matrix regulates the structure and molecular composition of cell-matrix adhesions. Molecular Biology of the Cell. 2000;11(3):1047-60.
204. Cukierman E, Pankov R, Stevens DR, Yamada KM. Taking cell-matrix adhesions to the third dimension. Science. 2001;294(5547):1708-12.
205. Beningo KA, Dembo M, Wang YI. Responses of fibroblasts to anchorage of dorsal extracellular matrix receptors. Proceedings of the National Academy of Sciences of the United States of America. 2004;101(52):18024-9.
206. Pelham RJ, Wang YL. Cell locomotion and focal adhesions are regulated by substrate flexibility (vol 94, pg 13661, 1997). Proceedings of the National Academy of Sciences of the United States of America. 1998;95(20):12070-.

207. Peyton SR, Putnam AJ. Extracellular matrix rigidity governs smooth muscle cell motility in a biphasic fashion. Journal of Cellular Physiology. 2005;204(1):198-209.
208. Trappmann B, Gautrot JE, Connelly JT, Strange DGT, Li Y, Oyen ML, et al. Extracellular-matrix tethering regulates stem-cell fate. Nature Materials. 2012;11(7):642-9.
209. Choi SJ, Kim HN, Bae WG, Suh KY. Modulus- and surface energy-tunable ultraviolet-curable polyurethane acrylate: properties and applications. Journal of Materials Chemistry. 2011;21(38):14325-35.
210. Khatiwala CB, Peyton SR, Metzke M, Putnam AJ. The regulation of osteogenesis by ECM rigidity in MC3T3-E1 cells requires MAPK activation. Journal of Cellular Physiology. 2007;211(3):661-72.
211. Peyton SR, Raub CB, Keschrumrus VP, Putnam AJ. The use of poly(ethylene glycol) hydrogels to investigate the impact of ECM chemistry and mechanics on smooth muscle cells. Biomaterials. 2006;27(28):4881-93.
212. Kim J, Kim HN, Lim KT, Kim Y, Pandey S, Garg P, et al. Synergistic effects of nanotopography and co-culture with endothelial cells on osteogenesis of mesenchymal stem cells. Biomaterials. 2013;34(30):7257-68.
213. Pompe T, Glorius S, Bischoff T, Uhlmann I, Kaufmann M, Brenner S, et al. Dissecting the Impact of Matrix Anchorage and Elasticity in Cell Adhesion. Biophysical Journal. 2009;97(8):2154-63.
214. Liu YX, Chan-Park MB. A biomimetic hydrogel based on methacrylated dextran-graft-lysine and gelatin for 3D smooth muscle cell culture. Biomaterials. 2010;31(6):1158-70.
215. Young S, Wong M, Tabata Y, Mikos AG. Gelatin as a delivery vehicle for the controlled release of bioactive molecules. Journal of Controlled Release. 2005;109(1-3):256-74.
216. Kumar PTS, Praveen G, Raj M, Chennazhi KP, Jayakumar R. Flexible, micro-porous chitosan-gelatin hydrogel/nanofibrin composite bandages for treating burn wounds. Rsc Advances. 2014;4(110):65081-7.
217. Kumar PTS, Raj NM, Praveen G, Chennazhi KP, Nair SV, Jayakumar R. In Vitro and In Vivo Evaluation of Microporous Chitosan Hydrogel/Nanofibrin Composite Bandage for Skin Tissue Regeneration. Tissue Engineering Part A. 2013;19(3-4):380-92.
218. Kumar PTS, Lakshmanan VK, Raj M, Biswas R, Hiroshi T, Nair SV, et al. Evaluation of Wound Healing Potential of beta-Chitin Hydrogel/Nano Zinc Oxide Composite Bandage. Pharmaceutical Research. 2013;30(2):523-37.
219. Wake MC, Patrick CW, Mikos AG. Pore morphology effects on the fibrovascular tissue-growth in porous polymer substrates. Cell Transplantation. 1994;3(4):339-43.
220. Druecke D, Langer S, Lamme E, Pieper J, Ugarkovic M, Steinau HU, et al. Neovascularization of poly(ether ester) block-copolymer scaffolds in vivo: Long-term investigations using intravital fluorescent microscopy. Journal of Biomedical Materials Research Part A. 2004;68A(1):10-8.
221. Adeloew C, Segura T, Hubbell JA, Frey P. The effect of enzymatically degradable poly(ethylene glycol) hydrogels on smooth muscle cell phenotype. Biomaterials. 2008;29(3):314-26.
222. Qiu YL, Bayomy AF, Gomez MV, Bauer M, Du P, Yang YF, et al. A role for matrix stiffness in the regulation of cardiac side population cell function. American Journal of Physiology-Heart and Circulatory Physiology. 2015;308(9):H990-H7.
223. Peyton SR, Kim PD, Ghajar CM, Seliktar D, Putnam AJ. The effects of matrix stiffness and RhoA on the phenotypic plasticity of smooth muscle cells in a 3-D biosynthetic hydrogel system. Biomaterials. 2008;29(17):2597-607.

224. Brown XQ, Bartolak-Suki E, Williams C, Walker ML, Weaver VM, JY W. Effect of substrate stiffness and PDGF on the behavior of vascular smooth muscle cells: Impli- cations for atherosclerosis. . J Cell Physiol 2010;225:115-22.
225. Saharinen P, Eklund L, Pulkki K, Bono P, Alitalo K. VEGF and angiopoietin signaling in tumor angiogenesis and metastasis. Trends in Molecular Medicine. 2011;17(7):347-62.
226. Saharinen P, Bry M, Alitalo K. How do angiopoietins Tie in with vascular endothelial growth factors? Current Opinion in Hematology. 2010;17(3):198-205.
227. Djonov V, Schmid M, Tschanz SA, Burri PH. Intussusceptive angiogenesis - Its role in embryonic vascular network formation. Circulation Research. 2000;86(3):286-92.
228. Gerhardt H, Golding M, Fruttiger M, Ruhrberg C, Lundkvist A, Abramsson A, et al. VEGF guides angiogenic sprouting utilizing endothelial tip cell filopodia. Journal of Cell Biology. 2003;161(6):1163-77.
229. Thurston G, Suri C, Smith K, McClain J, Sato TN, Yancopoulos GD, et al. Leakage-resistant blood vessels in mice transgenically overexpressing angiopoietin-1. Science. 1999;286(5449):2511-4.
230. Augustin HG, Koh GY, Thurston G, Alitalo K. Control of vascular morphogenesis and homeostasis through the angiopoietin-Tie system. Nature Reviews Molecular Cell Biology. 2009;10(3):165-77.
231. Thurston G. Role of Angiopoietins and Tie receptor tyrosine kinases in angiogenesis and lymphangiogenesis. Cell and Tissue Research. 2003;314(1):61-8.
232. Maisonpierre PC, Suri C, Jones PF, Bartunkova S, Wiegand S, Radziejewski C, et al. Angiopoietin-2, a natural antagonist for Tie2 that disrupts in vivo angiogenesis. Science. 1997;277(5322):55-60.
233. Suri C, Jones PF, Patan S, Bartunkova S, Maisonpierre PC, Davis S, et al. Requisite role of Angiopoietin-1, a ligand for the TIE2 receptor, during embryonic angiogenesis. Cell. 1996;87(7):1171-80.
234. Davis S, Aldrich TH, Jones PF, Acheson A, Compton DL, Jain V, et al. Isolation of Angiopoietin-1, a ligand for the TIE2 receptor, by secretion-trap expression cloning. Cell. 1996;87(7):1161-9.
235. Barton WA, Tzvetkova-Robev D, Miranda EP, Kolev MV, Rajashankar KR, Himanen JP, et al. Crystal structures of the Tie2 receptor ectodomain and the angiopoietin-2-Tie2 complex. Nature Structural & Molecular Biology. 2006;13(6):524-32.
236. Procopio WN, Pelavin PI, Lee WMF, Yeilding NM. Angiopoietin-1 and-2 coiled coil domains mediate distinct homo-oligomerization patterns, but fibrinogen-like domains mediate ligand activity. Journal of Biological Chemistry. 1999;274(42):30196-201.
237. Fagiani E, Christofori G. Angiopoietins in angiogenesis. Cancer Letters. 2013;328(1):18-26.
238. Yuan HT, Khankin EV, Karumanchi SA, Parikh SM. Angiopoietin 2 Is a Partial Agonist/Antagonist of Tie2 Signaling in the Endothelium. Molecular and Cellular Biology. 2009;29(8):2011-22.
239. Kim I, Kim JH, Moon SO, Kwak HJ, Kim NG, Koh GY. Angiopoietin-2 at high concentration can enhance endothelial cell survival through the phosphatidylinositol 3 '-kinase/Akt signal transduction pathway. Oncogene. 2000;19(39):4549-52.
240. Teichert-Kuliszewska K, Maisonpierre PC, Jones N, Campbell AIM, Master Z, Bendeck MP, et al. Biological action of angiopoietin-2 in a fibrin matrix model of angiogenesis is associated with activation of Tie2. Cardiovascular Research. 2001;49(3):659-70.
241. Daly C, Pasnikowski E, Burova E, Wong V, Aldrich TH, Griffiths J, et al. Angiopoietin-2 functions as an autocrine protective factor in stressed endothelial cells. Proceedings of the National Academy of Sciences of the United States of America. 2006;103(42):15491-6.

242. Hanahan D. Signaling vascular morphogenesis and maintenance. Science. 1997;277(5322):48-50.
243. Felcht M, Luck R, Schering A, Seidel P, Srivastava K, Hu JH, et al. Angiopoietin-2 differentially regulates angiogenesis through TIE2 and integrin signaling. Journal of Clinical Investigation. 2012;122(6):1991-2005.
244. Shibuya M. Vascular Endothelial Growth Factor (VEGF) and Its Receptor (VEGFR) Signaling in Angiogenesis A Crucial Target for Anti- and Pro-Angiogenic Therapies Genes Cancer 2011 Dec; 2(12): 1097–1105. 2012;2(12):1097-105.
245. Hurwitz H, Fehrenbacher L, Novotny W, Cartwright T, Hainsworth J, Heim W, et al. Bevacizumab plus irinotecan, fluorouracil, and leucovorin for metastatic colorectal cancer. New England Journal of Medicine. 2004;350(23):2335-42.
246. Sandler A, Gray R, Perry MC, Brahmer J, Schiller JH, Dowlati A, et al. Paclitaxel-carboplatin alone or with bevacizumab for non-small-cell lung cancer. New England Journal of Medicine. 2006;355(24):2542-50.
247. Shibuya M, Claesson-Welsh L. Signal transduction by VEGF receptors in regulation of angiogenesis and lymphangiogenesis. Experimental Cell Research. 2006;312(5):549-60.
248. Ingber DE. Tensegrity I. Cell structure and hierarchical systems biology. Journal of Cell Science. 2003;116(7):1157-73.
249. Elosegui-Artola A, Jorge-Penas A, Moreno-Arotzena O, Oregi A, Lasa M, Garcia-Aznar JM, et al. Image Analysis for the Quantitative Comparison of Stress Fibers and Focal Adhesions. Plos One. 2014;9(9).
250. Amano M, Chihara K, Kimura K, Fukata Y, Nakamura N, Matsuura Y, et al. Formation of actin stress fibers and focal adhesions enhanced by Rho-kinase. Science. 1997;275(5304):1308-11.
251. Tojkander S, Ciuba K, Lappalainen P. CaMKK2 Regulates Mechanosensitive Assembly of Contractile Actin Stress Fibers. Cell Reports. 2018;24(1):11-9.
252. Kuijpers AJ, Engbers GHM, Feijen J, De Smedt SC, Meyvis TKL, Demeester J, et al. Characterization of the network structure of carbodiimide cross-linked gelatin gels. Macromolecules. 1999;32(10):3325-33.
253. Birbrair A, Zhang T, Files DC, Mannava S, Smith T, Wang ZM, et al. Type-1 pericytes accumulate after tissue injury and produce collagen in an organ-dependent manner. Stem Cell Res Ther. 2014;5(6):122.
254. Siao CJ, Lorentz CU, Kermani P, Marinic T, Carter J, McGrath K, et al. ProNGF, a cytokine induced after myocardial infarction in humans, targets pericytes to promote microvascular damage and activation. J Exp Med. 2012;209(12):2291-305.
255. Avolio E, Rodriguez-Arabaolaza I, Spencer HL, Riu F, Mangialardi G, Slater SC, et al. Expansion and characterization of neonatal cardiac pericytes provides a novel cellular option for tissue engineering in congenital heart disease. J Am Heart Assoc. 2015;4(6):e002043.
256. Evans ND, Minelli C, Gentleman E, LaPointe V, Patankar SN, Kallivretaki M, et al. Substrate stiffness affects early differentiation events in embryonic stem cells. Eur Cell Mater. 2009;18:1-13; discussion -4.
257. Rowlands AS, George PA, Cooper-White JJ. Directing osteogenic and myogenic differentiation of MSCs: interplay of stiffness and adhesive ligand presentation. Am J Physiol Cell Physiol. 2008;295(4):C1037-44.
258. Ingber DE. Tensegrity I. Cell structure and hierarchical systems biology. J Cell Sci. 2003;116(Pt 7):1157-73.
259. Wozniak MA, Chen CS. Mechanotransduction in development: a growing role for contractility. Nat Rev Mol Cell Biol. 2009;10(1):34-43.

APPENDIX I: PUBLICATIONS, AWARDS AND PRESENTATIONS

1. **Naduthottathil M.R,** Avolio E, Carrabba M, Caputo M, Davis S, Madeddu P, Su B. Biomimetic gelatin nanofibrous scaffolds with tunable stiffness control human cardiac Pericyte behaviour **(Submitted to ACS Biomaterials Sciences and Engineering).**

2. Received best 3 Minute Thesis (3MT) quick-fire oral presentation award by presenting this work titled "Biomimetic gelatin nanofibrous scaffolds for the mechanical modulation of cardiac pericyte fate" at the Bristol Dental School Research Symposium (November 2018) Authors: **Naduthottathil M.R,** Avolio E, Carrabba M, Caputo M, Davis S, Madeddu P, Su B.

3. Delivered an oral presentation titled "Biomimetic gelatin nanofibrous scaffolds for the mechanical modulation of cardiac pericyte fate" in the International Nanoscience Students Conference (INASCON) 2017 held at Bristol (October 2017) Authors: Naduthottathil M.R, Avolio E, Carrabba M, Caputo M, Davis S, Madeddu P, Su B.

4. Presented a poster on the topic "Biomimetic gelatin nanofibrous scaffolds for the mechanical modulation of cardiac stem cell fate" in Nanofibers, Applications and Related Technologies (NART) 2017, held at Prague, Czech Republic (September 2017) Authors: Naduthottathil M.R, Avolio E, Carrabba M, Caputo M, Davis S, Madeddu P, Su B.

5. Presented this work titled "Biomimetic gelatin nanofibrous scaffolds for the mechanical modulation of cardiac pericyte fate" orally in the Bristol Centre for Functional Nanomaterials Annual Conference held at Bristol (May 2017) Authors: Naduthottathil M.R, Avolio E, Carrabba M, Caputo M, Davis S, Madeddu P, Su B.